AD-A154 070 TARGET DISCRIMINATION USING INFRARED TECHNIQUES: 1/2
THEORETICAL CONSIDERATIONS(U) STATE UNIV OF NEW YORK AT
SYRACUSE* M J DUGGIN ET AL. FEB 85 RADC-TR-84-29
UNCLASSIFIED F30602-81-C-0193 F/G 17/5 NL

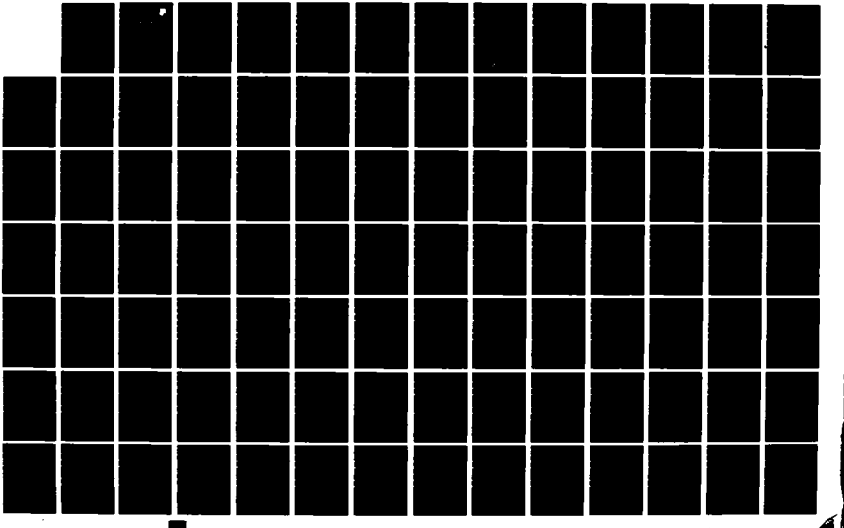

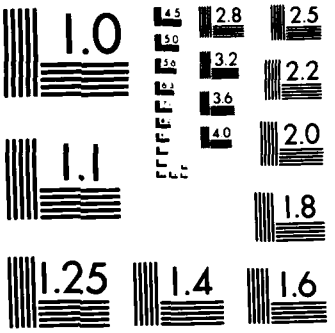

MICROCOPY RESOLUTION TEST CHART
NATIONAL BUREAU OF STANDARDS-1963-A

AD-A154 070

(2)

RADC-TR-84-29
Final Technical Report
February 1985

TARGET DISCRIMINATION USING INFRARED TECHNIQUES: THEORETICAL CONSIDERATIONS

State University of New York

Michael J. Duggin and Larry B. Schoch

APPROVED FOR PUBLIC RELEASE; DISTRIBUTION UNLIMITED

ROME AIR DEVELOPMENT CENTER
Air Force Systems Command
Griffiss Air Force Base, NY 13441

This report has been reviewed by the RADC Public Affairs Office (PA) and is releasable to the National Technical Information Service (NTIS). At NTIS it will be releasable to the general public, including foreign nations.

RADC-TR-84-29 has been reviewed and is approved for publication.

APPROVED: Randall K Blystone

RANDALL K. BLYSTONE
Project Engineer

APPROVED: Albert A Jamberdino

ALBERT A. JAMBERDINO
Acting Technical Director
Intelligence & Reconnaissance Division

FOR THE COMMANDER: John A. Ritz

JOHN A. RITZ
Acting Chief, Plans Office

If your address has changed or if you wish to be removed from the RADC mailing list, or if the addressee is no longer employed by your organization, please notify RADC (IRRE) Griffiss AFB NY 13441-5700. This will assist us in maintaining a current mailing list.

Do not return copies of this report unless contractual obligations or notices on a specific document requires that it be returned.

UNCLASSIFIED
SECURITY CLASSIFICATION OF THIS PAGE

REPORT DOCUMENTATION PAGE

1a. REPORT SECURITY CLASSIFICATION UNCLASSIFIED	1b. RESTRICTIVE MARKINGS N/A
2a. SECURITY CLASSIFICATION AUTHORITY N/A	3. DISTRIBUTION/AVAILABILITY OF REPORT Approved for public release; distribution unlimited
2b. DECLASSIFICATION/DOWNGRADING SCHEDULE N/A	
4. PERFORMING ORGANIZATION REPORT NUMBER(S) N/A	5. MONITORING ORGANIZATION REPORT NUMBER(S) RADC-TR-84-29
6a. NAME OF PERFORMING ORGANIZATION State University of New York 6b. OFFICE SYMBOL (If applicable)	7a. NAME OF MONITORING ORGANIZATION Rome Air Development Center (IRRE)
6c. ADDRESS (City, State and ZIP Code) Syracuse NY 13210	7b. ADDRESS (City, State and ZIP Code) Griffiss AFB NY 13441-5700
8a. NAME OF FUNDING/SPONSORING ORGANIZATION Rome Air Development Center 8b. OFFICE SYMBOL (If applicable) IRRE	9. PROCUREMENT INSTRUMENT IDENTIFICATION NUMBER F30602-81-C-0193
8c. ADDRESS (City, State and ZIP Code) Griffiss AFB NY 13441-5700	10. SOURCE OF FUNDING NOS. PROGRAM ELEMENT NO. 63789F; PROJECT NO. 2315; TASK NO. 06; WORK UNIT NO. P2
11. TITLE (Include Security Classification) TARGET DISCRIMINATION USING INFRARED TECHNIQUES: THEORETICAL CONSIDERATIONS	
12. PERSONAL AUTHOR(S) Michael J. Duggin, Larry B. Schoch	
13a. TYPE OF REPORT Final 13b. TIME COVERED FROM 30Jun83 TO 30Dec83	14. DATE OF REPORT (Yr., Mo., Day) February 1985 15. PAGE COUNT 132
16. SUPPLEMENTARY NOTATION N/A	

17. COSATI CODES		
FIELD	GROUP	SUB. GR.
09	04	

18. SUBJECT TERMS (Continue on reverse if necessary and identify by block number)
IR Imagery
Automatic Pattern Recognition
Image Exploitation
Algorithm Development

19. ABSTRACT (Continue on reverse if necessary and identify by block number)

This effort provides image processing systems, such as the RADC AFES (Automatic Feature Extraction System) and MIES (Multi-Imagery Exploitation System) testbeds an increased capability for discriminating tactical targets from the surface background in thermal infrared (IR) imagery. This investigation presents theories of the thermal emissivity and reflectivity of natural surfaces and applies these theories to develop a background model. This will hopefully lead to the construction of algorithms to be used as a background information filter to aid in the separation of targets from background.

20. DISTRIBUTION/AVAILABILITY OF ABSTRACT UNCLASSIFIED/UNLIMITED ☐ SAME AS RPT. ☒ OTIC USERS ☐	21. ABSTRACT SECURITY CLASSIFICATION UNCLASSIFIED
22a. NAME OF RESPONSIBLE INDIVIDUAL Randall K. Blystone	22b. TELEPHONE NUMBER (Include Area Code) (315) 330-3175 22c. OFFICE SYMBOL RADC (IRRE)

DD FORM 1473, 83 APR EDITION OF 1 JAN 73 IS OBSOLETE.

UNCLASSIFIED
SECURITY CLASSIFICATION OF THIS PAGE

TABLE OF CONTENTS

1. ABSTRACT

1.1 Objective

The objective of this effort has been to provide to image processing systems, such as the RADC AFES (Automatic Feature Extraction System) and MIES (Multi-Imagery Exploitation System) testbeds an increased capability for discriminating tactical targets from the surface background in thermal infrared (IR) imagery. The approach has been to investigate the present theories of the thermal emissivity and reflectivity of natural surfaces and to apply these theories to the development of a background model. This will hopefully lead to the construction of algorithms to be used as a background information filter to aid in the separation of targets from background.

1.2 Background

Target detection for thermal IR imagery is usually accomplished by pixel intensity thresholding routines. Hot targets (vehicles with engines running) appear as high intensity (bright) areas on IR imagery. A threshold limited detector shows all pixels above a specified intensity value as targets that have, at the time of imaging, a large temperature differential from the background. However, when a significant temperature differential is not present targets are very difficult to detect by simple thresholding.

1.3 Scope

This effort has addressed the problem of detecting targets which are close to ambient temperature. This was done by modelling the background and by using the model as a base for developing an understanding of physical processes and their variations, which will (with further work) lead to the construction of a filtering algorithm. This algorithm would be used to eliminate the background information causing any objects or targets with characteristics different from the model to stand out. We:

a. Investigated theories of emissivity and reflectivity of natural surfaces and determined which would best fulfill this effort's objective.

b. Adapted chosen theory to an imagery format.

c. Developed a simple model which simulates the emissivity and reflectivity of natural surfaces, leading to an understanding of the physical factors (and their variations) controlling the remote sensing process.

d. Developed an algorithm for the model, to study major remote sensing variables and their random and systematic variations, so that advances may be made towards developing an optimum parametric envelope for data acquisition and analysis.

e. Made recommendations for further relevant work.

f. In this initial examination of the problem we were forced by lack of data and by funding and time constraints to make the following assumptions for numerical calculations:

(i) goniometric isotropy of the target and background emissivities.

(ii) spectral invariance of the emissivity of ground target and background materials.

(iii) transmission through a homogeneous atmosphere, using typical published data.

(iv) zero atmospheric self-radiance

Further work is needed in which improved simulation models are used. Indeed, an end-to-end simulation of the remote sensing process is needed. It is necessary to consider the interaction of sensor point spread function with the heterogeneous field of view: something which was not possible in this project.

2. INTRODUCTION

Thresholding as a technique for target detection, identification and tracking and possibly for target quantification is of limited use. It is a technique which is not suitable for situations where the target differs by only small temperature differences from the background and for situations where both the target and the background show variations in radiance which can approach or exceed the differences between the mean values of the temperatures of the target and of the background. Under such situations, neither thresholding nor (probably) any other form of conventional signal processing can be useful in contrast enhancement or in target extraction.

One purpose of this study has been to concisely and clearly state the established principles which govern the detectability of different targets from each other and from their backgrounds in order to better understand factors determining the parametric envelope for optimum data acquisition and extraction. The reasons for this approach will become clear later in the report.

Those factors controlling the remote sensing process all need to be considered in concert, since the variance in sensor output obtained when viewing the target as compared to viewing the background will depend upon the variance in each of those parameters contributing towards the sensor

output. These are, for example, target and background emissivity and their variances with angular regime and with slope, aspect, soil moisture, microclimate and with a variety of other environmental factors. Also important are the variability of atmospheric transmission in the bandpass or combination of bandpasses used to observe the target and the background; transmission (and atmospheric self radiance) including the presence of scene obscurants . The interaction of the spectral radiance from the target with the spectral response of the sensor will be important in determining sensor output. The polarization of the radiance from the target and its interaction with the atmosphere (depolarizing effect due to multiple scattering) and with the inherent polarization of the sensor will be important in determining sensor output. Sky radiance will be an additional factor in determining composite sensor signal output.

In the case of a heterogeneous scene, consisting of a number of scene elements, each of which has its own angular anisotropy in emissivity and in bidirectional reflectance (optical reflective regime) the point spread function of the detector or of each element of the detector (in the case of an array) will interact with the heterogeneity of the target and with the angular disposition from which it (the target) is viewed.

Sensor noise, optical effects and stray radiation within the sensing device, tracking errors, the effects of sky radiance, cross-talk between different elements of an array, the magnitude and dimensions of the point spread function and its interaction with the composite scene, consisting of a number of different scene elements will all effect the overall output signal obtained for each pixel viewed by each instantaneous field of view, and will therefore affect the accuracy with which target and background may be discriminated.

Due to the short duration of this contract, it was considered important to consider those elements most important to the development of the ideas prevalent, indeed predominant in the statement of work. To this end, classical blackbody radiation theory, published atmospheric transmission data and multivariate statistical analysis were used to determine the relative advantages of single band and two-band data acquisition techniques for target detection, tracking and quantification. To the extent that detection implies discrimination the two terms in this report will be considered to be synonymous. The effects of atmospheric self-radiance and the effects of the point spread function were not considered for reasons of time.

Mathematical analysis has been performed for single band and for band ratio techniques in order to determine the feasibility of target discrimination at low target-to-background temperature differences. The examples selected are specific to a limited range of target and background emissivities, which are considered to be Lambertian. Atmospheric transmission is considered to be uniform and to consist of certain pre-selected values taken from the literature as typical. Variances for these parameters have been selected from an examination of the literature (e.g. the Infrared Handbook [14]) and are considered to be reasonable for a first order analysis.

A literature survey of the current state of the art as reported in the unclassified literature has been performed and is included in the discussion. Conclusions may be drawn with respect to promising new avenues of research for improved target tracking and discrimination, for the development of an optimum parametric envelope for data acquisition and analysis, for optimized target detection tracking and quantification. Suggestions are made for continuation and extension of this work in related areas which we had no time to investigate in this study such as, for example, dynamic viewing using staring two-dimensional pyro-electric or quantum effect arrays using CID or CCD devices. While the reported literature shows empirical comparison and evaluation of dynamic viewing of selected targets under ideal conditions, it is considered that far

more extensive modelling studies are required in order to determine the optimum parametric envelope for using two-dimensional arrays in a dynamic viewing method of operation.

These remarks apply to nadir-pointing sensors, but will apply even more to reasonably wide angle (10 - 20 degree field of view) scanned or two-dimensional sensor systems viewing obliquely towards (say) the horizon from space or from airborne platforms , or even at ground level.

A major emphasis in this report is to point the way towards future areas in which it is recommended that research efforts be concentrated.

3. FACTORS CONTROLLING THE RELATIONSHIP OF REMOTELY SENSED RADIANCE TO GROUND FEATURES

A.0 Introduction

While there has been a consideration of the many factors affecting the remote sensing process (e.g.[1]) and a consideration of those factors affecting the selection of bandpasses for smart sensors[2,3,157] there has been little work on the effects of systematic[4-9] and of random[10,11] variations on the accuracy with which targets may be discriminated using radiance data. We shall consider here each of the factors controlling remotely sensed radiance levels, the equations describing those factors and the level of variation which may be typically anticipated to occur in

totally effective. Duggin, Schoch and Gray[64,65] showed that up to 30% of the IFOV could be filled by cloud over a typical target, before the resulting pixel would be recognized as cloud, using current NOAA AVHRR data screening algorithms. Cloud contaminated pixels, once recognized, are discarded from further analysis, since there is no accurate way to correct for cloud without making assumptions about the degree of cloud contamination of flagged pixels. A qualitative illustration of the effects of cloud contamination is to point out that areas adjacent to cloud-covered regions usually have a modified color balance on interactive computer screens. That is, such areas may be viewed as "different". However, a far more quantitative test than human viewing of an interactive computer screen is needed to delete pixels which are cloud contaminated, or are suspected of being so.

Investigations are currently underway to study the off-nadir effects of unresolved cloud and haze on target discrimination for atmospheres of different turbidity.

5.1.f. The effect of random vs. systematic errors in recorded radiance levels.

As pointed out by Duggin[66] and by Duggin, et. al[67] there are both systematic and random errors in radiance levels recorded from targets which are to be discriminated and quantified. The systematic effects may be corrected for

This follows from the general case of a mixed (heterogeneous) pixel, as shown in Table 1. Here a_A is the fraction of the instantaneous field of view (IFOV) filled by target A, while a_C is the fraction of the IFOV filled by cloud. Thus, in addition to atmospheric effects mentioned previously, opaque cloud (or haze or cirrus) can alter the absolute radiance level recorded when viewing a given target and may (depending on the spectral reflectance characteristics of the cloud) alter the spectral distribution of target radiance.

Cloud which fills only a portion of the IFOV of the detector does not result in a radiance level or in a spectral distribution in radiance recorded by several channels, which characterizes cloud. However, unresolved cloud can have the same effect as cirrus or haze, namely to distort the spectral radiance signature from the target, which is to be discriminated from its surroundings or quantified in some manner. While the photointerpreter relies upon shapes, textures, relative positions and locations as well as on color and brightness, computer classification of multispectral imagery relies only upon the digital counts recorded from the target in each sensor channel. Therefore, unresolved cloud, cirrus and haze can result in errors of omission and/or of commission if there is not some means of detecting the cloud, haze or cirrus-contaminated pixels so that they are not considered in the analysis. So far, cloud screening algorithms are not

same areas and will permit comparisons to be made between images obtained over different areas. Such corrections are necessary to permit analysis for monitoring change in ground cover over large geographic areas and will enable quantitative evaluation of temporal change in the values and in the spectral distribution of recorded radiance.

Such angle-dependent effects are systematic and may, to some extent, be corrected for. This may be achieved by parallel empirical and theoretical (modelling) studies.

B.1.e. The effect of cloud and haze.

Cloud, haze and cirrus may be present in constant or in predictably varying quantities across a scene, in which case they will modify recorded radiance as reported by Duggin, et. al [64-67]. The overall recorded radiance signature in bandpass r will be, from a given target (A) (given that the cloud is a Lambertian reflector with a spectrally invariant reflectance factor R_C).

$$NS_r = \int_{\lambda_1}^{\lambda_2} I(\lambda)\cdot\left[\left\{\int_0^{\pi}\int_0^{\pi}(a_A \times R_A(\theta,\phi;\theta',\phi',\lambda) + a_c \times R_c)\cdot E_{Scatt}(\theta,\phi,\lambda)\cdot d\theta\cdot d\phi + L_T(\theta,\phi,\lambda)\left\{a_A R_A(\theta,\phi;\theta',\phi';\lambda) + a_c R_c\right\}\right\}\right.$$

$$\left.\times \exp\left\{-\int_0^{z}\int_{-\pi}^{\pi}\int_0^{\pi}\beta'_{ext}(\theta'',\phi'',\lambda,z)d\theta''\cdot d\phi''\cdot dz\right\} + \int_{-\pi}^{\pi}\int_0^{\pi}L_{path}(\theta,\phi;\theta',\phi',\lambda)d\theta\cdot d\phi\right]\cdot d\lambda$$

$$\Big/ \int_{\lambda_1}^{\lambda_2} I(\lambda)\cdot d\lambda \qquad (3.14)$$

(3.11). $I(\lambda)$ is the spectral response of the sensing device and equation (3.12) may be more fully expressed (so that the relative importance of the abovementioned factors may be appreciated) as:

$$NS_r = \frac{\int_{\lambda_1}^{\lambda_2} I(\lambda).\left[\left\{\int_0^{\pi}\int_0^{\pi} R(\theta,\phi;\theta',\phi',\lambda).E_{scatt}(\theta,\phi,\lambda).d\theta.d\phi + L_T(\theta,\phi,\lambda).R(\theta,\phi,\theta',\phi',\lambda)\right\} \times \exp\left\{-\int_0^{z}\int_0^{\pi}\int_0^{\pi} \beta'_{ext}(\theta'',\phi'',\lambda,z).d\theta''.d\phi''.dz\right\} + \int_0^{\pi}\int_0^{\pi} L_{path}(\theta,\phi;\theta',\phi',z)d\theta.d\phi\right] d\lambda}{\int_{\lambda_1}^{\lambda_2} I(\lambda).d\lambda} \qquad (3.13)$$

Here the sensor view and azimuth angles are θ' and ϕ'.

Not surprisingly, it has been shown that there is a significant dependence of recorded digital radiance levels on sun-target-sensor geometry [4-9] for the NOAA AVHRR, SPOT and MSS data [4]. There are indications [63] that this is also true for thematic mapper (TM) data. Empirical understanding of the dependence of recorded radiance on scan angle, season (solar declination) and latitude should lead to an approximate correction for these parameters, permitting radiometric comparisons (and therefore classifications on the basis of radiance levels) across images. Such corrections will also permit quantitative comparisons to be made between images obtained at different seasons over the

There are "zero power wavelengths" (λ_1, λ_2) which bound each sensor bandpass, and at which the response of the sensor is zero. However, between these wavelength limits, the response of the detector is not constant. Since the target radiance and the atmospheric transmission and path radiance also vary (each in a different manner) across each bandpass, interactions between the spectral response of the sensor, the spectral radiance from the target, the spectral backscatter from the atmosphere and the spectral extinction of the atmosphere along the path from the target to the sensor may be anticipated. This has been pointed out by Slater[59,60] and by Duggin, et. al [10,61,62].

The signal output of the sensor (normalized sensor response) is given by the equation:

$$NS_r = \frac{\int_{\lambda_1}^{\lambda_2} I(\lambda) . \left\{ L_D(\theta,\phi;\theta',\phi',\lambda) \right\} . d\lambda}{\int_{\lambda_1}^{\lambda_2} I(\lambda) . d\lambda} \qquad (3.12)$$

where $L_D(\theta,\phi;\theta',\phi',\lambda)$, the spectral radiance incident on the sensor is due to radiance reflected from the target for the sun-target-sensor geometry considered, after modification for the spectral extinction along the atmospheric path from the target to the sensor, plus the added spectral atmospheric backscatter (path radiance) for the same target-sensor-geometry as considered in equations (3.10) and

where $\sigma'_{ext}(\theta'', \phi'', \lambda, z)$ is the extinction coefficient at altitude Z along the path to the sensor and $L_{path}(\theta,\phi;\theta',\phi',\lambda)$ is the path radiance scattered into the sensor by the atmosphere in addition to radiance transmitted from the target at ground level.

It may be readily seen that the contrast in recorded radiance between two targets is reduced by both atmospheric extinction and by the addition of a background radiance level (e.g. ref.[50], pg. 206). The reason for this is that the level of useful signal is reduced by the atmosphere, while there is an addition of purely atmospheric signal which contains no useful information.

Some correction can be made for path radiance and for atmospheric extinction. However, methods currently used assume that the atmosphere is constant across the imaged area (e.g. [45]). Further, either approximations are made in that all signal from low albedo areas is supposed to arise from the atmosphere (e.g. [45]) or several meteorological inputs are required in order to compute the modelled corrections (e.g. [43]).

B.1.d. The effect of the detector.

The response of the detector is wavelength-dependent across those bandpasses to which it is sensitive. In other words, it is not either "on" or "off", depending upon wavelength. This is illustrated in Figs. 9 and 10.

goniometric hemispherical-directional reflectance factors[55-58]. Variations in global irradiance across an imaged area will also occur due atmospheric transmission fluctuations (that is, variations in time at a given location will be similar to variations with space at a given instant in time). Radiance from the ground will also be modified by the atmosphere, prior to detection.

B.1.c. The passage of reflected target radiance to the detector.

Radiance reflected from the target may be most exactly expressed by equation (3.10). However, some radiance is absorbed and scattered out of the reflected beam by the atmosphere[77 - 128]. This may be considered by using a modification of equation (3.2) allowing for the fact that extinction along the reflected path may differ from extinction along the path of the incident radiance falling on the target. Fig. 8 explains this relationship. Thus, the radiance falling on the detector is given by:

$$L_D(\theta,\phi;\theta',\phi',\lambda) = L_R(\theta,\phi;\theta',\phi',\lambda)\cdot\exp\left[-\int_0^z\int_{-\pi}^{\pi}\int_0^{\pi}\beta'_{ext}(\theta'',\phi'',\lambda,z)\cdot d\theta''\cdot d\phi''\cdot dz\right]$$

$$+\int_0^{\pi}\int_0^{\pi}L_{path}(\theta,\phi;\theta',\phi',\lambda)d\theta\cdot d\phi \qquad (3.11)$$

The relationship between incident, reflected and absorbed radiance is shown in Fig. 7. As pointed out by, for example, Kriebel [19] and by Kirchner, et al [52], it is the interaction of the polar distribution of the spectral irradiance field with the bidirectional spectral reflectance factor which determines the angular distribution (and the absolute value at any given angular orientation) of spectral reflected radiance. Thus, equation (3.9) may be more exactly expressed as:

$$L_R(\theta',\phi',\lambda) = \int_0^{\pi} \int_0^{\pi} R(\theta,\phi;\theta',\phi',\lambda) \cdot E_{scat}(\theta,\phi,\lambda) \cdot d\theta \cdot d\phi$$

$$+ L_T(\theta,\phi,\lambda) \cdot R(\theta,\phi;\theta',\phi',\lambda) \qquad (3.10)$$

where $R(\theta,\phi;\theta',\phi')$ is the bidirectional reflectance factor[53].

Thus, while equation (3.9) describes the spectral radiance reflected into a given direction, as a function of overall irradiance level, equation (3.10) takes into consideration the polar distribution of the incident spectral irradiant flux field.

It has been shown (e.g. [10,11,19,52]) that the scalar global spectral irradiance and its polar distribution are time-dependent. Therefore, both the scalar value and the polar distribution of this quantity may vary between sequential ground measurements of target radiance and irradiance, giving errors in estimates of spectral

The radiance reflected into any polar direction may be expressed as:

$$L_R(\theta',\phi',\lambda)=R(2\pi;\theta',\phi',\lambda)\cdot E(\theta,\phi,\lambda) \qquad (3.9)$$

where $R(2\pi;\theta',\phi'\lambda)$ is the hemispherical-directional spectral reflectance factor [53], which relates the spectral radiance reflected into any selected direction (selected by the scan angle and by the ground track of the sensor platform) to the total scalar (global) spectral irradiance. The angular notation used is shown in Figs. 4 and 5.

There can be considerable angular anisotropy in the spectral hemispherical-directional reflectance factor. Indeed, a polar plot of this factor generally produces a non-spherical surface, whose irregularity is indicative of the degree of angular anisotropy in the spectral bidirectional reflectance factor. Experimental evidence of such anisotropy has already been widely published (e.g. [26-36]): furthermore, theoretical calculations indeed predict such anisotropy (e.g. [20 - 25]) in a manner which has been experimentally confirmed (e.g. [28, 54]). Fig. 6 shows the variation of the bidirectional reflectance factor with wavelength and scan angle for wheat at a growth stage of 3.5 on the modified Feeks scale, calculated from published data [27,36, 70]. The solar azimuth and zenith angles are taken to correspond to those for the NOAA-6 advanced very high resolution radiometer (AVHRR).

where

h = altitude (km)

σ_r = Rayleigh scattering cross section (m^2)

n_r = atmospheric number density (m^{-3})

n_p = aerosol number density (m^{-3})

A_v = ozone absorption coefficient (cm^{-1})

D_3 = ozone concentration ($cm\ km^{-1}$).

B.1.b. The reflection of radiance from the target.

The situation at the target is shown in Fig. 3. The total resolved component of radiance falling perpendicularly on the surface is shown as the scalar quantity $E(\lambda)$. This quantity will depend upon the solar zenith angle , upon the various atmospheric extinction coefficients and upon the amount and polar distribution of cloud ([8-11,19,50-52]).

There will be some energy which will be absorbed by the ground target. This is $E_{abs}(\theta',\phi',\lambda)$ and will depend upon polar direction, since there will probably be angular anisotropy in the absorbing properties of the ground.

The energy reflected in a given polar direction will be $L_R(\theta', \phi', \lambda)$. There will be a net balance as given by the equation:

$$E(\lambda) = \int_0^{\pi} \int_0^{\pi} L_R(\theta',\phi',\lambda)\cos\theta' \cdot d\theta'\, d\phi' + \int_0^{\pi} \int_0^{\pi} E_{abs}(\theta'_1,\phi'_1,\lambda)\cos\theta' \cdot d\theta'_1 \cdot d\phi'_1 \qquad (3.8)$$

where $\beta_{ext}(\theta'',\phi'',\lambda,z) = \beta_r(\theta'',\phi'',\lambda,z) + \beta_p(\theta'',\phi'',\lambda,z) + \beta_3(\theta'',\phi'',\lambda,z)$ (3.3)

Here $\beta_{ext}(\theta'',\phi'',\lambda,z)$ is the total extinction coefficient

$\beta_r(\theta'',\phi'',\lambda,z)$ is the coefficient for Rayleigh scattering.

$\beta_p(\theta'',\phi'',\lambda,z)$ is the coefficient for aerosol scattering.

$\beta_3(\theta'',\phi'',\lambda,z)$ is the coefficient for ozone absorption.

The total irrradiance on the target at wavelength λ is given by the sum of the radiance from the sun's disk $L_T(\theta,\phi,\lambda)$ and the irradiance from the sky (scattered radiation), see Figs. 2 and 3.

$$E(\lambda) = L_T(\theta,\phi,\lambda)\ \mathrm{Cos}\ \theta + \int_0^{\pi}\int_0^{\pi} E_{scatt}(\theta,\phi,\lambda)\ \mathrm{Cos}\ \theta\ d\theta.d\phi \qquad (3.4)$$

Here $E(\lambda)$ is a scalar quantity; while $E_{scatt}(\theta,\phi,\lambda)$ is a polar vector which represents the scattered radiance from each point in the sky. Integration of the component $E_{scatt}(\theta,\phi,\lambda)$ over the hemisphere of the sky gives a scalar quantity which represents the total "sky" irradiance. $L_T(\theta,\phi,\lambda).\mathrm{Cos}\ \theta$ is the resolved component of the radiance from the solar disk which falls perpendicular to the ground.

Approximate values for the extinction coefficients, in terms of readily measured physical quantities are given by (e.g.) Slater[50].

$$\beta_r(h) = \sigma_r n_r(h) \times 10^3 \qquad (3.5)$$

$$\beta_p(h) = \beta_p(0).\frac{n_p(h)}{n_p(0)} \qquad (3.6)$$

$$\beta_3(h) = A_v D_3(h) \qquad (3.7)$$

B.1 The optical-reflective region of the spectrum

In the optical-reflective region, we shall consider the remote sensing process in three parts; the passage of radiant energy from the sun to the target, the reflection of energy by the target and the interaction of the atmosphere with reflected radiance before it reaches the sensor.

B.1.a. The passage of radiant energy to the target.

Fig. 2 shows the passage of solar radiance through the atmosphere to the target on the ground. The solar zenith and azimuth angles are determined by the local time, season (solar declination δ) and latitude ϕ. In fact, the solar zenith angle θ is given by the equation:

$$\text{Cos } \theta = \text{Sin } \phi.\text{Sin } \delta + \text{Cos } \phi.\text{Cos } \delta \text{ Cos } 15 \left(TH + \frac{TM}{60} - SLN\right) \quad (3.1)$$

where TH is the local time in hours, TM the local time in minutes and where SLN is solar noon, the time at which the sun crosses the meridian.

Losses from the radiant beam from the sun's disk occur due to scattering and absorption. Broadly, the radiance reaching the target along the direct beam from the sun's disk is (e.g. [50]).

$$L_T(\theta,\phi,\lambda) = L_0(\theta,\phi,\lambda) \left\{ \exp\left[- \int_0^Z \int_0^{\pi} \int_0^{\pi} \beta_{ext}(\theta'',\phi'',\lambda,z).d\theta''.d\phi''.dz \right] \right\} \quad (3.2)$$

effect of the atmosphere, in order to correct for it (e.g. [17,37-49]). Such models generally assume that the atmosphere is not turbulent, but rather consists of a series of steady-state, layered media, with discrete and constant aerosol, molecular and particle concentrations.

Before dealing with variations in these quantities, we must quantitatively describe the entire remote sensing process in an overall manner as outlined by (e.g.) Maxwell[1].

some of those factors (on the basis of what very limited experimental data exists). The effect of such variation on recorded radiance levels, on target discrimination and quantification, on system design and on data collection and analysis optimization will be considered.

B.0 Discussion

The interactions occurring between solar radiance incident on the top of the atmosphere, the atmosphere, the ground and the sensor are shown broadly in figure 1. It is seen that solar radiance (L_o) incident on the top of the earth's atmosphere is subject to losses in each polar direction (θ, ϕ) caused by scattering ($L_s(\theta, \phi)$) and absorption ($L_a(\theta,\phi)$) (e.g. [13-19]) during its passage through the atmosphere. The total energy which reaches the earth's surface is given by the sum of the radiance from the solar disk, plus the energy scattered from the sky to the earth's surface (diffuse irradiance or "sky radiance"). The earth's surface reflects radiation in an anisotropic manner, which has been described analytically [20-25] and which has been observed experimentally (e.g. [26 - 36]). The radiance reflected from a ground target into the direction of the sensor is again subject to scattering and absorption. Some radiance reflected from adjacent target areas is scattered into the reflected beam and radiance is scattered from the atmosphere into the sensor ("path radiance" or "backscatter"). Models have been developed to describe the

empirically, using regression equations developed by studying a large volume of data [6,68]. However, the nature of random errors prevents their correction. The best that may be achieved is to determine the magnitude of the random errors and to determine their effect upon feature identification and quantification [10]. The effects on sensor output of random and systematic errors in various remote sensing variables are shown in flow-chart form for the optical-reflective part of the spectrum in Fig. 11 and for the thermal infrared region in Fig. 12.

Thus, in the event that two targets, A and B are to be discriminated and there is no visible cloud in the sky, then the radiance difference needed to perform a discrimination with 95% confidence would be given by the expression [11]:

$$HW\left\{(\bar{L}_A) - (\bar{L}_B)\right\} = \frac{t_{0.5,m-1}}{\sqrt{m}}\left\{(\sigma_{LL})_A + (\sigma_{LL})_B\right\}^{1/2} \qquad (3.15)$$

where H.W. denotes half the width of the 95% confidence interval on the difference $(\bar{L}_r)_A - (\bar{L}_r)_B$ and where $(\bar{L}_r)_A$ and $(\bar{L}_r)_B$ are the mean radiance values in bandpass r from targets A and B. The means are obtained in each case from m pixels. $t_{0.5,m-1}$ is the student factor where (m) is the number of observations used in estimating $(\bar{L}_r)_A$ and $(\bar{L}_r)_B$. The evaluation of equation (3.15) using equation (3.14) would be complex. However, if we use the concept of hemispherical-directional reflectance, in equation (3.9) then we can obtain a simple solution from the works of

(e.g.) Davis [69], such as proposed by Duggin [66], as given in equation (3.16).

$$HW\{(L)_A - (L)_B\} =$$

$$\frac{t_{0.5,m-1}}{\sqrt{m}} \left\{ \left(a_A . R_A(z_1,\phi_1;\theta_1',\phi_1',\lambda) . \tau(\theta_1',\lambda) + a_C . R_C(\lambda) . \tau(\theta_1',\lambda) \right)^2 . \sigma_{EE} + E^2(z_1,\lambda) . R_A^2(z_1,\phi_1;\theta_1',\phi_1',\lambda) \tau^2(\theta_1',\lambda) . \sigma_{a_A a_A} \right.$$

$$+ E^2(z_1,\lambda) . R_C^2(\lambda) . \tau^2(\theta_1',\lambda) . \sigma_{a_C a_C} + E^2(z_1,\lambda) . a_A^2 . \tau^2(\theta_1',\lambda) . \sigma_{R_A R_A} + E^2(z_1,\lambda) . a_C^2 . \tau^2(\theta',\lambda) . \sigma_{R_C R_C}$$

$$+ E^2(z_1,\lambda) . \left(a_A . R_A(z_1,\phi_1;\theta_1',\phi_1',\lambda) + a_C . R_C(\lambda) \right)^2 . \sigma_{\tau\tau} + E^2(z_2,\lambda) . R_B^2(z_2,\phi_2;\theta_2',\phi_2',\lambda) \tau^2(\theta_2',\lambda) . \sigma_{a_B a_B}$$

$$+ \left(a_B . R_B(z_2,\phi_2;\theta_2',\phi_2',\lambda) . \tau(\theta_2',\lambda) + a_C' . R_C(\lambda) . \tau(\theta_2',\lambda) \right)^2 . \sigma_{EE} + E^2(z_2,\lambda) . R_C^2(\lambda) . \tau^2(\theta_2',\lambda) . \sigma_{a'_C a'_C}$$

$$+ E^2(z_2,\lambda) . a_B^2 . \tau^2(\theta_2',\lambda) . \sigma_{R_B R_B} + E^2(z_2,\lambda) . a_C'^2 . \tau^2(\theta_2',\lambda) . \sigma_{R_C R_C} + E^2(z_2,\lambda) \left(a_B . R_B(z_2,\phi_2;\theta_2',\phi_2',\lambda) + a_C' . R_C(\cdot) \right)^2 .$$

$$\left. + 2\sigma_{L_p L_p} + 2E^2(z_1,\lambda) . R_C(\lambda) . R_A(z_1,\phi_1;\theta_1',\phi_1',\lambda) . \tau^2(\theta_1',\lambda) . \sigma_{a_A a_C} + 2E^2(z_2,\lambda) . R_C(\lambda) . R_B(z_2,\phi_2;\theta_2',\phi_2',\lambda) . \tau^2(\theta_2',\lambda) . \sigma_{a_B a'_C} \right\}^{1/2}$$

$$\text{and } H.W.\{(\bar{L}_A)_r - (\bar{L}_B)_r\} = \int_{\lambda_1}^{\lambda_2} H.W.\{(\bar{L}_A)_\lambda - (\bar{L}_B)_\lambda\} \, d\lambda \qquad (3.16)$$

where $(z_1,\phi_1;\theta_1',\phi_1')$ describes the sun-target-sensor geometry for the group of pixels in target A and where $(z_2,\phi_2;\theta_2',\phi_2')$ describes the sun-target-sensor geometry for the group of pixels in target B. Here $\theta = z$.

Here we refer to mean radiance differences at a specific wavelength λ, instead of across bandpass r. τ is the atmospheric transmission. Note that we assume a fraction of cloud a_c in the pixels over target A, while we assume a fraction of cloud a'_c in the pixels over target B. This formula would need to be computed for each scan angle, putting in the values for each variable relating to the appropriate sun-target-sensor geometry.

It should be noted that if we consider the radiance output from the sensor (recorded radiance rather than the radiance incident on the sensor as considered above), then for each wavelength λ equation (3.16) becomes, more fully expressed in equation (3.19) *(next page)*. These equations enable us to compute the necessary mean radiance difference between two targets for target discrimination with a 95% probability of being correct. The computation is unique to each sun-target-sensor geometry and will depend not only on the angular anisotropy of each target reflectance, but will also depend upon the angular anisotropy of the atmospheric scattering functions. The computation is also sensor-specific.

In detail, the sensor output difference Δ for m pixels obtained over each target, each partly filled by a proportion of (Lambertian) cloud would then be:

$$\Delta = \frac{\int_{\lambda_1}^{\lambda_2} I(\lambda)\cdot\bar{L}_A(\lambda)\cdot d\lambda \; - \; \int_{\lambda_1}^{\lambda_2} I(\lambda)\cdot\bar{L}_B(\lambda)\cdot d\lambda}{\int_{\lambda_1}^{\lambda_2} I(\lambda)\cdot d\lambda} \tag{3.17}$$

$$\Delta = \frac{\int_{\lambda_1}^{\lambda_2} I(\lambda)\cdot\left\{\bar{L}_A(\lambda) - \bar{L}_B(\lambda)\right\}\cdot d\lambda}{\int_{\lambda_1}^{\lambda_2} I(\lambda)\cdot d\lambda} \tag{3.18}$$

In order to be 95% confident that the two features are indeed seperable on the basis of reflected radiance using a bandpass r, whose upper and lower zero-power wavelength limits are λ_2 and λ_1, the difference must exceed the value of the following function:

$$\text{H.W.}\left\{(\bar{L}_r')_A - (\bar{L}_r')_B\right\} = \frac{\int_{\lambda_1}^{\lambda_2} \text{H.W.}\left\{I(\lambda).\bar{L}_A(\lambda) - I(\lambda).\bar{L}_B(\lambda)\right\}.d\lambda}{\int_{\lambda_1}^{\lambda_2} I(\lambda)\cdot d\lambda} \tag{3.19}$$

where H.W. $\left\{(\bar{L}_r')_A - (\bar{L}_r')_B\right\}$ is the minimum recorded radiance difference Δ necessary to be 95% confident of discrimination on the basis of sensor output. Of course, we can perform such calculations for any pre-determined confidence level.

Factors which will control the discriminability of targets, where

$$\text{Discriminability} = \text{D.F.} = \frac{\text{H.W.} \left\{ (\overline{L_r'})_A - (\overline{L_r'})_B \right\}}{|\Delta|}$$

function

as given by (e.g. Duggin [66]) are several. These effects are mentioned but have not been investigated in this study. For discrimination to be possible D.F. < 1.0.:

(i) relative areas in the IFOV occupied by unresolved cloud and by target.

(ii) atmospheric extinction and its variation (here shown as atmospheric transmission τ) for the sensor bandpasses.

(iii) variation in the relative proportions of the IFOV occupied by the target and by cloud. [64-67]

(iv) path radiance for the sensor bandpasses and its variation across the imaged area. (e.g. [64])

(v) relative albedos of the targets to be distinguished in the bandpasses used and of the cloud present in the IFOV where unresolved cloud exists. [64-66]

(vi) variations in atmospheric turbidity and the average value of this quantity across the imaged area. (e.g. [68])

(vii) The overall level and spectral distribution of global irradiance.

(viii) The spectral responses of the sensors in those bandpasses used, and the interaction of such responses with the target radiance.

(ix) random variability of the spectral bidirectional reflectance factor across the sampled area. This can be caused by (e.g.) topographic variations, textural variations, slight changes in pixel composition, etc.

(x) the dependence on sun-target-sensor geometry of the spectral bidirectional reflectance factor, spectral path radiance, spectral atmospheric extinction and target discriminability. Due to angular anisotropy of ground reflectance, it may be that discrimination of some targets is optimal (target/background contrast is maximum) at certain angular regimes (i.e. at certain solar elevations and azimuths and at certain, possibly off-nadir view angles).

(xi) The interaction of the point-spread function of the detector with the heterogeneity of the pixel, consisting of different scene components. This point is made clear in Fig. 13. Here, the point-spread function of the sensor is shown superimposed upon a nominal pixel (projection of the defined earlier (IFOV) on the ground) containing several different scene

elements. Each scene element will have its own, different angular spectral reflectance and emissivity anisotropy and so the movement of the sensor such that the IFOV is shifted by a fraction of a pixel will produce a considerable change in sensor output. This important point has so far received very little attention.

An example [66, 67] of the effects of scan angle, unresolved cloud and atmospheric turbidity on contrast ratio is shown in Figs. 14 (clear atmosphere: meteorological range > 50 km) and 15 (turbid atmosphere: meteorological range < 10 km). Here vegetated targets (70% wheat, 30% soil) and 100% wheat at a growth stage of 3.5 on the modified Feeks scale (boot stage) are considered. In each case, a vegetative index (VIN) is used to typify the target: the VIN used is the radiance recorded in AVHRR band 2 (0.713-0.986 μm; reflected infrared) divided by the radiance recorded in AVHRR band 1 (0.570-0.686 μm; visible). Three facts emerge: firstly the contrast ratio (VIN_{MAX}/VIN_{MIN}) is greatly reduced by unresolved cloud (and therefore by haze and cirrus). Secondly, the contrast ratio is scan angle dependent. Thirdly, the contrast ratio is reduced in a scan angle-dependent manner by unresolved cloud for a turbid (meteorological range < 10 km) atmosphere as compared to a clear (meteorological range > 50 km) atmosphere.

B.2. THE THERMAL INFRARED REGION OF THE SPECTRUM

Evidence exists to snow that there is angular anisotropy of the emissivity of ground targets [71-76]. In the case of emitted thermal radiance, atmospheric attenuation consists principally of absorption, so that equation (3.10) should be re-written, for emitted thermal infrared radiance at ground level, as:

$$L_R(\theta',\phi',\lambda) = \varepsilon(\theta',\phi',\lambda).\ W(T,\lambda) \qquad (3.20)$$

where $\varepsilon(\theta',\phi',\lambda)$ is the directional radiant spectral emittance and $W(T,\lambda)$ is the spectral radiant exitance of a blackbody at temperature T (degrees Kelvin). The assumption here is that the radiator is a graybody.

Therefore, in the case of emitted thermal radiance, the equivalent equation to the optical-reflective equation (3.11) is:

$$L_D(\theta',\phi',\lambda) = L_R(\theta',\phi',\lambda).\exp\left\{-\int_0^Z \int_{-\pi}^{\pi} \int_0^{\pi} \beta'_{ext}(\theta'',\phi'',\lambda,z)\, d\theta''.d\phi''.dz\right\}$$

$$+ L_{sky}(\theta',\phi',\lambda) \qquad (3.21)$$

Here, it is assumed that the predominant atmospheric effect is absorption, e.g. [77-89, 95, 96, 100, 103]. There is also an atmospheric self radiance term:

$$L_{sky}\ (\theta',\phi',\lambda)$$

This situation is illustrated by Fig. 16.

The interaction of this spectral thermal radiance with the detecting device is given by the expression for the recorded radiance NS_r.

$$NS_r = \frac{\int_{\lambda_1}^{\lambda_2} I(\lambda)\ \left[\varepsilon(\theta',\phi',\lambda)\cdot W(T,\lambda)\cdot \exp\left\{-\int_0^z -\int_{\pi}^{\bar{\pi}} \int_0^{\pi} \beta'_{ext}(\theta'',\phi'',\lambda)\cdot d\theta''\cdot d\phi''\cdot dz\right\} + L_{sky}\ (\theta',\phi',\lambda)\right]\cdot d\lambda}{\int_{\lambda_1}^{\lambda_2} I(\lambda)\cdot d\lambda} \qquad (3.22)$$

Equations (3.15) and (3.16) would also be different, of course, for the thermal infrared case than for the optical reflective case. Here, we ignore the (generally trivial) covariance terms.

$$HW\left\{L(\lambda)_A - L(\lambda)_B\right\} = \frac{\tau_{.05,m}}{\sqrt{n}} \left\{\left(\varepsilon_A^2(\theta',\phi',\lambda)\cdot S_{\tau\tau} + \tau^2(\theta',\phi',\lambda)\cdot S_{\varepsilon_A\varepsilon_A}\right)\cdot W(T_A,\lambda) + \left(\varepsilon_B^2(\theta',\phi',\lambda)\cdot S_{\tau\tau} + \tau^2(\theta',\phi',\lambda)\cdot S_{\varepsilon_B\varepsilon_B}\right)\cdot W(T_B,\lambda) + 2\, S_{L_{sky}L_{sky}}\right\}^{\frac{1}{2}} \quad (3.23)$$

where $S_{\tau\tau}$, $S_{\varepsilon_A\varepsilon_A}$, $S_{\varepsilon_B\varepsilon_B}$ and $S_{L_{sky}L_{sky}}$ represent sample variances in atmospheric transmission, emissivity of target A, emissivity of background B and sky radiance L_{sky}. Atmospheric transmission τ is given by

$$\tau = \exp\left\{-\int_0^z \int_{-\pi}^{\pi} \int_0^{\pi} \beta'_{ext}(\theta'',\phi'',\lambda)\, .d\theta''.d\phi''.dz\right\}$$

More discussion will be made of this derivation later.

Equation (3.23) could then be substituted into equations (3:18) and (3.19) to determine the value of a discriminability function (DF) such that:

$$D.F. = \frac{HW\left\{(\bar{L}')_A - (\bar{L}')_B\right\}}{|\Delta|} \quad (3.24)$$

and D.F. must always be less than 1, for discrimination of target from background with a 95% (or some other predetermined level) of confidence.

The well-known physical factors controlling the remote sensing process have been discussed and represented in relevant form in this section. The relative importance of some already reported random and systematic variations on recorded radiance and on target discriminability and contrast have also been discussed. These factors need to be borne in mind when designing instrumentation or when optimizing imaging conditions.

Assuming that the wavelengths for the bandpasses used by the sensing device have been best chosen for the task at hand, (and this has been the case only so far as is possible with limited data) it is possible that discrimination of the target will be more effective for some sun-target-sensor geometries than for others. It is also likely that there are upper limits for unresolved cloud, haze, obscurants and cirrus for which discrimination of targets of different, selected albedos is possible. In order to understand the principles controlling both the systematic and random variations discussed above, which control the accuracy with which selected targets may be discriminated, it is necessary to use both empirical and mathematical simulation studies for the atmosphere, [37-49, 90-128] for sensing devices, [2,3, 5-10,14,59-62,136,164,241-266] and for the variability of recorded radiance and its effect on contrast [10-12,204-240].

In order to test and calibrate the mathematical models it is necessary to have sufficient measurements of the reflectance factors and emissivity of the earth's surface at various angular geometries. Unfortunately, few such data currently exist and there is little agreement on the methods by which such critical data should be obtained.

While it is necessary to be pragmatic regarding the best use of existing data, it is suggested that few advances in sensor design, in data collection optimization or in an understanding of the effects of random and systematic errors on target discriminability will be possible until theoretical studies are performed to parallel present experimental studies to increase our understanding of those factors discussed above. Only such studies will make possible the collection and analysis of digital multispectral radiance data so as to minimize errors of omission and comission in automated or semi-automated analysis.

4. SENSORS

Sensing devices can consist of either scanners, pushbroom array devices or staring arrays [129-203, 261-286]. The scanner has the advantage of utilizing a limited number of detectors whose spectral response and point spread function may be relatively well known (although this is apparently not the case for (e.g.) the Landsat Multi-

spectral scanner (MSS). Neither the MSS, nor the TM had documented inherent polarization measurements performed, nor was the spectral response of each of the channels of each of the bands on these devices well documented in the open literature. (e.g. [59-62])

As discussed in section 3, the point spread function of a sensor means that the central portion of the IFOV, has a higher sensitivity than the outermost portions of the IFOV. For a heterogeneous field of view or for a target which does not completely fill the field of view, the position of a small (sub-pixel sized) target with respect to the peak of the point spread function is therefore obviously important. This fact appears so far to have received relatively little attention and it is recommended that more work is needed here. Pushbroom scanners may consist of a single array of sensors which obtains information in one spectral bandpass or may consist of a two-dimensional detector array placed behind a wedge interference filter where the axis perpendicular to the ground track obtains spatially varying information from different pixels and the axis alongtrack obtains information in different wavebands. Such a device clearly entails considerable problems in so far as high data rates involved, coupled with varying instrument spectral responses between detectors, varying filter transmissions in front of each of the sensing elements, absolute detector calibration variation from element-to-element and

spheric transmission was allowed to vary from 0.8 to 1.00 in increments of 0.02. For band 2 (11.0 - 12 μm) the atmospheric transmission was allowed to vary from 0.60 to 1.00 in increments of 0.04. This resulted in a range of ratios (τ_2/τ_1). The coefficients of variation in both τ_1 and τ_2 was allowed to vary from 0.01 to 0.05 in 0.01 increments which was an estimate based upon the literature.

The discrimination function (D.F.) described in equation (5.19) was plotted as a function of the relative atmospheric transmissions τ_1 and τ_2 in the two bandpasses used and as a function of the temperature of the target T_A. The target temperature was allowed to vary from 265° K to 285° K in one degree increments. The background temperature was always 275° K. The target was assumed to have a spectral invariant emissivity. Examples of the three-dimensional plots are shown in Figs. C1 to C3. The vertical axis is DF, while the horizontal axes are the ratio (τ_2/τ_1) of the atmospheric transmissions in the two bands used and the target temperature T_A. Fig. C1 shows the case where the correlation coefficients between the recorded radiances is 0.01, while the coefficient of variation in each of the atmospheric transmission values τ_1 and τ_2 for bands 1 and 2 is 0.01. Fig. C2 shows a case which is identical, except that the coefficients of variation for τ_1 and τ_2 are 0.05: clearly the increased variation in atmospheric transmission reduces the discriminability (i.e. increases D.F.) for any given temperature. The D.F. is relatively insensitive to τ_2/τ_1 in either case.

Similarly, for target B:

$$S_{RR_B} = \left(\frac{BB_{22}}{BB_{21}}\right)^2 \cdot \left(\frac{\varepsilon_{B_2}}{\varepsilon_{B_1}}\right)^2 \cdot \left(\frac{\tau_2}{\tau_1}\right)^2 \cdot S_{\tau_1\tau_1} + \left(\frac{BB_{22}}{BB_{21}}\right)^2 \cdot \left(\frac{\varepsilon_{B_2}}{\varepsilon_{B_1}}\right)^2 \cdot \left(\frac{1}{\tau_1}\right)^2 \cdot S_{\tau_2\tau_2}$$

$$2\left(\frac{BB_{22}}{BB_{21}}\right)^2 \cdot \left(\frac{\varepsilon_{B_2}}{\varepsilon_{B_1}}\right)^2 \cdot \left(\frac{\tau_2}{\tau_1^2}\right) \cdot \left(\frac{1}{\tau_1}\right) \cdot \ldots \cdot \left(S_{\tau_2\tau_2} \cdot S_{\tau_1\tau_1}\right)^{\frac{1}{2}} \qquad (5.18)$$

where BB_{21} is the blackbody radiant emittance from background B in band 1 and BB_{22} is the blackbody radiant emittance from blackbody B in band 2.

The discrimination function D.F., which must be less than 1.00 for discrimination of target from background using the recorded radiance ratios $R_A = L_{A_2}/L_{A_1}$ and $R_B = L_{B_2}/L_{B_1}$ at the 95% confidence level (equation 5.13) is given by:

$$D.F. = \frac{\left(\frac{t_{0.5,m-1}}{\sqrt{m}}\right)\left\{\left(S_{RR}\right)_A + \left(S_{RR}\right)_B\right\}^{\frac{1}{2}}}{\left|\left(S_{RR}\right)_A - \left(S_{RR}\right)_B\right|} \qquad (5.19)$$

Calculations of D.F. were made and tabulated. Here, as for the single band calculations, samples of 20 pixels were assumed to exist in the target and in the background areas. For bandl (3.5-4.1μm) the atmos-

Starting from this point, we may use arguments similar to those embodied in equations (5.7) and (5.8) to deduce that the major contribution to the variance in the ratio between bands 1 and 2 of the radiance from target A may be attributed to atmospheric transmission variation.

That is,

$$R_A = \frac{L_{A_2}}{L_{A_1}} = \frac{BB_{12} \cdot \varepsilon_{A_2} \cdot \tau_2}{BB_{11} \cdot \varepsilon_{A_1} \cdot \tau_1} \qquad (5.15A)$$

$$S_{RR} = \left(\frac{\partial R}{\partial \tau_1}\right)^2 \cdot S_{\tau_1\tau_1} + \left(\frac{\partial R}{\partial \tau_2}\right)^2 \cdot S_{\tau_2\tau_2} + 2\rho \left(\frac{\partial R}{\partial \tau_1}\right) \cdot \left(\frac{\partial R}{\partial \tau_2}\right) \cdot \left(S_{\tau_2\tau_2} \cdot S_{\tau_1\tau_1}\right)^{\frac{1}{2}} \qquad (5.16)$$

since the variation in ε_{A_2} and in ε_{A_1} is such that $\frac{\varepsilon_{A_2}}{\varepsilon_{A_1}}$ is always constant and since BB_{12} and BB_{11} are physical constants which depend only on blackbody temperature. We may obtain an estimate of the sample variance in the radiance ratio for target A:

$$(S_{RR})_A = \left(\frac{BB_{12}}{BB_{11}}\right)^2 \cdot \left(\frac{\varepsilon_{A_2}}{\varepsilon_{A_1}}\right)^2 \cdot \left(\frac{-\tau_2}{\tau_1^2}\right)^2 \cdot S_{\tau_1\tau_1} + \left(\frac{BB_{12}}{BB_{11}}\right)^2 \cdot \left(\frac{\varepsilon_{A_2}}{\varepsilon_{A_1}}\right)^2 \cdot \left(\frac{1}{\tau_1}\right)^2 \cdot S_{\tau_2\tau_2}$$

$$+ 2\left(\frac{BB_{12}}{BB_{11}}\right)^2 \cdot \left(\frac{\varepsilon_{A_2}}{\varepsilon_{A_1}}\right)^2 \cdot \left(-\frac{\tau_2}{\tau_1^2}\right) \cdot \left(\frac{1}{\tau_1}\right) \cdot \rho \cdot \left(S_{\tau_2\tau_2} \cdot S_{\tau_1\tau_1}\right)^{\frac{1}{2}} \qquad (5.17)$$

Further modelling calculations were performed on the ratio of the radiance from the target, compared to that from the background in two different bands. That is, the ratio:

$$\frac{L_{A_2}}{L_{A_1}} = \frac{B_{12}}{B_{11}} \cdot \frac{\varepsilon_{A_2}}{\varepsilon_{A_1}} \cdot \frac{\tau_2}{\tau_1} \qquad (5.15)$$

where L_{A_2} is the radiant emittance from target A in band 2 (11.0-12.0 μm) and L_{A_1} is the radiant emittance from target A in band 1 (3.5-4.1 μm). B_{12} is the blackbody radiant exitance from target A in band 2 while B_{11} is the blackbody radiant exitance from target A in band 1.

If ε_{A_1} and ε_{A_2} are the average emissivities of the target A in bands 1 and 2, then, from the work of (e.g.) Maxwell[302] it is reasonable to assume that there is little wavelength dependence of the emissivities, so that;

$$\frac{\varepsilon_{A_2}}{\varepsilon_{A_1}} = 1.0 \text{ (approximately)}$$

Further variations in ε_{A_2} will be very strongly correlated to those in ε_{A_1}, so that the ratio;

$$\frac{\varepsilon_{A_2}}{\varepsilon_{A_1}}$$

will change very little with variations in ε_A: the same reasoning may be applied to the emissivity of target B.

Three graphs are shown of the same calculations at different rotations, in order to best present detail. Like calculations were performed for the 11.0-12.0 μm bandpass. Examples of these calculations are shown in Figs. B1 to B6. Figures B1 through B3 show calculations of D.F. as a function of (T_A, ($1 - \varepsilon_A$)) at different rotations about the vertical (D.F.) axis where $\tau = 1.00$ and $\varepsilon_B = 0.90$. Figs. B4 through B6 show similar calculations, with like rotations about the D.F. axis, for $\tau = 0.60$ and $\varepsilon_B = 0.85$. The D.F. peaks where target and background emissivities are similar, especially at target temperatures close to that of the background, as one would expect. However, discrimination of target from background with even turbid, variable atmospheric transmission and with variable target and background emissivities appears possible, for some circumstances even with temperature differences as small as 1 degree Kelvin. The three-dimensional plots show the interactive effect of target-to-background emissivity contrast and temperature differences, for different atmospheric transmissions. As expected, the higher atmospheric turbidity and higher atmospheric variability yielded a larger D.F.. Where the temperatures and emissivities of target and background were similar discrimination was impossible. The variation of the recorded exitance would cause blurring of the characteristic radiant exitance vs. wavelength curves for both target and background. The closer the emissivity values, the closer (and less seperable) the curves.

In calculations performed, the covariance term was always small. The target temperature was allowed to vary at 1 degree K increments from 265K to 285K . The background temperature was always taken to be 275K . The target emissivity was allowed to vary at 0.10 increments from 0.05 to 0.95. The emissivity of the background was taken to be 0.85 and (in a separate run) 0.90. Atmospheric transmission was taken to be 0.60 to 1.00 in 0.10 increments. The coefficient of variation (standard deviation divided by the mean) for the emissivities was taken to be 0.05, while that of the atmospheric transmission was taken to be 0.05 also. Selected examples of the results of these comprehensive calculations for the bandpass 3.5-4.1 μm are shown in Figs. A1 to A6. For each data plot, the discrimination function (D.F.) is shown as the vertical axis, while the two horizontal; mutually orthogonal axes are target temperature (T_A)(temperature of background (T_B) always assumed equal to 275K) and ($1 - \varepsilon_A$). Figs. A1 through A3 show, for different rotations about the vertical (D.F.) axis, the value of D.F. plotted as a function of (T_A, ($1 - \varepsilon_A$)). For these calculations ε_B = 90 and atmospheric transmission τ = 1.00. Figs. A4 through A6 show similar calculations, with like rotations about the D.F. axis, for τ = 0.70 and ε_B = 0.85. Each plot of D.F. as a function of (T_A, ($1 - \varepsilon_A$)) is plotted for selected constant background emissivity and atmospheric transmission values.

Now, as discussed in section 3, the half-width of the 95 percent confidence interval (or of any other pre-selected confidence interval) on the mean radiance difference from samples of pixels taken over target and background must be greater than the difference in the mean radiance levels (for the bandpass used).

$$\text{i.e.} \qquad \text{D.F.} = \frac{\text{H.W.} \left\{ \bar{L}_A - \bar{L}_B \right\}}{\left| \bar{L}_A - \bar{L}_B \right|} \qquad (5.13)$$

must be smaller than 1.0 for discrimination to occur. We considered samples of 20 pixels in computing the student t-factor $t_{0.5,m}$ for the 95% confidence interval;

$$\left(\frac{t_{0.5,m-1}}{\sqrt{m}} \right) \cdot \left\{ S_{L_A L_A} + S_{L_B L_B} \right\}^{\frac{1}{2}} = \text{H.W.} \left\{ \bar{L}_A - \bar{L}_B \right\} \qquad (5.14)$$

Thus the discrimination function (D.F.) may be calculated from equations (5.11) - (5.14).

Thus, for a single bandpass:

$$S_{L_A L_A} = \left(\frac{\partial L_A}{\partial \varepsilon_A}\right)^2 \cdot S_{\varepsilon_A \varepsilon_A} + \left(\frac{\partial L_A}{\partial \tau}\right)^2 \cdot S_{\tau\tau} + 2\left(\frac{\partial L_A}{\partial \varepsilon_A}\right) \cdot \left(\frac{\partial L_A}{\partial \tau}\right) \cdot S_{\varepsilon_A \tau} \tag{5.9}$$

$$S_{L_B L_B} = \left(\frac{\partial L_B}{\partial \varepsilon_B}\right)^2 \cdot S_{\varepsilon_B \varepsilon_B} + \left(\frac{\partial L_B}{\partial \tau}\right)^2 \cdot S_{\tau\tau} + 2\left(\frac{\partial L_B}{\partial \varepsilon_B}\right) \cdot \left(\frac{\partial L_B}{\partial \tau}\right) \cdot S_{\varepsilon_B \tau} \tag{5.10}$$

from equations (5.5) - (5.10), the sample variances in the radiance recorded from target and from background in a selected band are, respectively:

$$S_{L_A L_A} = \tau^2 \cdot BB_{1r}^2 \cdot S_{\varepsilon_A \varepsilon_A} + \varepsilon_A^2 \cdot BB_{1r}^2 \cdot S_{\tau\tau} + 2\varepsilon_A \cdot \tau \cdot BB_{1r}^2 \cdot \rho(S_{\tau\tau} \cdot S_{\varepsilon_A \varepsilon_A})^{\frac{1}{2}} \tag{5.11}$$

$$S_{L_B L_B} = \tau^2 \cdot BB_{2r}^2 \cdot S_{\varepsilon_B \varepsilon_B} + \varepsilon_B^2 \cdot BB_{2r}^2 \cdot S_{\tau\tau} + 2\varepsilon_B \cdot \tau \cdot BB_{2r}^2 \cdot \rho(S_{\tau\tau} \cdot S_{\varepsilon_B \varepsilon_B})^{\frac{1}{2}} \tag{5.12}$$

while that from the background was:

$$L_{Br} = \varepsilon_{BR} \cdot \tau_r \cdot BB_{2r} \qquad (5.6)$$

where:

ε_{Ar} = emissivity of the target A in bandpass r.

ε_{Br} = emissivity of the background B in bandpass r.

τ_r = atmospheric transmission in band r.

BB_{1r} = blackbody emissivity for the target (1) at temperature T_1.

BB_{2r} = blackbody emissivity for the background (2) at temperature T_2

It may be shown (e.g. [69, 58]) that where a dependent variable (v) is a function of two other variables (x,y), then the sample variance in the dependent variable (v) is given by:

$$S_{VV} = \left(\frac{\partial v}{\partial x}\right)^2 \cdot S_{xx} + \left(\frac{\partial v}{\partial y}\right) \cdot S_{yy} + \left(\frac{\partial v}{\partial x}\right) \cdot \left(\frac{\partial v}{\partial y}\right) \cdot S_{xy} + \text{lower order terms} \qquad (5.7)$$

Here the terms of a lower order of magnitude are generally negligible where the coefficient of variation of each of the variables x, y is less than about 0.20 and the covariance may be expressed using the well-known formula:

$$S_{xy} = \rho \cdot \left(S_{xx}\right)^{\frac{1}{2}} \cdot \left(S_{yy}\right)^{\frac{1}{2}} \qquad (5.8)$$

where ρ is the correlation coefficient between the two sample distributions.

different bandpasses.

Studies of the Infrared Handbook [14] showed that atmospheric transmission is maximum in the regions 3.5-4.1 μm and 10.0-12.0 μm. For the purposes of this study, we have, for reasons of time, restricted our attention to target discriminability in each of the bands 3.5-4.1 μm and 11.0-12.0 μm and for the ratio of the radiance recorded in these bands. We considered the effect of random variations in target and background emissivities and in atmospheric transmission on the discriminability of target from background. The case of the thermal infrared region may be seen from the general principles referred to in section 3 to be simpler than the optical-reflective region: scattering processes cause fluctuations in target illumination, with a consequent effect on target radiance fluctuation only in the optical-reflective region.

We considered first the case where a target was to be discriminated from background in each of the above-mentioned two bandpasses. Here the radiance from the target was:

$$L_{Ar} = \varepsilon_{AR} \cdot \tau_r \cdot BB_{1r} \qquad (5.5)$$

This expression may be written as:

$$M_\lambda = \frac{C_1 \lambda^{-5}}{\left\{\exp\left\{\frac{C_2}{\lambda T}\right\} - 1\right\}} \qquad (5.2)$$

where $C_1 = 2\pi hc^2$

and $C_2 = \frac{hc}{k}$

The total (i.e., integrated over the electromagnetic spectrum) radiant exitance of a blackbody is given by:

$$M_{TOT} = \frac{C_1}{C_2^4} \cdot \frac{\pi^4}{15} \cdot T^4 \quad (W m^{-2}) \qquad (5.3)$$

Of course, the quantities used in the above expressions could just as easily be expressed in c.g.s. units, so that $M\lambda$ and M_{TOT} would appear in c.g.s. units.

The in-band radiance $M_{\Delta\lambda}$ is approximately expressed as:

$$M_{\Delta\lambda} = \frac{C_1}{C_2^4} T^4 \left[\sum_{n=1}^{\infty} \cdot \frac{1}{n^4} \left\{ (n\lambda)^3 + 3(n\lambda)^2 + 6n\lambda + 6 \right\} e^{-n\lambda} \right]_{\lambda=\lambda_1}^{\lambda=\lambda_2} \qquad (5.4)$$

This expression was used to calculate tabular values of blackbody exitance for different temperatures and for

In this case, because of the broad aims of the study, it has been decided to use the assumption that the target and background act as Lambertian greybodies with almost wavelength-independent emissivities at any given wavelength. (e.g. [302]). This is a simplistic assumption. However, for first-order calculations, in the light of conversations with several researchers in the field and after a perusal of available unclassified literature, this was considered to be a reasonable starting point.

The Planck radiation law may be used to calculate the total radiant exitance of a blackbody at a selected temperature. This is shown in equation (5.1).

$$M_\lambda = \frac{2\pi hc^2}{\lambda^5} \left\{ \frac{1}{\exp\left\{\frac{hc}{K\lambda T}\right\} - 1} \right\} \qquad (5.1)$$

where M_λ is the energy radiated per unit wavelength per second, per unit area of the blackbody (W_m^{-2} $A^{0-1'}$) (radiant exitance)

h = Planck's constant (J sec^{-1})

c = speed of light (m sec^{-1})

k = Boltzmann constant (J $°K^{-1}$)

λ = wavelength

T = absolute temperature (°K)

accumulation of scene elements, each of which has its own angular anisotropy, considerable difficulty may arise in consistent target detection, discrimination, tracking and quantification, depending upon the location of the target with respect to the maximum of the point spread function of each detector element, if the target occupies less than 1 or 2 pixels. Preliminary studies have shown that there are possibilities of improving contrast enhancement by dynamic viewing or "dithering" (e.g. [282]) the two dimensional array. At present, very few studies have been reported in the unclassified literature. There is a real need to be aware of the interaction of scene heterogeneity, atmospheric transmission fluctuations, obscurants [77-89], and target aspect with the sensing device in order to be able to define the optimum parametric envelope for target discrimination, detection, tracking and quantification. Much more work appears to be needed here.

5. MODELLING STUDIES

A considerable body of theory exists for the modelling of the interaction of electromagnetic radiation with dielectric media. Generally, these models have been idealized (e.g. [14, 302-326]).

varying point spread function from detector element to detector element. However, the advantages of such a system are that it does not entail moving components such as the oscillating mirror or rotating mirror utilized in scanning devices and should therefore have enhanced reliability. It is suggested that the success of such devices will rely heavily upon the development of adequate onboard preprocessing facilities (smart sensor devices e.g. [157]).

A staring array consists of a two-dimensional matrix of either quantum detectors (such as silicon) or of pyroelectric detectors which record information in the optical reflective, mid-infrared or thermal infrared parts of the spectrum. In the case where charge coupled devices (CCD's) or charge injection devices (CID's) are utilized, most of the area occupied by the array can consist purely of sensing elements. Where the photodetectors and the circuitry involved in transferring the charge to different registers is located on a single plane, then perhaps only 50% of the "real estate" of the array element may be occupied by sensors. The disadvantages of the two-dimensional array are the same as mentioned for the multispectral pushbroom scanner. The point-spread function may look something like that shown in Figure 13 for each element of the array. There may be slight differences from element to element, and there may be slight differences in the absolute calibration (radiometrically) of each element. Thus, when a staring array views a scene consisting of a heterogeneous

Fig. C3 shows a case where the coefficients of variation for τ_1 and τ_2 are 0.05 and where the correlation coefficient between radiance recorded in the two bands is 0.90: clearly, an increased correlation between radiance recorded in bands 1 and 2 (3.5 - 4.1 and 11.0 - 12.0 μm) increases the discriminability of target from background (reduces D.F.). In general we found that as might be expected, the more variable the atmosphere, the larger D.F.. However, the discrimination function (D.F.) is generally < 1.0 where the target temperature is within 1^{o} K of that of the background.

It is significant that discrimination is independent of target/background emissivity contrast using the ratio method and that for target/background contrasts of 1^{o}K (or less) discrimination appears more probable at the 95% confidence level than for either of the single bands, for the levels of atmospheric turbidity variance considered. Thus, the ratio method would appear superior to the single-channel method and would seem to be free of the dependence on emissivity variation.

6. CONCLUSIONS, RECOMMENDATIONS AND SUGGESTIONS FOR FURTHER WORK

Here, we present the conclusions drawn from this study, plus general suggestions which one of us (MJD) has long thought necessary steps in a research program to increase the accuracy of target detection, classification, quantification and tracking.

1. The discrimination of targets from background under the selected atmospheric conditions used in the modelling calculations demonstrates the feasibility of detection for small (e.g. 1 degree Kelvin = $1^{o}C$) temperature differences. It appears that, for atmospheric transmission and ground emissivity random variations which may be expected the technique of using ratioed radiance values for the bandpasses 3.5-4.1 μm and 11.0 - 12.0 μm for reasons discussed above offers advantages over the discrimination possible using radiance data recorded in either of the single bands 3.5 - 4.1 μm and 11.0 - 12.0 μm.

2. Real time contrast enhancement using histogram stretching, geometric stretching or other contrast enhancement techniques with micro-chip technology appears to be a possibility, providing that the target occupies that portion of the instantaneous field of view (IFOV) which has the maximum point spread function: (an area which needs research). Clearly if the target is smaller than the pixel

(IFOV at ground level) then the contrast between the pixel containing the target and the pixels containing only background material will depend upon the position of the point spread function with respect to the target. This is an area which needs considerable study. It is suggested that little data exists on the point spread function of any detecting device and that little is known about improvements in contrast between target containing pixels and background pixels using dynamic viewing or "dithering" techniques. This area is a major gap in present technology and must be closed, otherwise predictable discrimination, identification and quantification of targets may not be possible.

3. The inherent polarization of detection devices is a relatively unexplored field. Work in the optical reflective region (e.g. [287-301]) shows target radiance to be polarized: studies performed in 1974 by Maxwell et al in the emitted infrared part of the spectrum [302] show polarization to exist in an angularly anisotropic manner in the thermal infrared region. Although considerable angular anisotropy in polarization differences with vertical and horizontal polarizations have been detected, little is apparently known about the interaction of such polarized scene radiance with inherent sensor polarization effects: indeed inherent polarization of detectors appears to have received little attention.

Quantitative measurements are necessary here in order to ensure predictable accuracy of targeting data. It is essential that the interaction of polarized scene radiance, the depolarizing effect of the atmosphere, the polarized sky radiance and the inherent polarization of the sensing devices be investigated to provide optimum targeting data. That is, it is essential to minimize failure to detect targets, to minimize misclassification of targets and to utilize all potentially available information to detect, quantify and track targets.

4. The possible combination of multiband approaches in which polarization effects are utilized appears attractive, since polarization differences in scene radiance or in target versus sky radiance are markedly greater in the ultraviolet part of the spectrum as compared to, for example, the emitted infrared part of the spectrum. Such considerations are, it is suggested, of vital importance in horizon and nadir-viewing sensors based on satellite or high altitude airborne platforms. They may also be of use in skytracking camera and in missile terminal guidance systems.

5. The utilization of staring sensors to detect target motion necessitates the knowledge of the point-spread function of each element of the array or of any other device which is used to image a scene. This is because a movement of less than 1 pixel in sensor pointing will change the radiometric and spectral signature from the scene because of the movement of the point-spread function with respect to the target/background composite scene.

6. The effects of scene obscurants and their interaction with elements of two-dimensional arrays needs to be further studied. Clearly, each element will have a slightly different absolute radiometric sensitivity, spectral response, inherent polarization (especially in the case of ferroelectric pyroelectric devices) and also point spread function. Such inter-detector differences can lead to errors in an image.

7. Cirrus and unresolved cloud, as well as localized obscurants will manifest themselves as scene elements (i.e. components of a heterogeneous pixel). The effects of these components upon radiometric signatures needs considerable study in so far as it effects target detection, tracking and quantification. Modelling studies would be inexpensive and a logical first step.

8. A model for the two-dimensional array in which the point-spread functions are mapped in a two-dimensional diagram is necessary before it is possible to determine the optimum method of dynamic viewing. It is suspected that this will depend upon the angular viewing regime and upon the target-to-background contrast as well as upon the portion of the pixel occupied by the target and upon target aspect.

9. Further modelling studies should be performed and should integrate terrestrial vegetation emittance models in order to predict parametric envelopes for optimum data acquisition and analysis. For reasons discussed in section 3, it will be necessary to model sensor output for each sensor element in a two-dimensional array, pushbroom array, or scanning device so as to take into account the radiometric point or line spread functions spectral response, polarization characteristics, detector noise, and the interaction of each of these parameters with spectral scene radiance. The importance of the difference in angular anisotropy in scene radiance from each scene component will depend upon the point-spread function of each scene element. Models of typical arrays could be used mathematically to predict optimum dynamic viewing conditions to optimize target-to-background discrimination under different atmospheric and meteorological conditions, for different geographical regions and for different sensor types. Further, utilizing the techniques of modelling studies could suggest possible new sensor combinations to optimize target discrimination, tracking and quantification.

10. It is strongly recommended that this work be continued and that modelling studies incorporating some or all of the above be pursued as a matter of urgency in order

to better define optimum parametric envelopes for optimal data acquisition and real-time processing. It has been shown that targets and backgrounds which are similar in temperature may be discriminated under a variety of atmospheric conditions. The suite of data used in such studies should be expanded, the models made more sophisticated so as to include spectral and point-spread function information on the sensing devices. Random and systematic error sources described above should also be further investigated in order to determine their effects on target detection, tracking and quantification accuracy.

Acknowledgement

Appreciation is expressed for support of this work under U.S. Air Force contract F 30602-81-C-0193. We appreciate the assistance of D. Piwinski with computing and extensive work by Melanie Johnson in library research, word processing, collation of data and deciphering the handwriting of the principal investigator.

FIGURE CAPTIONS

Fig. 1. Overall picture of interactions between incident and reflected radiance, the atmosphere and the earth's surface.

Fig. 2. Interactions between solar radiance and the earth's atmosphere.

Fig. 3. Nomenclature for the interactions of light energy at the earth's surface. Hemispherical-directional reflectance.

Fig. 4. Angular notation relating incident and reflected radiance. Bidirectional reflectance.

Fig. 5. Angular notation for reflected target radiance.

Fig. 6. Wavelength dependence and view zenith angle dependence of bidirectional reflectance factor for wheat at boot stage, for solar zenith and azimuth angles typical for NOAA-6 ephemeris. The LARSPEC data base was used in this calculation[36,70].

Fig. 7. The relationship between incident, absorbed and reflected radiance.

Fig. 8. The relationship between radiance from the target, absorbed radiance and radiance scattered from the beam to the sensor.

Fig. 9. Wavelength dependence of those factors which determine sensor output.

Fig. 10. Showing that two sensors with the same nominal half-power and zero-power bandpass values and wavelength limits can differ so as to produce different sensor outputs when viewing the same target.

Fig. 11. Flow chart showing those factors controlling variations in sensor output in the optical reflective part of the spectrum.

Fig. 12. Flow chart showing those factors controlling variations in sensor output in the thermal infrared part of the spectrum.

Fig. 13. The superposition of a hypothetical contoured point-spread function for a detector on a heterogeneous pixel, showing that the movement of the instanteous field of view by a fraction of a pixel can change the sensor output.

Fig. 14. The dependence of the vegetation index contrast ratio (VIN_{MAX}/VIN_{MIN}) on view zenith angle and on the percentage of unresolved cloud in the IFOV over the targets to be distinguished (percentage of cloud assumed to be the same in each case). Here (VIN = AVHRR2/AVHRR1) and the atmosphere is clear (meteorological range > 50 km).

Fig. 15. The dependence of the contrast ratio (VIN_{MAX}/VIN_{MIN}) on view zenith angle and on the percentage of unresolved cloud in the IFOV over the targets to be distinguished (percentage of cloud assumed to be the same in each case). Here (VIN = AVHRR2/AVHRR1) and the atmosphere is turbid (meteorological range < 10 km).

Fig. 16. The relationship between emitted thermal target radiance, atmospheric extinction and radiance incident on the sensor.

Figs. A1-A3. The calculated relationship between the discriminability function (D.F.) for detector bandpass 3.5-4.1 μm, target temperature T_A and $(1 - \varepsilon_A)$ where ε_A = target emissivity for background temperature $T_B = 275^{\circ}K$, background emissivity $\varepsilon_B = 0.90$ and atmospheric transmission $\tau = 1.00$. The degree of variation in emissivity and atmospheric transmission considered is discussed in the text. Three different rotations of the same calculated data are shown.

Figs. A4-A6. Similar to Figs. A1-A3, but for $\tau = 0.70$ and $\varepsilon_B = 0.85$.

Figs. B1-B3. Similar to Figs. A1-A3 but for detector bandpass 11.0 - 12.0 μm: $\tau = 1.00$ and $\varepsilon_B = 0.90$.

Figs. B4-B6. Similar to Figs. B1-B3 but for $\tau = 0.60$ and $\varepsilon_B = 0.85$.

Fig. C1. The discriminability function (D.F.) is shown as a function of the ratio of the atmospheric transmission values τ_1 and τ_2 in two bandpasses and as a function of target temperature T_A. The correlation coefficient between the radiance recorded from the target in each bandpass is taken to be 0.1 Here the coefficients of variation in the emissivities of target ε_A and of background ε_B and in atmospheric transmission values τ_1, τ_2 are taken as 0.01. The emissivity of the target is assumed to be spectrally invariant.

Fig. C2. As Fig. C1 but with the coefficients of variation in ε_A, ε_B, τ_1 and τ_2 = 0.05.

Fig. C3. As Fig. C1 . but with the correlation coefficient between the radiance values recorded from the target in bands 1 and 2 (3.5 - 4.1 μm and 11.0 - 12.0 μm respectively) taken to be 0.90.

REFERENCES

1. Maxwell, E.L., 1976, Multivariate system analysis of multispectral data. Photogramm. Eng. Rem. Sens. 42, 1173.

2. Huck, F.O.; Halyo, N. and Park, S.K., 1981, Information efficiency of line-scan imaging mechanisms. Appl. Optics 20, 1990.

3. Park, S.K.; Davis, R.E.; Huck, F.O. and Arduini, R.F., 1980, Multispectral data acquisition and classification: computer modeling for smart sensor design. Proc. AIAA Conf. Sensor Systems for the 80's, Colorado Springs, Colo., Dec. 2-4.

4. Kaneko, T. and Engvall, J.L., 1977, View angle effect in Landsat imagery. Proc. 11th Internat. Symp. on Remote Sens. of Environ., Ann Arbor, MI, pp. 945-951.

5. Duggin, M.J.; Piwinski, D.; Whitehead, V. and Ryland, G., 1982, The scan angle dependence of radiance recorded by the NOAA-AVHRR, Proc. AIAA/SPIE Tech. Meeting, San Diego, Calif., August 23-27, in press.

6. Piwinski, D.; Schoch, L.B.; Duggin, M.J.; Whitehead, V. and Ryland, G., 1983, Dependence of NOAA-AVHRR recorded radiance on scan angle, atmospheric turbidity and unresolved cloud, Proc. 17th Internat. Symp. on Remote Sens. of Environ., Ann Arbor, MI, in press.

7. Duggin, M.J.; Piwinski, D.; Whitehead, V. and Ryland G., 1982, Evaluation of NOAA-AVHRR data for crop assessment, Appl. Optics 21, 1873.

8. Schnetzler, C.C., 1981, Effect of sun and sensor geometry, canopy structure and density and atmospheric conditions on the spectral response of vegetation, with particular emphasis on across-track pointing. Proc. Conf. Signatures Spectrales d'objets en teledetection, Avignon, 8-11 Sept., pp. 509-520.

9. Kirchner, J.A. and Schnetzler, C.C., 1981, Simulated directional radiances of vegetation from satellite platforms, Int. J. Remote Sensing 2, 253.

10. Duggin, M.J., 1983, The effect of irradiation and reflectance variability on vegetation condition assessment, Int. J. Remote Sensing, 4, 601.

11. Duggin, M.J., 1974, On the natural limitations of target differentiation by means of spectral discrimination techniques, Proc. 9th Internat. Symp. on Remote Sens. Environ., Ann Arbor, Mich., pp. 499-516.

12. Daughtry, C.S.T.; Vanderbilt, V.C. and Pollara, V.J., 1981, Variability of reflectance measurements with sensor altitude and canopy type. NASA AgRISTARS Supporting Research Document NAS9-15466: SR-P1-04191.

13. Gast, P.R.; Jursa, A.S., Castelli, J.; Basu, S. and Aarons, J., 1965, Solar electromagnetic radiation, in Handbook of Geophysics and Space Environments, Air Force Cambridge Research Lab. ed. S.L. Valley. Ch. 16.

14. Wolfe, W.L. and Zissis, G.J., 1978, The Infrared Handbook, Environmental Research Inst. of Michigan.

15. Turner, R.E.; Malila, W.A. and Nalepka, R.F., 1971, Importance of atmospheric scattering in remote sensing. Proc. 7th Int. Symp. on Remote Sensing of Environ., Ann Arbor, MI., pp. 1651-1697.

16. Fraser, R.S., Bahethi, Om. P.; Al-Abbas, A.H., 1977, The effect of the atmosphere on the classification of satellite observation to identify surface features. Remote Sensing of Environ. 6, 229-249.

17. Herman, B.M. and Browning, S.R., 1975, The effect of aerosols on the earth-atmospheric albedo. J. Atmos. Sci. 32, 1430.

18. Ellis, P.E. and Duggin, M.J., 1978, Atmospheric measurements, in Landsat 2 Over New Zealand: Monitoring our Resources from Space. New Zealand Department of Scientific and and Industrial Research DSIR Bulletin 221, pp. 83-101.

19. Kriebel, K.T., 1976, On the variability of the reflected radiation field due to differing distributions of the irradiation. Remote Sensing Environ. 4, 257-264.

20. Smith, J.A. and Oliver, L.E., 1972, Plant canopy models for simulating composite scene spectroradiance in the 0.4 to 1.05 micrometer region. Proc. Eighth Internat. Symp. on Remote Sensing of Environ., Ann Arbor, MI., 1333-1353.

21. Suits, G.H., 1972, The calculation of the directional reflectance for a vegetative canopy, Remote Sens. Environ. 2, 117.

22. Suits, G.H., 1972, The causes of azimuthal variations in directional reflectance of vegetative canopies, Remote Sens. Environ. 2, 175.

163. Janssens, T.J., Valdes, S.F., 1981, Smear compensation for a pushbroom scan. Proc. of SPIE, Vol. 304, pp. 101-107

164. Jobson, D.J., 1980, Programmable performance - one aspect of smart sensing systems. AIAA Sensor Systems for the 80's Conference, pp. 113-116

165. Johnson, L.F., 1972, On the performance of infrared sensors in earth observations. Technical Report RSC-37, supported by NASA Grant NsG 239-62, NASA Contract NAS 9-11155, August.

166. Joy, M.L.G., Gilday, D.L., Fenaud, L., 1981, Fourier Multiaperture Emision Tomography: Quantum Noise Calculations. Optical Engineering, Vol. 20, No. 5, pp. 736-739

167. Kates, J.C., Jr., 1982, Omew field measurement capabilities for EW signature measurements. Proc. of SPIE, Vol. 356, pp. 68-75

168. Keene, G.T., 1981, A concept for an advanced earth resources satellite system. Proc. of the 15th Int. Symp. on Remote Sensing of Environment, Vol. 1, pp. 33-44

169. Kondratyev, K.Y., Rokrovsky, O.M., 1979, A factor analysis approach to optimal selection of spectral intervals for multipurpose experiments in remote sensing of the environment and earth resources. Remote Sensing of Environment, Vol. 8, pp. 3-10

170. Lange, S.R., Greynolds, A.W., 1980, Prototype designs for a wide-field high-resolution low-scatter image device. Proc. of SPIE, Vol. 226, pp. 98-107

171. Lienesch, J.H., Bauer, B.P., Goddard, B.B., 1975, SMS Infrared Observations: Their accuracy and calibration. Proc. of the 10th Int. Symp. on Remote Sensing of Environment, Volume I, October 6-10, pp. 149-158

172. Lotspeich, J.F., Stephens, R.R., Henderson, D.M., 1981, Electro-Optic Tunable Filter. Optical Engineering, Vol. 20, No. 6, pp. 830-836

173. Lucy, R.F., 1981, Spectritek - A multispectral electro-optic pushbroom camera. Presented at the 15th Int. Symp. on Remote Sensing of Environment, pp. 715-720

152. [illegible], R.D., Stermer, R.L., Jr., 1982, Bubble domain technology for spacecraft onboard memory. Proc. of SPIE, Vol. 363, pp. 136-146

153. Helfrich, R., 1981, Hardware for non-uniformity correction devices for non-scanned systems (Unicorns). Interim Technical Report for March 1981 to August 1981, Prepared for: Night Vision & Electro-Optics Laboratory, U.S. Army Electronics R&D Command, Fort Belvoir, VA 22060., pp. 1-18

154. Hier, R.G., Beaver, E.A., Bradley, S.E., Burbidge, E.M., Harms, R.J., McIlwain, C.E., Schmidt, G.W., Smith, R.D., 1982, Charge-coupled device (CCD) digicon detector system concepts. Proc. of SPIE, Vol. 363, pp. 57-65.

155. Hodgson, R.M., Cady, F.M., Pairman, D., 1981, A solid-state airborne sensing system for remote sensing. Photogrammetric Engineering and Remote Sensing, Vol. 47, pp. 177-182

156. Houston, J.B., Jr., 1981, The potential for acousto-optics in instrumentation; an overview for the 1980's. Optical Engineering, Vol. 20, No. 5, pp. 712-718.

157. Huck, F.O., Davis, R.E., Park, S.K., Aherron, R.M., Arduini, R.F., 1981, Computational modeling for smart multispectral sensor design. Proc. of SPIE, Vol. 278, pp. 83-101

158. Hurwitz, C.E., 1981, Detectors for the 1.1 to 1.6 um wavelength region. Optical Engineering, Vol. 20, No. 4, pp. 658-664

159. Husain-Abidi, A.S., Ostrow, H., Rubin, B., 1980, Thermal IR imaging system using a self-scanned HgCdTe/CCD detector array. Proc. of SPIE, Vol. 226, pp. 10-17

160. Ingersoll, K.A., Liquid filters for the ultraviolet, visible, and near infrared. Applied Optics, Vol. 11, No. 11, pp. 2473-2476

161. Arons, J., Wharton, S., 1980, Earth array pushbroom radiometer data analysis. Earth Survey Applications Division Research Report, pp. 299-302.

162. Jain, Y.K., Kalakrishnan, B., 1979, Use of pyroelectric detectors in horizon sensors. Optical Engineering, Vol. 18, No. 6, pp. 634-637

141. Elabd, H., Villani, T.S., 1982, High density schottky barrier IRCCD sensors for SWIR applications at intermediate temperature. RCA Laboratories, Princeton, New Jersey.

142. Engel, J.L., 1980, Thematic mapper - An interim report on anticipated performance. AIAA Sensor Systems for the 80's conference.

143. Fischer, R.E., 1980, Design considerations for a reflective IR imager. Proc. of SPIE, Vol. 226, pp. 83-90

144. Forshaw, M.R.B., Haskell, A., Miller, P.F., Stanley, D.J., Townshend, J.R.G., 1983, Spatial resolution of remotely sensed imagery, a review paper. Int. Journal of Remote Sensing, Vol. 4, No. 3, pp. 497-520

145. Gasser, G.C., Friedman, M.G., 1981, Effects of internal-compartment turbulence on camera optical performance. Optical Engineering, Vol. 20, No. 6, pp. 893-898.

146. General Electric Company, 1978, MSS standard interface document. Contract NAS5-24167, prepared for Goddard Space Flight Center, Greenbelt, MD

147. Godfrey, T.E., Clark, W.M., 1981, Boresighting of airborne laser designator systems. Optical Engineering, Vol. 20, No. 6, pp. 854-860

148. Grinberg, J., Efron, U., Little, M.J., Bleha, W.P., 1980, Visible-to-infrared image converter for dynamic infrared target simulation applications. Proc. of SPIE, Vol. 226, pp. 129-132.

149. Gunning, W.J., 1981, Electro-optically tuned spectral filters; a review. Optical Engineering, Vol. 20, No. 6, pp. 837-845

150. Harney, R.C., 1980, Dual active/passive infrared imaging systems. Proc. of SPIE, Vol. 226, pp. 74-82

151. Harrington, R.F., 1980, The development of a stepped frequency microwave radiometer and its application to remote sensing of the earth. NASA TM 81847-N80-28637, 166 pgs., 65 refs.

130. Cabrieres, B., Cazaux, J.C., Weill, G., 1980, Spot program. Proc. of the 14th Int. Symp. on Remote Sensing of Environment, Vol. II, pp. 931-940

131. Cabrieres, B., Cazaux, J.C., Weill, G., 1979, Spot - First French remote sensing satellite geometrical performance. Proc. of the 13th Int. Symp. on Remote Sensing of Environment, Vol. II, pp. 867-877

132. Carnahan, S.U., Eargle, J.R., Noll, R.E., Schaff, F.L., Williams, V.L., 1981, Solid-State shuttle-launched meteorological sensor. Proc. of SPIE, Vol. 304, pp. 143-147

133. Chan, W.S., 1981, Focal plane architecture; an overview. Optical Engineering, Vol. 20, No. 4, pp. 574-578

134. Chang, I.C., 1981, Electronically tunable optical spectral filters. Optical Engineering, Vol. 20, No. 6, pp. 805-814.

135. Chang,I.C., 1981, Electronically tunable optical spectral filters. Optical Engineering, Vol. 20, No. 6, pp. 824-829

136. Clark, J., Bryant, N.A., 1977, Landsat-D thematic mapper simulation using aircraft multispectral scanner data. Proc. of the 11th Int. Int. Symp. on Remote Sensing of Environment, Vol. I, pp. 483-491

137. Cordray, D.M., Searles, S.K., Hanley, S.T., Dowling, D.A., Gott, C.O., 1981, Experimental mesurements of turbulence induces beam spread and wander at 1.06, 3.8, and 10.6 um. Proc. of SPIE, Vol. 305, pp. 273-280

138. Cox, J.A., 1982, Signal-to-noise ratio dependence on frame time, time delay and integration (TDI), and pulse shaping. Optical Engineering, Vol. 21, No. 3, pp. 528-536

139. Darnell, W.L., Harriss, R.C., 1983, Satellite sensing capabilities for surface temperature and meteorological parameters over the ocean. Int. Journal of Remote Sensing, Vol. 4, No. 1, pp. 65-92

140. Due, C.T., Peterson, L.M., 1982, Optical-mechanical, active/passive imaging systems - Volume 1. An IRIA State-of-the-Art Report, Vol. 1, Office of Naval Research, Dept. of the Navy, Arlington, VA 22217, Contract Nos. N00014-77-C-0125, N00014-80-C-0510, and N00014-81-C-0425.

120. Malick, J.D., 1981, Review of cirrus cloud optical properties and effects on infrared sensors. Proc. of SPIE, Vol. 305, pp. 70-78

121. Gimmestad, G.G., Winchester, L.W., Lee, S.M., 1981, Measurements of infrared and visible extinction in adverse weather, Proc. of SPIE, Vol. 305, pp. 99-105

122. Hering, W.S., 1981, Assessment of operational techniques for estimating visible spectrum contrast transmittance. Proc. of SPIE, Vol. 305, pp. 119-125

123. Bradford, R., 1972, An experimental model for the automated detection, mesurement, and quality control of low-level cloud motion vectors from geosynchronous satellite data. Proc. of the 8th Int. Symp. on Remote Sensing of Environment, Vol. I, pp. 441-462.

124. Coakley, J.A., Bretherton, F.P., 1982, Cloud cover from high-resolution scanner data: detecting and allowing for partially filled fields of view. Journal of Geophysical Research, Vol. 87, No. C7, pp. 4917-4932

125. Embury, J.F., 1983, Extinction by clouds of polydisperse and randomly oriented nonspherical particles at arbitrary wavelengths. Optical Engineering, Vol. 22, No. 1, pp. 71-77

126. Malick, J.D., 1981, Review of cirrus cloud optical properties and effects on infrared sensors. Proc. of SPIE, Vol. 305, pp. 70-78

127. Welch, R.M., Cox, S.K., Zdunkowski, W.G., 1980, Calculations of the variability of ice cloud radiative properties at selected solar wavelengths. Applied Optics, Vol. 19, No. 18, pp. 3057-3067

128. Selby, J.E.A., 1982, Influence of atmospheric uncertainties on predicting infrared atmospheric attenuation and radiance. Proc. of SPIE, Vol. 356, pp.. 20-25

129. Brown, T.J., 1980, Development of an earth resource pushbroom scanner utilizing a 90-element 8-14 micrometer (Hg, Cd) Te array. Proc. of SPIE, Vol. 226, pp. 18-37

110. Slater, P.N., Jackson, R.D., 1982, Transforming ground-measured reflectances to radiances measured by various space sensors through clear and turbid atmospheres, pp. 1-11.

111. Sutherland, R.A., Hoock, D.W., Gomez, R.B., 1983, Objective summary of U.S. Army electro-optical modeling and field testing in an obscuring environment. Optical Engineering, Vol. 22, No. 1, pp. 2-19

112. Switzer, P., Kowalik, W.S., Lyon, R.J.P., Estimation of atmospheric path-radiance by the covariance matrix method. Photogrammetric Engineering and Remote Sensing, Vol. 47, pp. 1469-1476

113. Turner, R.E., 1975, Signature variations due to atmospheric effects. Proc. of the 10th Int. Symp. on Remote Sensing of Environment, Vol. II, pp. 671-682

114. Turner, R.E., 1978, Elimination of atmospheric effects from remote sensor data. Proc. of the 12th Int. Symp. on Remote Sensing of Environment, Vol. II, pp. 783-793

115. Ben-Shalom, A., Devir, A.D., Lipson, S.G., Oppenheim, U.P., Trahovsky, E., 1982, New developments in instrumentation for long path atmospheric transmittance and radiance measurements. Proc. of SPIE, Vol. 356, pp. 98-105

116. Watson, K., Hummer-Miller, S., 1981, A simple algorithm to estimate the effective regional atmospheric parameters for thermal-inertia mapping. Remote Sensing of Environment, Vol. 11, pp. 455-462

117. Fronterhouse, D.C., Heath, W.B., Smith, D.M., Shively, F.T., 1980, Simulation studies of infrared signatures from remote aerosols. Proc. of SPIE, Vol. 226, pp. 149-156.

118. Seagraves, M.A., 1981, Optical characteristics of windblown dust. Proc. of SPIE, Vol. 305, pp. 45-52.

119. Ebersole, J.F., 1981, Transmission effects of explosion-produced dust clouds on downward viewing airborne platforms. Proc. of SPIE, Vol. 305, pp. 53-68

100. Malick, J.D., 1981, Review of Cirrus cloud optical properties and effects on infrared sensors. Proc. of SPIE, Volume 305, pp. 70-78

101. Martinez-Sanchez, M., Yousefian, V., Dvore, D., Vaglio-Lauren, R., 1983, Numerical modeling of optically significant characteristics of falling snow. Optical Engineering, Volume 22, No. 1, pp. 78-85

102. McClatchey, R.A., 1981, Atmospheric transmission and radiance calculations for satellite applications. Proc. of the 15th Int. Symp. on Remote Sensing of Environment, Vol. 1, pp. 111-124.

103. Bliamptis, E.E., 1970, Nomogram relating true and apparent radiometric temperatures of graybodies in the presence of an atmosphere. Remote Sensing of Environment, Vol. 1, p. 93-94.

104. Coney, T.A., Salzman, J.A., 1979, A comparison of measured and calculated upwelling radiance over water as a function of sensor altitude. Proc. of the 13th Int. Symposium on Remote Sensing of Environment, Vol. III, pp. 1707-1720

105. Dave, J.V., 1980, Effect of atmospheric conditions on remote sensing of a surface nonhomogeneity. Photogrammetric Engineering and Remote Sensing, Vol. 46, pp. 1173-1180.

106. Otterman, J., Fraser, R.S., 1976, Earth-atmosphere system and surface reflectivities in arid regions from Landsat MSS data. Remote Sensing of Environment, Vol. 5, pp. 247-266

107. Pitts, D.E., McAllum, W.E., Dillinger, A.E., The effect of atmospheric water vapor on automatic classification of ERTS data. Proc. of the 9th Int. Symp. on Remote Sensing of Environment, Vol. I, pp. 483-497

108. Potter, J., Shelton, M., 1974, Effect of atmosphere haze and sun angle on automatic classification of ERTS-1 data. Proc. of the 9th Int. Symp. on Remote Sensing of Environment, Vol. II, pp. 865-874

109. Potter, J.F., 1977, The correction of Landsat data for the effects of haze, sun angle, and background reflectance. Presented at the 1977 Machine Processing of Remotely Sensed Data Symp. Laboratory for Application of Remote Sensing, Purdue University, West Lafayette, Indiana, June 21-23, 1977.

89. Sutherland, R.A., 1982, Field measurement requirements for electro-optical obscuration modeling. Proc. of SPIE, Vol. 356, pp. 62-67.

90. Dave, J.V., 1980, Effect of atmospheric conditions on remote sensing of vegetation parameters. Remote Sensing of Environment, Vol. 10, pp. 87-90

91. Dave, J.V., 1981, Influence of illumination and viewing geometry and atmospheric composition on the "tasseled cap" transformation of Landsat MSS data. Remote Sensing of Environment, Vol. 11, pp. 37-55

92. Dave, J.V., 1979, Contrast attenuation factors for remote sensing, IBM Journal of research and development, Vol. 23, No. 2.

93. Dozier, J., Frew, J., Atmospheric corrections to satellite radiometric data over rugged terrain, Remote Sensing of Environment, Vol. 11, pp. 191-205

94. Englander, A., Slatkine, M., Karoubi, R., Bensimon, D., 1983, Probabilistic diffraction limited imaging through turbulence. Optical Engineering, Vol. 22, No. 1, pp. 145-148

95. Fronterhouse, D.C., Heath, W.B., Smith, D.M., Shively, F.T., 1980, Simulation studies of infrared signatures from remote aerosols. Proc. of SPIE, Vol. 226, pp. 149-156

96. Gemoets, L.A., McIntyre, R.G., Gemoets, E.E., Hockett, L.J., 1981, Sequential process method of modeling thermo-gradients and the dynamics of fire plumes. Proc. of SPIE, Vol. 305, pp. 31-36

97. Kiang, R.K., 1979, Atmospheric effects on cluster analyses, Proc. of 13th Int. Symposium on Remote Sensing of Environment, Volume II, pp. 1189-1197

98. Kowalik, W.S., Lyon, R.J.P., Switzer, P., 1983, The effects of additive radiance terms on ratios of Landsat data. Photogrammetric Engineering and Remote Sensing, Vol. 49, No. 5, pp. 659-669

99. Lambeck, P.F., 1979, Spatially varying xstar haze correction. NASA New Technology Report, NASA Contract No: NAS9-15476

77. Duncan, L.D.,Shirkey, R.C., 1983, EOSAEL 82: A library of battlefield obscuration models. Optical Engineering, Vol. 22, No. 1, pp. 20-23.

78. Ebersole, J.F., 1981, Transmission Effects of Explosion-Produced Dust Clouds on Downward Viewing Airborne Platforms. Proc. of SPIE, Vol. 305, pp. 53-68.

79. Embury, J.F., 1981, Extinction by Aerosol Clouds of Nonspherical Particles at Arbitrary Wavelengths. Proc. of SPIE, Vol. 305, pp. 24-27.

80. Farmer, W.M., 1982, Relationships between battlefield obscurart parameters measured over large and small distance scales. Proc. of SPIE, Vol. 356, pp. 53-60

81. Farmer, W.M., Krist, K.L., 1981, Comparison of methods used to determine the mass extinction coefficient for phosphorus smokes. Proc. of SPIE, Vol. 305, pp. 7-16.

82. Krist, K.L., Farmer, W.M., 1982, Measurement of battlefield obscurant parameters with the point characterization instrumentation system. Proc. of SPIE, Vol. 356, pp. 45-52.

83. Nelson, J.G., 1982, Applications overview of battlefield obscurant parameters measured in U.S. Army tests. Proc. of SPIE, Vol. 356, pp. 34-38.

84. Seagraves, M.A., 1981, Optical characteristics of windblown dust. Proc. of SPIE, Vol. 305, pp. 45-52.

85. Shirkey, R.C., 1981, Effects of atmospheric and man-made obscurants on visual contrast. Proc. of SPIE, Vol. 305, pp. 37-44.

86. Smalley, H.M., 1982, Dugway proving ground smoke and obscurant field measurement technology. Proc. of SPIE, Vol. 356, pp. 39-44.

87. Stuebing, E.W., 1981, Future optical and electro-optical (EO) instrumentation requirements of the Army smoke research program. Proc. of SPIE, Vol. 305, pp. 2-6.

88. Sutherland, R.A., Hoock, D.W., Gomez, R.B., 1983, Objective summary of U.S. Army electro-optical modeling and field testing in an obscuring environment. Optical Engineering, Vol. 22, No. 1, pp. 2-19.

71. Jackson, R.D. 1981, Interactions between canopy geometry and thermal infrared measurements, Proc. Conf. Signatures Spectrales D'objets en teledetection, Avignon, 8-11 Sept. g.II.5. 291

72. Kimes, D.A., 1981, Remote Sensing of temperature profiles in vegetation canopies using multiple view angles and inversion techniques, IEEE Transactions on Geoscience and Remote Sensing, Vol. GE-19, No. 2, April 1981, 85.

73. Kimes, D.S., Idso, S.B., Pinter, P.J., Reginato, R.J., and Jackson, R.D., 1980, View angle effects in the radiometric measurement of plant canopy temperatures., Remote Sensing of Environment 10, 273.

74. Kimes, D.S., 1981, Azimuthal radiometric temperature measurements of wheat canopies, Applied Optics, 20, 1119.

75. Kimes, D.S. and Kirchner, J.A., 1983, Directional radiometric measurements of row-crop temperatures, Int. Journal of Remote Sensing, 4, 299.

76. Kimes, D.S., 1983, Remote sensing of row crops structure and component temperatures using directional radiometric temperatures and inversion techniques, Remote Sensing of Environment, 13,33

61. Duggin, M.J., Slater, P.N. and Somers, S.L., 1980, A method for calibrating multispectral scanners to allow for the spectral dependence of instrument response. Proc. AIAA Conf., "Sensor Systems for the 80's," Colorado Springs, CO., Dec. 2-4, 76-83.

62. Duggin, M.J., 1980, Effect of instrument spectral response on use of the Landsat MSS for vegetative disease assessment. Appl. Optics 19, 2081.

63. Duggin, M.J. and Lindsay, J., in preparation.

64. Duggin, M.J., Schoch, L.B. and Gray, T.I., 1982, Effect of subpixel-sized cloud on target discrimination from satellite data. Appl. Optics 21, 2649.

65. Duggin, M.J., Schoch, L.B. and Gray, T.I., 1982, Effect of sub-pixel sized cloud on vegetation assessment from satellite data, Proc. SPIE meeting Advanced Multispectral Remote Sensing Technology and Applications, May 6-7, Arlington, Virginia, pp. 97-101.

66. Duggin, M.J., 1982, The effects of variable unresolved cloud and haze on digital multichannel data from large scan angles. Proc. Conf. on Remote Sensing and the Atmosphere, Liverpool, 15-17 December, pp.

67. Duggin, M.J., Schoch, L.B. and Moreton, G.E., 1982, The effect of variable sub-pixel sized cloud and haze on discrimination of ground features. Proc. Conf. on Remote Sensing and the Atmosphere, Liverpool, 15-17 December, pp.

68. Duggin, M.J. and Piwinski, D., 1982, Study to assess the importance of errors introduced by applying NOAA 6 and NOAA 7 AVHRR data as an estimator of vegetative vigor: feasibility study of data normalization. Final Report to NASA, contract 9-1663.

69. Davis, O.L. (ed.), 1961, Statistical Methods in Research and Production, 3rd Edition, Oliver and Boyd, London and Edinburgh, pg. 41.

70. LARSPEC data base, Purdue University, Laboratory for the Applications of Remote Sensing.

48. Dave, J.V., 1975, A direct solution of the spherical harmonics approximation to the radiative transfer equation for an arbitrary solar elevation. Part 1: theory. J. Atmos. Sci. 32, 790-798.

49. Dave, J.V., 1980, Simulation colorimentry of the earth-atmosphere system. Remote Sensing of Environ. 9, 301-324.

50. Slater, P.N., 1981, Remote Sensing: Optics and Optical Systems, Addison Wesley. Advanced Book Program, Reading, Mass., pp. 211, et seq.

51. Hulstrom, R.L., 1972, The cloud bright spot, Photogramm. Eng. 39, 370.

52. Kirchner, J.A.; Youkhana, S. and Smith, J.A., 1982, Influence of sky radiance distribution on the ratio technique for estimating bidirectional reflectance. Photogrammetric Eng. and Remote Sens. 48, 955-959.

53. Nicodemus, F.E.; Richmond, J.C.; Hsia, J.J.; Ginsbert, J.W.; and T. Limperis, 1977, Geometrical consideration and nomenclature for reflectance. NBS Monograph 160, Institute for Basic Standards, U.S. Dept. Commerce. Rept. No. NBSMN-160, Washington, D.C.

54. Chance, J.G. and LeMaster, E.W., 1977, Suits reflectance models for wheat and cotton: theoretical and experimental tests. Appl. Optics 16, 407.

55. Duggin, M.J., 1980, The field measurement of reflectance factors. Photogramm. Eng. and Rem. Sensing 46, 643.

56. Duggin, M.J. and Philipson, W.R., 1982, Field measurements of reflectance: some major considerations. Appl. Optics 21, 2833.

57. Duggin, M.J., 1981, Simultaneous measurement of irradiance and reflected radiance in field determination of spectral reflectance. Appl. Optics 20, 3816.

58. Duggin, M.J. and Cunia, T., 1983, Ground reflectance measurements: some observations on technique. Proc. 17th Int. Symp. on Remote Sens. Environ., Ann Arbor, MI, May 9-13, in press.

59. Slater, P.N., 1979, A re-examination of the Landsat MSS, Photogramm. Eng. and Remote Sens. 45, 1497.

60. Slater, P.N., 1980, Remote Sensing: Optics and Optical Systems. Addison Wesley, Reading, Mass., p. 473 et seq.

35. Kollenkark, J.C.; Vanderbilt, V.C.; Daughtry, C.S.T. and Bauer, M.E., 1982, Influence of solar illumination angle on soybean canopy reflectance. Appl. Optics, 21, 1179-1184.

36. Biehl, L., 1982, Private communication.

37. Rogers, R.H. and Peacock, K., 1973, A Technique for correcting ERTS data for solar and atmospheric effects. Symp. on Significant Results Obtained from the Earth Resources Technology Satellite - 1, March. NASA SP-327, Vol. 1, p. 1115.

38. Rogers, R.H., 1973, Investigation of Techniques for correcting ERTS data for solar and atmospheric effects. Bendix Aerospace Systems Div., Rept. MNC 655, October.

39. Kowalik, W.S., 1981, Ph.D. Thesis, Atmospheric Correction to Landsat data for limonite discrimination, Stanford University, 363 pp.

40. Switzer, P.; Kowalik, W.S. and Lyon, R.J.P., 1981, Estimation of atmospheric path radiance by the covariance matrix method. Photogramm. Eng. and Remote Sensing 47, 1469-1476.

41. Potter, J.F. and Mendlowitz, M.A., 1975. On the determination of haze levels from Landsat data. Proc. Tenth Int. Symp. on Remote Sensing of Environ., Ann Arbor, MI., pp. 695-703.

42. Potter, J.F., 1977. The correction of Landsat data for the effects of haze, sun angle and background reflectance. Proc. Symp. on Machine Processing of Remotely Sensed Data, IEEE 77Ch 1218-7MPRSD, June, pp. 24-32.

43. Turner, R.E., 1978, Elimination of atmospheric effects from sensor data. Proc. 12th Int. Symp. on Remote Sensing of Environ., Ann Arbor, MI., pp. 783-793.

44. Otterman, J. and Fraser, R.S., 1976, Earth-atmosphere system and surface reflectivities in arid regions from Landsat MSS data. Remote Sensing of Environ. 5, 247-266.

45. Johnson, W.R. and Sestak, M.L., 1981, AgRISTARS Report NASA SR-LI-04071; JSC-17127.

46. Dave, J.V., 1978, Extensive data sets of the diffuse radiation in realistic atmospheric models with aerosols and common absorbing gases. Solar Energy 21, 361-369.

47. Dave, J.V., Canosa, J., 1974. A direct solution of the radiactive transfer equation: application to atmospheric models with arbitrary vertical nonhomogenities, J. Atmos. Sci. 32, 790-798.

23. Verhoef, W. and Bunnik, N.J.J., 1976, The spectral directional reflectance of row crops. Part 1: Consequences of non-Lambertian behavior for automatic classification. Part 2: Measurements on wheat and simulations by means of a reflectance model for row crops. Tech. Rpt. No. NIWARS-Publ. 35. NIWARS, Delft, The Netherlands.

24. Chance, J.E. and LeMaster, E.W., 1978, Plant canopy light absorption model with application to wheat. Appl. Optics 17, 2629-2636.

25. Berry, J.K. and Smith, J.A., 1977, An overview of vegetation canopy modeling for signature correction and analysis. 4th Annual Symp. on Machine Processing of Remotely Sensed Data, p. 194.

26. Kriebel, K.T., 1977, Reflection properties of vegetated surfaces: tables of measured spectral biconical reflectance factors. Universitat Munchen - Meterorologisches Inst. Wissenschaftliche Mietteilung, Nr 29.

27. Bauer, M.E.; Biehl, L.L.; Daughtry, C.S.T.; Robinson, B.F.; and Stoner, E.R., 1979, AgRISTARS Supporting Research, Final Report NAS9-15466, vol. 1.

28. Suits, G.H. and Safir, G., 1972, Verification of a reflectance model for mature corn with applications to corn blight detections. Remote Sens. Environ. 2, 183.

29. Smith, J.A., 1979, MRS Literature Survey of bidirectional reflectance. ORI, Inc., 1400 Spring Rd., Silver Spring, MD.

30. Colwell, J.E., 1974, Vegetation canopy reflectance. Remote Sens. Environ. 3, 175-183.

31. Coulson, K.L., 1966, Effects of reflection properties of natural surfaces in aerial reconnaissance. Appl. Optics 5, 905-917.

32. Coulson, K.L.; Bouricius, C.M. and Gray, E.L., 1965, Optical reflection properties of natural surfaces. J. Geophysical Res. 70, 4601-4611.

33. Egbert, D.D. and Ulaby, F.T., 1972, Effects of angles on reflectivity. Photogrammetric Eng. 38, 556-564.

34. Duggin, M.J., 1977, Likely effects of solar elevation on the quantification of changes in vegetation with maturity using sequential Landsat imagery. Appl. Optics 16, pp. 521-523.

171. Mann, A., 1981, Infrared zoom lens system for target detection. Proc. of SPIE, Vol. 304, pp. 160-170.

175. Markham, B.L., Townshend, J.R.G., 1981, Land cover classification accuracy as a function of sensor spatial resolution. Proc. of the 15th Int. Symp. on Remote Sensing of Environment, Vol. III, May 11-15, pp. 1075-1090.

176. Markham, B.L., Baker, J.L., 1983, Spectral characterization of the Landsat-4 MSS sensors. Photogrammetric Engineering and Remote Sensing, Vol. 49, No. 6, pp. 811-833.

177. Mazaika, P.K., 1981, Jitter-induced clutter in staring sensors arising from background spatial radiance gradients. Proc. of SPIE, Vol. 304, August 27-8, San Diego, CA.

178. Molain, P., 1980, Visible and Infrared Radiometer on Seasat-1. IEEE Journal of Oceanic Engineering, Vol. OE-5, No. 2, April, pp. 164-168.

179. Mobasseri, B.G., Anuta, P.E., Mcgillem, C.D., 1980, A parametric model for multispectral scanners. AgRISTARS report # SR-P1-04169, NAS9-15466, Purdue University/LARS, 4 pp.

180. Montuori, J.S., 1980, Image scanner technology. Photogrammetric Engineering and Remote Sensing, Vol. 46, pp. 49-61.

181. Otterman, J., Salomonson, V.V., Atlas, D., Sheck, W., Maxwell, M.S., Pitts, D.E., 1983, A case for gonrem: geosynchronous orbit high resolution earth monitoring. Presented at the 17th Int. Symp. on Remote Sensing of Environment, Ann Arbor, Michigan, May 9-13.

182. Peckham, G.E., Flower, D.A., 1981, The Design of Optimum Remote Sensing Instruments. Int. Journal of Remote Sensing, Vol. 4, No. 2, pp. 457-463.

183. Pauch, H.E., Bohteld, J.J., 1980, System Design for a Staring Mosaic Sensor. Proc. of SPIE, Vol. 226, pp. 53-60.

184. Richmond, J.C., 1980, Errors in passive infrared imaging systems due to reflected ambient flux. Proc. of SPIE, Vol. 226, pp. 110-114.

185. Rifman, S.S., Ronski, A.T., Shortwell, C.P., 1979, Multi-sensor Landsat MSS registration. Proc. of the 13th Int. Symp. on Remote Sensing of Environment, Vol. I, pp. 245-258.

186. Robinson, B.F., 1979, Multiband radiometer for field research. Proc. of Photo-Optical Instrumentation Engineers, Vol. 196.

187. Schnetzler, C., Thompson, L.L., 1979, Multispectral Resource Sampler: An Experimental Satellite Sensor for the Mid-1980's. Proc. of the SPIE Tech. Symp. Vol. 183.

188. Scheler, C., 1983, Thematic Mapper Protoflight Model Line Spread Function. Presented at the 17th Int. Symp. on Remote Sensing of Environment, May 9-13, 1983.

189. Slater, P.N., 1977, Comparison of photographic and digital imagery from film and solid-state-array remote sensing cameras. Photographic Science and Engineering, Vol. 21, No. 4, pp. 198-203.

190. Sprague, R.A., Turner, W.D., 1981, High Resolution Multispectral Linear Focal Plane Using an Area Image Sensor. Optical Engineering, Vol. 20, No. 6, pp. 873-880.

191. Tanaka, S.C., 1979, Coping with Charge Transfer Inefficiency Affecting Modulation Transfer Function (MTF) of Charge-Coupled Devices (CCD). Optical Engineering, Vol. 18, No. 5, pp. 504-512.

192. Taranik, J.V., 1981, Advanced Aerospace Remote Sensing Systems for Global Resource Applications. Proc. of the 15th Int. Symp. on Remote Sensing of Environment, Vol. 1, pp. 3-20.

193. Taranik, J.V., 1978, Characteristics of the Landsat Multispectral Data System. Open-file report 78-187, U.S. Geological Survey, Sioux Falls, South Dakota, January 1978.

194. Thomson, F.J., Erickson, J.D., Koerber, K., Harnage, M.J., 1975, A thematic mapper performance optimization study. Proc. of the 10th Int. Symp. on Remote Sensing of Environment, Volume 1, pp. 85-98.

195. Title, A.M., Rosenberg, W.J., 1981, Tunable birefringent filters. Optical Engineering, Vol. 20, No. 6, pp. 815-823.

196. Toler, O.E., Grey, D.S., 1980, Simulation model for infrared imaging systems. Proc. of SPIE, Vol. 226, pp. 121-128.

197. Townshend, J.R.G., 1980, The spatial resolving power of earth sources satellites: a review. NASA Technical Memorandum 82020, September 1980.

198. Welch, R., 1981, Spatial Resolution and Geometric Potential of Planned Earth Satellite Missions. Presented at the 15th Int. Symp. on Remote Sensing of Environment, pp. 1-9.

199. Wellman, J.B., 1981, Technologies for the multispectral mapping of earth resources. Proc. of the 15th Int. Symp. on Remote Sensing of Environment, Vol. I, pp. 45-64.

200. Wells, C.W., Potter, A.E., Morgan, T.H., 1980, Near Infrared Spectral Imaging Michelson Interferometer for Astronomical Applications. Proc. of SPIE, Vol. 226, pp. 61-64.

201. Wharton, S.W., Irons, J.R. Hoegel, F., 1981. LAPR: An experimental pushbroom scanner. Photogrammetric Engineering and Remote Sensing, Vol. 47, pp. 631-639.

202. Wiersma, D.J., Landgrebe, D.A., 1980, Analytical design of multispectral sensors. AgRISTARS, Report #SR-P1-04163, NAS9-15466, Purdue University/LARS, 1980.

203. Wolfe, W.L., 1980, Comparison of coherent and incoherent imaging in the location of point sources. Proc. of SPIE, Vol. 226, pp. 115-120.

204. Zweibaum, F.M., Chapelle, E.W., 1979, Making real-time sun reflectance measurements with a micropreocessor-based spectroradiometer. Soc. of Photo-Optical Instrumentation Engineers, Vol. 180, 14 pages.

205. Carrison, C.L., Foss, N.A., 1980, Fixed Pattern Noise Compensation Techniques for Staring Infrared Focal Planes. Optical Engineering, Vol. 19, No. 5, pp. 753-757.

206. Cordray, D.M., Searles, S.K., Hanley, S.T., Dowling, D.A., Gott, C.O., 1981, Experimental measurements of turbulence induces beam spread and wander at 1.06, 3.8, and 10.6 um. Proc. of SPIE, Vol. 305, pp. 273-280.

207. Cox, J.A., 1982, Signal-to-noise ratio dependence on frame time, time delay and integration (TDI), and pulse shaping. Optical Engineering, Vol. 21, No. 3, pp. 528-536.

208. Daughtry, C.S.T., Vanderbilt, V.C., Pollara, V.J., 1981, Variability of reflectance measurements with sensor altitude and canopy type. AgRISTARS, SR-P1 04191, NAS9-15466, Purdue University.

209. Dozier, J., Frew, J., 1981, Atmospheric corrections to satellite radiometric data over rugged terrain. Remote Sensing of Environment, Vol. 11, pp. 191-205.

210. Guyot, G., 1980, Analysis of factors acting on the variability of spectral signatures of natural surfaces. Int. Soc. for Photogrammetry, 14th Cong., Hamburg, W. Germany, July 13-25, 1980, 12 pp.

211. Holben, B.N., Justice, C.O., 1979, Evaluation and modeling of the topographic effect on the spectr l response from nadir pointing sensors. NASA Technical Memorandum 80305, June 1979, Goddard Space Flight Center, Greenbelt, Maryland.

212. Horwitz, H.M., Nalepka, R.F., Hyde, P.D., Morgenstern, J.P., 1971, Estimating the Proportions of Objects within a Single Resolution Element of A Multispectral Scanner. Proc. of the 7th Int. Symp. on Remote Sensing of Environment, Vol. II, May 17-21, pp. 1307-1320.

213. Hsing, T.R., Poularikas, A.D., 1981, The change of limiting resolution of electro-optical systems due to atmospheric effects. Proc. of SPIE, Vol. 305, pp. 268-272.

214. Hugli, H., Frei, W., 1983, Understanding anisotropic reflectance in mountainous terrain. Photogrammetric Engineering and Remote Sensing, Vol. 49, No. 5, pp. 671-683.

215. Janssens, T.J., Valdes, S.F., 1981, Smear Compensation for a Pushbroom Scan. Proc. of SPIE, Vol. 304, pp. 101-107.

216. Joy, M.L.G., Gilday, D.L., Renaud, L., 1981, Fourier Multiaperture Emission Tomography; Quantum Noise Calculations. Optical Engieering, Vol. 20, No. 5, pp. 736-739.

217. Kates, J.C., Jr., 1982, Omew field measurement capabilities for EW signature measurements. Proc. of SPIE, Vol. 356, pp. 68-75.

218. Kimes, D.S., Kirchner, J.A., Newcomb, W.W., 1983, Spectral radiance errors in remote sensing ground studies due to nearby objects. Applied Optics, Vol. 22, No. 1, 2 pp.

219. Kimes, D.S., Kirchner, J.A., 1982, Radiative transfer model for heterogeneous 3-D scenes. Applied Optics, Vol. 21, No. 22, pp. 4119-4129.

220. Kimes, D.S., Ranson, K.J., Smith, J.A., 1980, A monte carlo calculation of the effects of canopy geometry on PhAR absorption. Photosynthetics, Vol. 14, No. 1, pp.. 55-64.

221. Kimes, D.S., Smith, J.A., 1980, Simulation of solar radiation absorption in vegetation canopies. Applied Optics, Vol. 19, No. 16, pp. 2801-2811.

222. Kitcho, C.A., 1979, Optimum Landsat sun angles for extreme contrasts of terrain. Proc. of the 13th Int. Symp. on Remote Sensing of Environment, Vol. II, pp. 1213-1221.

223. Koepke, P., Kriebel, K.T., 1978, Influence of measured reflection properties of vegetated surfaces on atmospheric radiance and its polarization. Applied Optics, Vol. 17, No. 2, pp. 260-264.

224. Kriebel, K.T., 1979, Albedo of vegetated surfaces: its variability with differing irradiances. Remote Sensing of Environment, Vol. 8, pp. 283-290.

225. Kriebel, K.T., 1978, Average variability of the radiation reflected by vegetated surfaces due to differing irradiations. Remote Sensing of Environment, Vol. 7, pp. 81-83.

226. Maksymowicz, A.T., Bankus, R.A., Davis, W.W., Pecora, V.J., Wald, L.H., Statistical modeling of scene variability. Proc. of SPIE, Vol. 304, pp. 116-124.

227. Mazaika, P.K., 1981, Jitter-induced clutter in staring sensors arising from background spatial radiance gradients. Proc. of SPIE, Vol. 304, August 27-8.

228. Otterman, J., Dishon, M., Rehavi, S., 1983, Point spread functions in imaging a lambert surface from zenith through a thin scattering layer. Proc. of Int. Journal of Remote Sensing, Vol. 4, No. 3, pp. 583-599.

229. Pitts, D.E., Badhwar, G., 1980, Field size, length, and width distributions based on lacie ground truth data. Remote Sensing of Environment, Vol. 10, pp. 201-213.

230. Polara, V.J., Daughtry, C.S.T., Vanderbilt, V.C., Robinson, B.F., 1980, Variability of reflectance measurements with sensor altitude and canopy type. Purdue University, Lafayette, Indiana, June 2-6, 1980.

231. Piwinski, D.J., Schoch, L.B., Duggin, M.J., Whitehead, V., Ryland, E., 1983, Dependence of NOAA-AVHRR recorded radiance on scan angle, atmospheric turbidity and unresolved cloud. Presented at the 17th Int. Symp.. on Remote Sensing of Environment, Ann Arbor, MI, May.

232. Richmond, J.C., 1980, Errors in passive infrared imaging systems due to reflected ambient flux. Proc. of SPIE, Vol. 226, pp. 110-114.

233. Sadowski, F.G., Malila, W.A., Sarno, J.E., Nalepka, F., 1977, The influence of multispectral scanner spatial resolution on forest feature classification, Proc. of the 11th Int. Symp. on Remote Sensing of Environment, Vol. II, pp. 1279-1288.

234. Steinberg, R.A., 1981, Quantum-noise-limited signal processors for infrared surveillance. Optical Engineering, Vol. 20, No. 5, pp. 726-735.

235. Tappan, G., Miller, G.E., 1981, Area estimation of environmental phenomena from NOAA-n satellite data. AgRISTARS report, Early Warning and Crop Conditon Assessment, November 1981.

236. Tucker, C.J., 1980, Radiometric resolution for monitoring vegetation - how many bits are needed? International Journal of Remote Sensing, Vol. 1, pp. 241-254.

237. Vanderbilt, V.C., Kollenkark, J.C., Biehl, L.L., Robinson, B.F., Bauer, M.E., Ranson, K.J., 1981, Diurnal changes in reflectance factor due to sun-row direction interactions. AgRISTARS report #SR-P1-04140, NAS9-15466, Purdue University, Laboratory for Applications of Remote Sensing.

238. Vanderbilt, V.C., Kilgore, R.W., 1981, Application of computer axial tomagraphy (CAT) to measuring crop canopy. AgRISTARS report #SR-P1-04141, NAS9-15466, Purdue University.

239. Wang, C.D., 1982, Adaptive spatial/temporal/spectral filters for background clutter suppression and target detection. Optical Engineering, Vol. 21, No. 6, pp. 1033-1038.

240. Wolfe, W.L., 1980, Effects of reflected background radiation on radiometric temperature measurement. Proc. of SPIE, Vol. 226, pp. 133-135.

241. Abotteen, R., Levy, S., Mendlowitz, M., Moritz, T., Potter, J., Thadani, S., Wehmanen, O., 1977, Performance tests of signature extension algorithms. Proc. of the 11th Int. Symp. on Remote Sensing of Environment, Vol. II, April 25-29, pp. 1523-1532.

242. Dalton, J.T., Winkert, G.E., 1979, Quadratic image destriping. Proc. of the 13th Int. Symp. on Remote Sensing of Environment, Vol. III, pp. 1697-1705.

243. Drexler-Salmon, B.C., 1977, Reducing Landsat data to parameters with physical significance and signature extension-A view of Landsat capabilities. Proc. of the 11th Int. Symp. on Remote Sensing of Environment, Vol. II, pp. 1289-1299.

244. Duggin, M.J., Piwinski, D., Whitehead, V., Ryland, G., 1982, Scan angle dependence of radiance recorded by the NOAA-AVHRR. Proc. of SPIE, Vol. 363, pp. 98-103.

245. Egan, W.G., Fischbein, W.L., 1975, Optical atmospheric scattering and absorption limitations on offset pointing from earth observatory satellite (EOS) sensors. Proc. of the 10th Int. Symp. on Remote Sensing of Environment, Vol. II, pp. 783-792.

246. Goodenoogh, D.G., Guindon, B., Teillet, P.M., 1979, Correction of synthetic aperture radar and multispectral scanner data sets. Proc. of the 13th Int. Symp. on Remote Sensing of Environment, Vol. I, pp. 259-270.

247. Hoffer, R.M., Goodrick, F.E., 1971, Variables in automatic classification over extended remote sensing test sites. Proc. of the 7th Int. Symp. on Remote Sensing of Environment, Vol. III, pp. 1967-1981.

248. Holben, B.N., Justice, C.O., 1980, The topographic effect on spectral response from nadir-pointing sensors. Photogrammetric Engineering and Remote Sensing, Vol. 46, pp. 1191-1200.

249. Hutchinson, C.F., 1982, Techniques for combining Landsat and ancillary data for digital classification improvement. Photogrammetric Engineering and Remote Sensing, Vol. 48, pp. 123-130.

250. Janssens, T.J., Valdes, S.F., 1981, Smear compensation for a pushbroom scan. Proc. of SPIE, Vol. 304, pp. 101-107.

251. Kitcho, C.A., 1979, Optimum Landsat sun angles for extreme contrasts of terrain. Proc. of the 13th Int. Symp. on Remote Sensing of Environment, Vol. II, pp. 1213-1221.

252. Lambeck, P..F., Kauth, R., Thomas, G.S., 1978, Data screening and preprocessing for Landsat MSS data. Proc. of the 12th Int. Symp. on Remote Sensing of Environment, Vol. II, pp. 999-1008.

253. Lambeck, P.F., 1977, Signature extension preprocessing for Landsat MSS data. NASA CR-ERIM 122700-32-F, Final report.

254. Lienesch, J.H., Bauer, B.P., Goddard, B.B., 1975, SMS Infrared Observations: their accuracy and calibration. Proc. of the 10th Int. Symp. on Remote Sensing of Environment, Vol. I, October 6-10, pp. 149-158.

255. Malila, W.A., Gleason, J.M., Sadowski, F.G., Cicone, R.C., Crist, E.P., 1978, Applications of Modeling to Analysis and Preprocessing of Landsat Data, Proc. of the 12th Int. Symp. on Remote Sensing of Environment, Vol. II, pp. 917-926.

256. Nelson, R., Grebowsky, G., 1982, Evaluation of temporal registration of Landsat scenes. International Journal of Remote Sensing, Vol. 3, pp. 45-50.

257. Roller, N.E.G., Cox, S., 1980, Comparison of Landsat MSS and merged MSS/RBV data for analysis of natural vegetation. Proc. of the 14th Int. Symp. on Remote Sensing of Environment, Vol. II, pp. 1001-1007.

258. Schnetzler, C.C., 1981, On the use of off-nadir pointing for increased temporal resolution of earth observing satellite systems, NASA Tech. Memorandum 82139, Goddard Space Flight Center, Greenbelt, MD.

259. Schott, J.R., Tourin, R.H., 1975, A completely airborne calibration of aerial infrared water-temperature measurements. Proc. of the 10th Int. Symp. on Remote Sensing of Environment, Vol. I, pp. 477-484.

260. Schowengerdt, R.A., 1980, Reconstruction of multispatial, multispectral image data using spatial frequency content. Photogrammetric Engineering and Remote Sensing, Vol. 46, pp. 1325-1334.

261. Arens, J.F., Lamb, G.M., Peck, M.C., 1983, Infrared camera for ten micrometer astronomy. Optical Engineering, Vol. 22, No. 2, pp. 267-268.

262. Bly, V.T., 1982, Passive visible to infrared transducer for dynamic infrared image simulation. Optical Engineering, Vol. 21, No. 6, pp. 1079-1082.

263. Capone, B.R., Taylor, R.W., Kosonocky, W.F., 1982, Design and characterization of a schottky infrared charge coupled device (IRCCD) focal plane array. Optical Engineering, Vol. 21, No. 5, pp. 945-950.

264. Coffeen, D.L., Hansen, J.E., 1972, Airborne infrared polarimetry. Proc. of the 8th Int. Symp. on Remote Sensing of Environment, Vol. 1, pp. 515-522.

265. Craine, E.R., 1980, Optical infrared sky survey instrumentation. Optical Engineering, Vol. 19,, No. 3, pp. 397-403.

266. Desrochers, A.A., 1982, On the analysis of an all-reflective zoom optical system for the infrared. Optical Engineering, Vol. 21, No. 5, pp. 868-871.

267. Eden, R.C., Deyhimy, I., 1981, Gaas Integrated Circuits and Charge-Coupled Devices for High Speed Signal Processing. Optical Engineering, Vol. 20, No. 6, pp. 947-952.

268. Ewing, W.S., Shepherd, S.D., Capps, R.W., Dereniak, E.L., 1983, Applications of an infrared charge-coupled device schottky diode array in astronomical instrumentation. Optical Engineering, Vol. 22, No. 3, pp. 334-338.

269. Harney, R.C., 1981, Dual active/passive infrared imaging systems. Optical Engineering, Vol. 20. No. 6, pp. 976-980.

270. Jain, Y.K., Kalakrishnan, B., 1979, Use of pyroelectric detectors in horizon sensors. Optical Engineering, Vol. 18, No. 6, pp. 634-637.

271. Kahle, A.B., Schieldge, J.P., Abrams, M.J., Alley, R.E., LeVine, C.J., 1981, Geological application of thermal inertia imaging using "HCMM" data. JPL Publication 81-55, 200 pp.

272. Kahle, A.B., Madura, D.P., Soha, J.M., 1980, Middle infrared multispectral aircraft scanner data: analysis for geological applications. Applied Optics, Vol. 19, No. 14, pp. 2279-2290.

273. Mann, A., 1982, Infrared zoom lens system for target detection. Optical Engineering, Vol. 21, No. 4, pp. 786-793.

274. McDowell, M.W., Klee, H.W., 1980, Method of improving the performance of lenses for use in thermal infrared. Optical Engineering, Vol. 19, No. 5, pp. 748-752.

275. Pasko, J.G., Tracy, J., Elser, W., 1981, Liquid crystal infrared modulation. Optical Engineering, Vol. 20, No. 6, pp. 970-975.

276. Kassal, T., Selby, J.E.A., Waters, R., 1981, Balloon atmospheric mosaic measurements (Bammo IIA phenomenology and band selection). Proc. of SPIE, Vol. 304, pp. 70-82.

277. Tanaka, S.C., 1979, Coping with charge transfer inefficiency affecting modulation transfer function (MTF) of charge-coupled devices (CCD). Optical Engineering, Vol. 18, No. 5, pp. 504-512.

278. Toler, O.E., Grey, D.S., 1980, Simulation model for infrared imaging systems. Proc. of SPIE, Vol. 226, April 10-11, pp. 121-128.

279. Brown, T.J., 1980, Development of an earth resource pushbroom scanner utilizing a 90 element 8-14 micrometer (Hg,Cd) Te Array. Proc. of SPIE, Vol. 226, pp. 18-37.

280. Fischer, R.E., 1980, Design considerations for a reflective IR imager. Proc. of SPIE, Vol. 226, pp. 83-90.

281. Marshall, D.E., Jr., 1980, Focal plane array design for optimum system performance. Proc. of SPIE, Vol. 226, pp. 66-73.

282. Nordbryhn, A., 1978, The dynamic sampling effect with CCD imagers. SPIE 1978 Technical Symposium East, March, Washington, DC.

283. Nummedal, K., 1980, Wide-field imagers--Pushbroom or whiskbroom scanners. Proc. of SPIE, Vol. 226, pp. 38-52.

284. Roth, J.A., 1982, Mobile tracking imaging radiometer. Proc. of SPIE, Vol. 356, pp. 90-97.

285. Singer, S.M., Rogne, T.J., Smith, F.G., White, K.O., 1982, Development of a high frame rate infrared digital imagery system for characterizing battlefield events. Proc. of SPIE, Vol. 356, pp. 84-89.

286. Tanaka, S.C., 1979, Coping with charge transfer inefficiency affecting modulation transfer function (MTF) of charge-coupled devices (CCD). Optical Engineering, Vol. 18, No. 5, pp. 504-512.

287. Coffeen, D.L., Hansen, J.E., 1972, Airborne Infrared Polarimetry, Proceedings of the 8th Int. Symp. on Remote Sensing of Environment, Volume I, pp. 515-522.

288. Coulson, K.L., 1966, Effects of reflection properties of natural surfaces in aerial reconnaissance. Applied Optics, Vol. 5, No. 6, pp. 905-917.

289. Curran, P.J., 1978, A photographic method for the recording of polarised visible light for soil surface moisture indications. Remote Sensing of Environment, Vol. 7, pp. 305-322.

290. Curran, P.J., 1979, The use of polarized panchromatic and false-color infrared film in the monitoring of soil surface moisture. Remote Sensing of Environment, Vol. 8, pp. 249-266.

291. Egan, W.G., 1970, Optical stokes parameters for farm crop identification. Remote Sensing of Environment, Vol. 1, pp. 165-180.

292. Halajian, J., Hallock, H., 1972, Principles and techniques of polarimetric mapping. Proc. of the 8th Int. Symp. on Remote Sensing of Environment, Vol. 1, pp. 523-540.

293. Koepke, P., Kriebel, K.T., 1978, Influence of measured reflection properties of vegetated surfaces on atmospheric radiance and its polarization. Applied Optics, Vol. 17, No. 2, pp. 260-264.

294. Stockhoff, E.H., Frost, R.T., 1971, Polarization of light scattered from moist soils. Proc. of the 7th Int. Symp. on Remote Sensing of Environment, Vol. 1, pp. 345-364.

295. Stockhoff, E.H., Frost, R.T., 1974, Remote detection of soil surface moisture. Proc. of the 9th Int. Symp. on Remote Sensing of Environment, Vol. 1, pp. 707-723.

296. Vanderbilt, V.C., 1980, A model of plant canopy polarization. AgRISTARS report #SR-P1-04170, NAS9-15466, Purdue University, LARS, 1980, 10 pp.

297. Vanderbilt, V.C., Biehl, L.L., Bauer, M.E., Vanderbilt, A.S., 1981, Linear polarization of light by two wheat canopies measured at many view angles. AgRISTARS, SR-P1-04139, NAS9-15466, Purdue University, Indiana.

298. Coulson, K.L., Walraven, R.L., Weigt, G.I., Soohoo, L.B., 1974, Photon-counting polarizing radiometer. Applied Optics, Vol. 13, No. 3, pp. 497-498.

299. Coulson, K.L., 1968, Effect of surface reflection on the angular and spectral distribution of skylight. Journal of Atmospheric Sciences, Vol. 25, No. 5, pp. 759-770.

300. Coulson, K.L., Bouricius, G.M.B., Gray, E.L., 1965, Effects of surface reflection on radiation emerging from the top of a planetary atmosphere. Technical Information Series, R65SD64, General Electric, Missile and Space Division.

301. Curran, P.J., 1982, Polarized visible light as an aid to vegetation classification. Remote Sensing of Environment, Vol. 12, pp. 491-499.

302. Maxwell, J.R., Vincent, R., Weiner, S., 1974, Polarized radiance Vol. II: Polarized spectral emittance from 4 to 14 um. Prepared by Environmental Institute of Michigan, P.O. Box 618, Ann Arbor, Michigan, report no. 155.

303. Brown, R.J., Cihlar, J., Teillet, P.M., 1981, Quantitative residential heat loss study. Photogrammetric Engineering and Remote Sensing, Vol. 47, No. 9, pp. 1327-1333.

304. Byrne, G.F., Davis, J.R., 1980, Thermal inertia, thermal admittance, and the effect of layers. Remote Sensing of Environment, Volume 9, pp. 295-300.

305. Djermakoye, B., Kong, J.A., 1979, Radiative-transfer theory for the remote sensing of layered random media. Journal of Applied Physics, Vol. 50, No. 11, pp. 6600-6604.

306. Gauffre, G., 1981, Aircraft infrared radiation modeling. Rech. Aerosp. pp. 21-41.

307. Idso, S.B., 1981, On the systematic nature of diurnal patterns of differences between calculations and measurements of clear sky atmospheric thermal radiation. Quarterly Journal Royal Meteorological Society, Vol. 107, pp. 737-741.

308. Idso, S.B., 1981, A set of equations for full spectrum and 8- to 14-um and 10.5- to 12.5-um thermal radiation from cloudless skies. Water Resources Research, Vol. 17, No. 2, pp. 295-304.

309. Idso, S.B., 1983, On calculating thermal radiation from cloudless skies. Arch. Met. Geoph. Biocl. Ser. B. 32, pp. 53-57.

310. Kahle, A.B., Schieldge, J.P., Abrams, M.J., Alley, R.E., LeVine, C.J., 1981, Geological application of thermal inertia imagering using "HCMM" data. JPL publication 81-55, 200 pp.

311. Kimball, B.A., Idso, S.B., 1982, A model of thermal radiation from partly cloudy and overcast skies. Water Resources Research, Vol. 18, No. 4, pp. 931-936.

312. Kimes, D.A., 1981, Remote sensing of temperature profiles in vegetation canopies using multiple view angles and inversion techniques. IEEE Transactions on Geoscience and Remote Sensing, Vol. GE-19, No. 2, pp.. 85-90.

313. Kimes, D.S., Kirchner, J.A., 1982, Radiative transfer model for heterogeneous 3-D scenes. Applied Optics, Vol. 21, No. 22, pp. 4119-4129.

314. Kong, J.A., Shin, R., Shiue, J.C., Tsang, L., Theory and experiment for passive microwave remotee sensing of snowpacks. Journal of Geophysical Research, Vol. 84, No. B10, pp. 5669-5673.

315. Lillesand, T.M., Keifer, R.W., 1979, Aerial thermography. Remote Sensing and Image Interpretation, Chapter 7, pp. 382-441.

316. Matson, M., Dozier, J., 1981, Identification of subresolution high temperature sources using a thermal IR sensor. Photogrammetric Engineering and Remote Sensing, Vol. 47, No. 9, pp. 1311-1318.

317. Nieuwenhuis, G.J.A., 1979, Influence of atmosphere on thermal infrared radiation. Instituut voor Cultuurtechniek en Waterhuishouding, Wageningen, NOTA 1159, Dec. 1979.

318. Pratt, D.A., 1980, Two-dimensional model variability in thermal inertia surveys. Remote Sensing of Environment, Vol. 9, pp. 325-338.

319. Ren-Hua, Z., Guo-Liang, T., 1980, Emissivity measurement of objects at usual temperature. Int. Symp. on Remote Sensing of Environment, Proc. 14th, San Jose, Cost Rica, April 23-30, Vol. 1, pp. 153-158.

320. Shin, R.T., Kong, J.A., 1981, Radiative transfer theory for active remote sensing of a homogenous layer containing spherical scatters. Journal of Applied Physics, Vol. 52, No. 6, pp. 4221-4230.

321. Tsang, L., Kong, J.A., 1980, Energy conservation for reflectivity and transmissivity at a very rough surface. Journal of Applied Physics, Vol. 51, No. 1, pp. 673-680.

322. Tsang, L., Kong, J.A., 1977, Thermal microwave emission from a random inhomogenous layer over a homogeneous medium using the method of invariant imbedding. Radio Science, Vol. 12, No. 2, pp. 185-194.

AD-A154 070 TARGET DISCRIMINATION USING INFRARED TECHNIQUES: 2/2
THEORETICAL CONSIDERATIONS(U) STATE UNIV OF NEW YORK AT
SYRACUSE* M J DUGGIN ET AL. FEB 85 RADC-TR-84-29
UNCLASSIFIED F30602-81-C-0193 F/G 17/5 NL

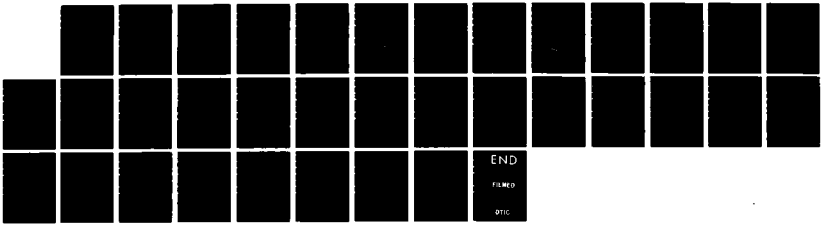

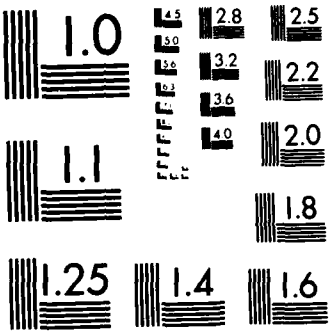

MICROCOPY RESOLUTION TEST CHART
NATIONAL BUREAU OF STANDARDS-1963-A

323. Watson, K., 1980. Direct computation of the sensible heat flux. Geophysical Research Letters, Vol. 7, No. 8, pp. 616-618.

324. Becker, F., 1981, Angular reflectivity and emissivity of natural media in the thermal infrared bands. Signatures spectrales d'objets en teledetection, Avignon, Sept. 8-11, 1981, pp. 57-72.

325. DeCarolis, C., Amodeo, P., 1980, Basic problems in the reflectance and emittance properties of vegetation. Remote Sensing Application in Agriculture and Hydrology, In the framework of A.A. Balkema, Rotterdam, 11 pp, 14 refs.

326. Jackson, R.D., 1981, Interactions between canopy geometry and thermal infrared measurements. Signatures spectrales D'objets en teledetection, Avignon, 8-11, Sept., pp. 291-302.

HETEROGENEOUS (MIXED) SCENE IN IFOV (MIXED PIXEL) OMITTING

FUNCTION INTERACTION

$$\left[\begin{array}{c}\text{RELATIVE}\\ \text{SENSOR}\\ \text{OUTPUT}\\ \text{IN BAND}\\ r\end{array}\right] = \frac{\displaystyle\int_{\lambda_1}^{\lambda_2} I(\lambda).\left\{\left[\begin{array}{c}\text{SPECTRAL}\\ \text{RADIANCE}\\ \text{FROM}\\ \text{TARGET}\\ \text{ELEMENT 1}\end{array}\right] + \left[\begin{array}{c}\text{SPECTRAL}\\ \text{RADIANCE}\\ \text{FROM}\\ \text{TARGET}\\ \text{ELEMENT 2}\end{array}\right] +\ldots+ \left[\begin{array}{c}\text{SPECTRAL}\\ \text{RADIANCE}\\ \text{FROM}\\ \text{TARGET}\\ \text{ELEMENT n}\end{array}\right] +\ldots+ \left[\begin{array}{c}\text{SPECTRAL}\\ \text{RADIANCE}\\ \text{FROM}\\ \text{ATMOSPHERE}\end{array}\right]\right\}.d\lambda}{\displaystyle\int_{\lambda_1}^{\lambda_2} I(\lambda).d\lambda}$$

WHERE: (OPTICAL REFLECTIVE CASE)

$$\left[\begin{array}{c}\text{SPECTRAL}\\ \text{RADIANCE}\\ \text{FROM}\\ \text{TARGET}\\ \text{ELEMENT n}\end{array}\right] = \left[\sum_{\text{HEMISPHERE}} \left(\begin{array}{c}\text{SPECTRAL}\\ \text{SKY}\\ \text{RADIANCE}\\ \text{FROM}\\ \theta,\phi\end{array}\right) \times \left(\begin{array}{c}\text{SPECTRAL}\\ \text{BIDIRECTIONAL}\\ \text{REFLECTANCE}\\ \text{FACTOR}\\ R_n(\vartheta,\varphi;\theta',\varphi',\lambda)\end{array}\right) \times \left(\begin{array}{c}\text{FRACTION}\\ \text{OF IFOV}\\ \text{(PIXEL)}\\ \text{FILLED BY}\\ \text{TARGET n}\end{array}\right)\right.$$

$$\left. + \left(\begin{array}{c}\text{SPECTRAL}\\ \text{SOLAR}\\ \text{RADIANCE}\\ \text{FROM } \theta,\phi\end{array}\right) \times \left(\begin{array}{c}\text{SPECTRAL}\\ \text{BIDIRECTIONAL}\\ \text{REFLECTANCE}\\ \text{FACTOR}\\ R_n(\vartheta,\phi;\theta',\phi',\lambda)\end{array}\right) \times \left(\begin{array}{c}\text{FRACTION}\\ \text{OF IFOV}\\ \text{(PIXEL)}\\ \text{FILLED BY}\\ \text{TARGET n}\end{array}\right)\right] \times \left[\begin{array}{c}\text{SPECTRAL}\\ \text{ATMOSPHERIC}\\ \text{EXTINCTION}\\ \text{COEFFICIENT}\end{array}\right] + \left[\begin{array}{c}\text{SPECTRAL}\\ \text{ATMOSPHERIC}\\ \text{PATH}\\ \text{RADIANCE}\end{array}\right]$$

TABLE 1

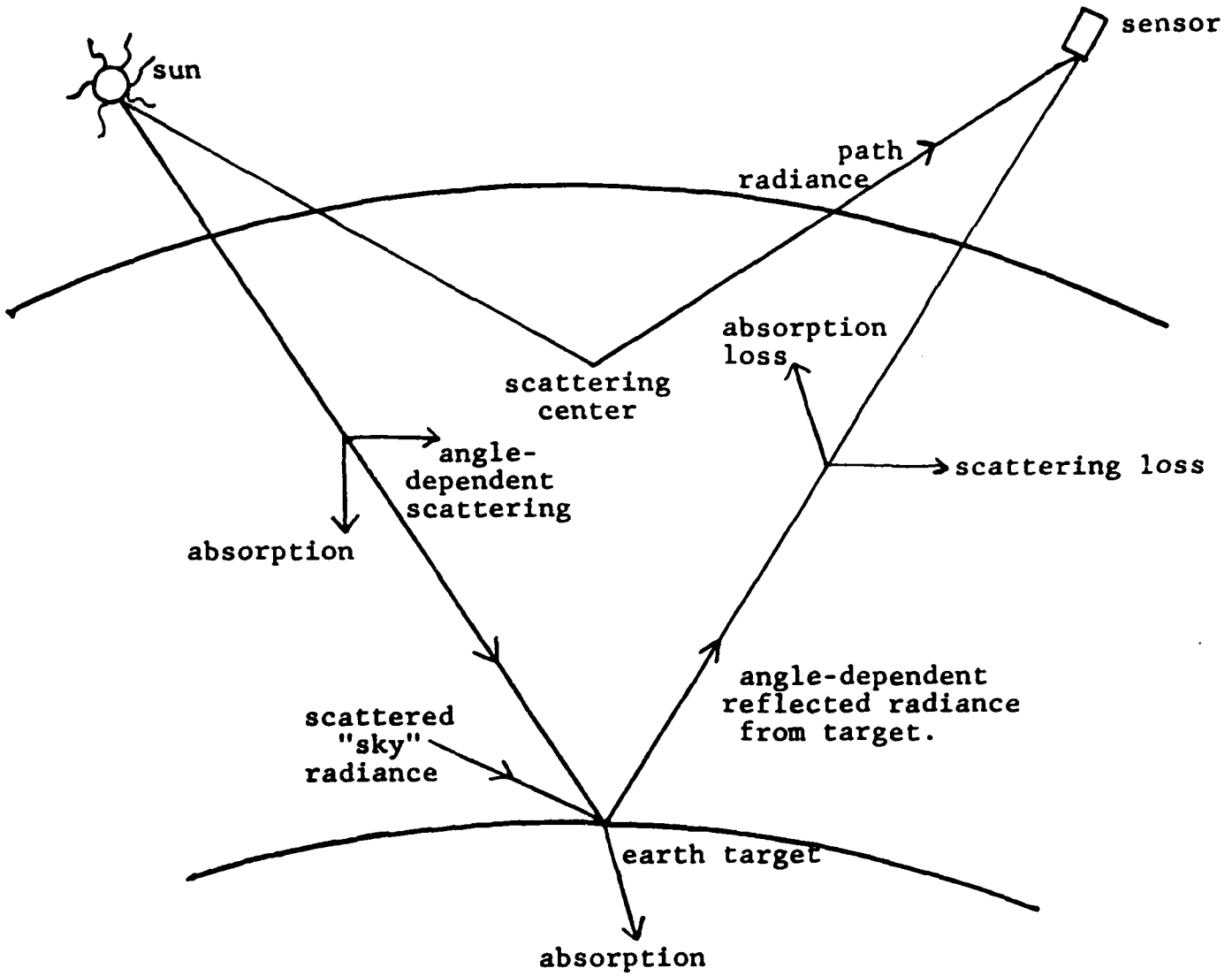
sensor
sun
path
radiance
absorption
loss
scattering
center
angle-
dependent
scattering
scattering loss
absorption
angle-dependent
reflected radiance
from target.
scattered
"sky"
radiance
earth target
absorption

FIG. 1

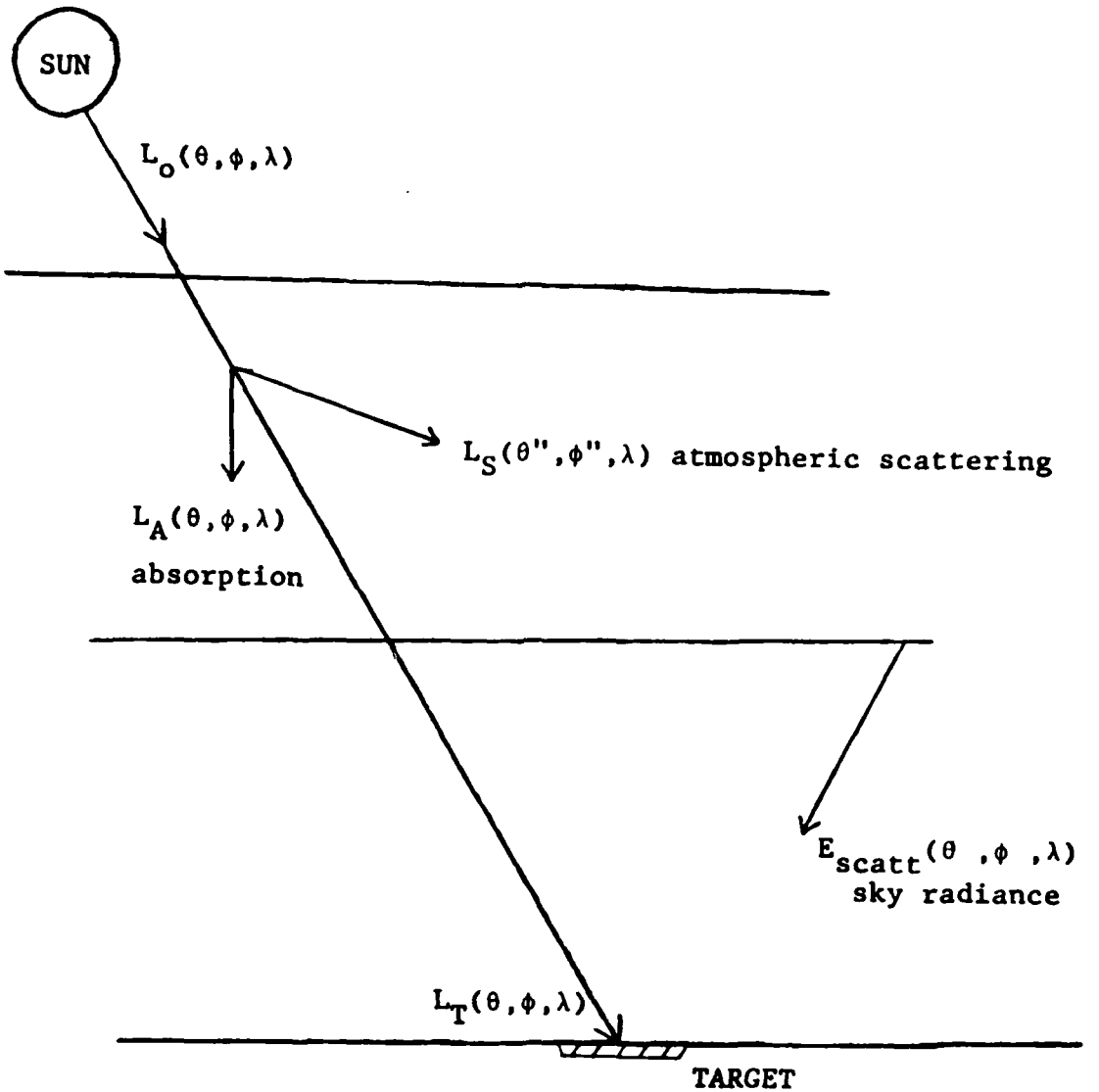
SUN
$L_o(\theta,\phi,\lambda)$
$L_S(\theta'',\phi'',\lambda)$ atmospheric scattering
$L_A(\theta,\phi,\lambda)$
absorption
$E_{scatt}(\theta,\phi,\lambda)$
sky radiance
$L_T(\theta,\phi,\lambda)$
TARGET

FIG. 2

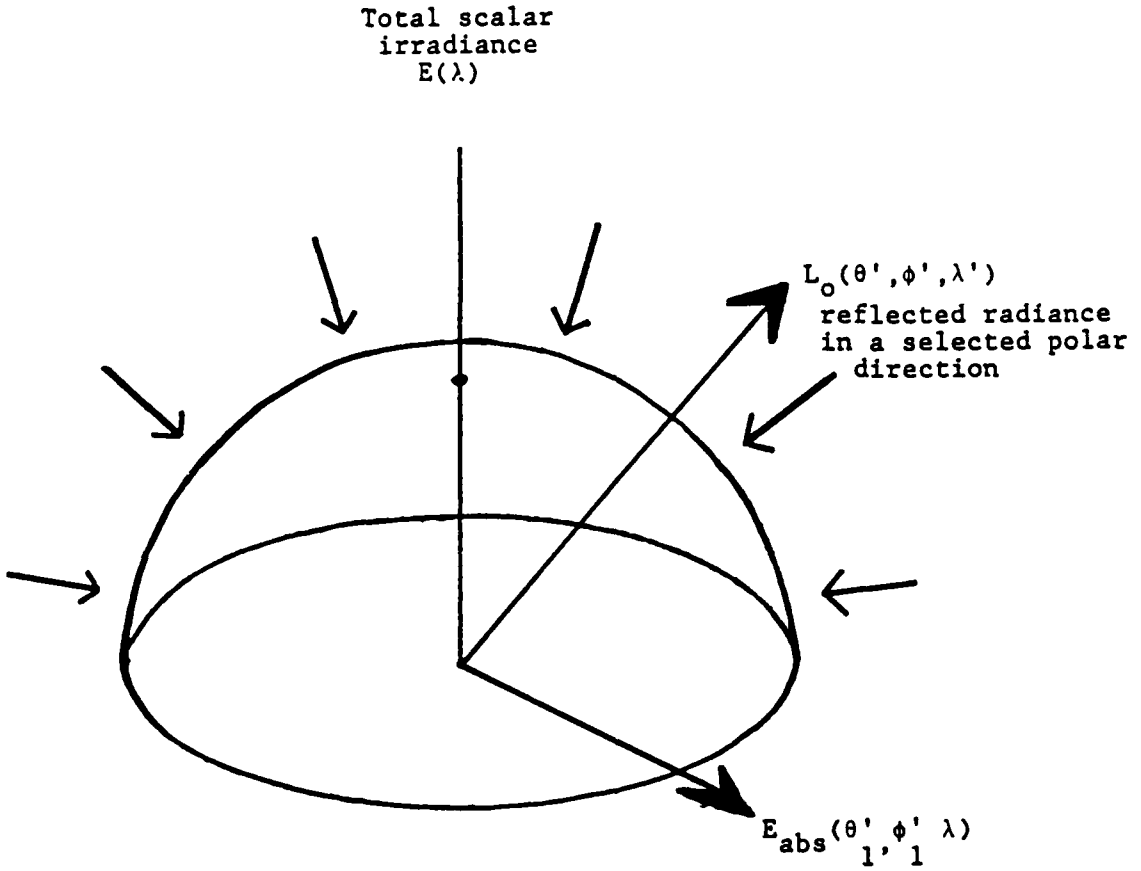
Total scalar
irradiance
E(λ)
$L_o(\theta',\phi',\lambda')$
reflected radiance
in a selected polar
direction
$E_{abs}(\theta'_1, \phi'_1, \lambda)$

Fig. 3.

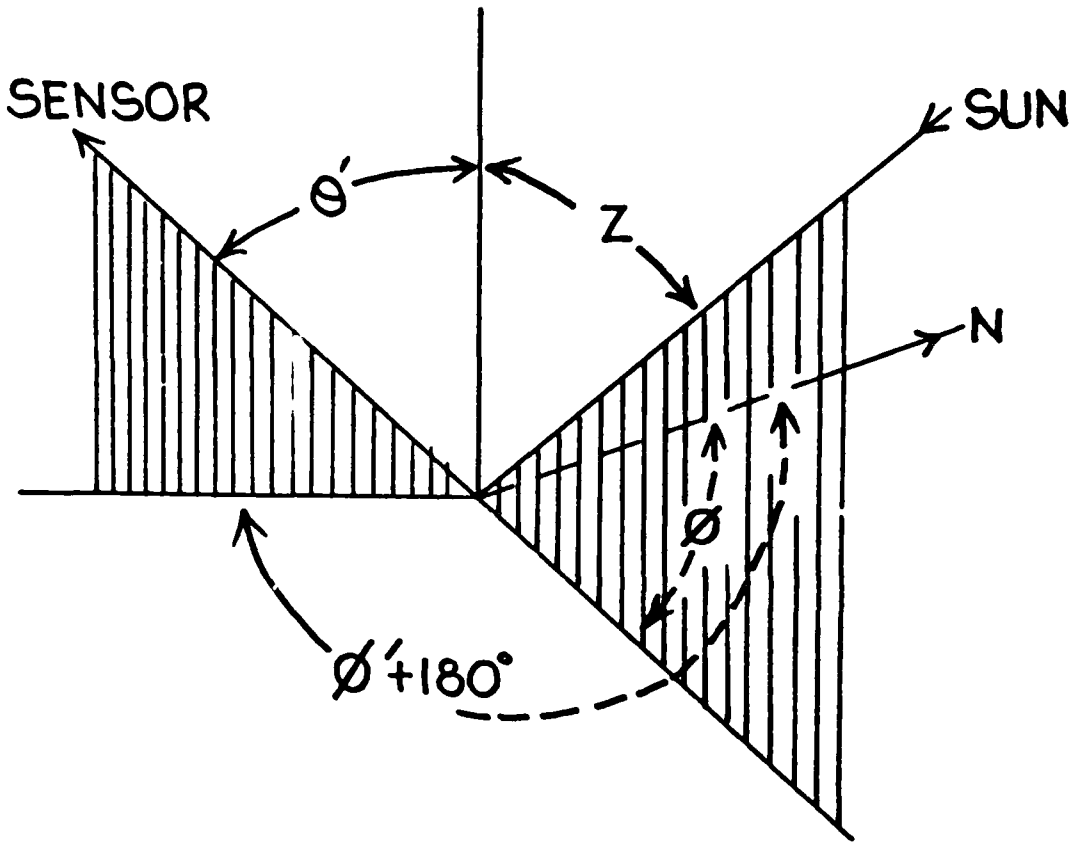

ø = solar azimuth
(ø′+180) = detector azimuth (view azimuth)
Z = solar zenith angle
θ′ = view zenith angle

Fig. 4.

REFLECTED TARGET RADIANCE

$$\begin{bmatrix}\text{SPECTRAL}\\ \text{RADIANCE}\\ \text{FROM}\\ \text{TARGET}\end{bmatrix} - \begin{bmatrix}\text{SPECTRAL}\\ \text{REFLECTED}\\ \text{SKY}\\ \text{RADIANCE}\end{bmatrix} + \begin{bmatrix}\text{SPECTRAL}\\ \text{REFLECTED}\\ \text{SOLAR}\\ \text{RADIANCE}\end{bmatrix}$$

$$L_R(\theta,\phi;\theta',\phi',\lambda) = \int_0^{\pi}\int_0^{\pi} R(\theta,\phi;\theta',\phi',\lambda).\ E_{scatt}\ (\theta,\phi,\lambda)\ .d\theta\ .\ d\phi$$

$$+ L_T\ (\theta,\phi,\lambda).\ R\ (\theta,\phi;\theta',\phi',\lambda).$$

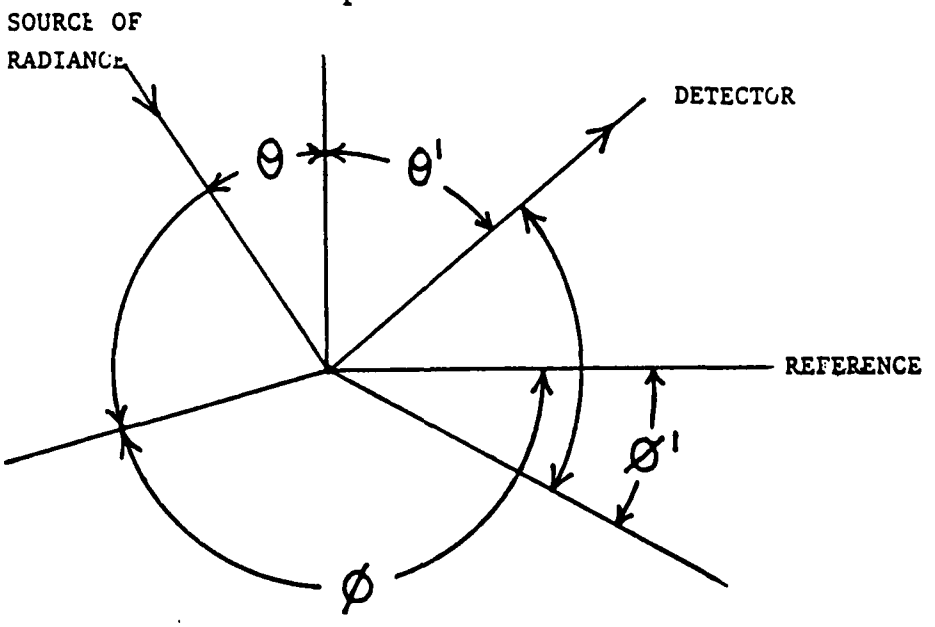

Fig. 5.

BIDIRECTIONAL REFLECTANCE FACTOR
AS A FUNCTION OF SCAN ANGLE AND WAVELENGTH
WHEAT AT 3.5 BOOT STAGE

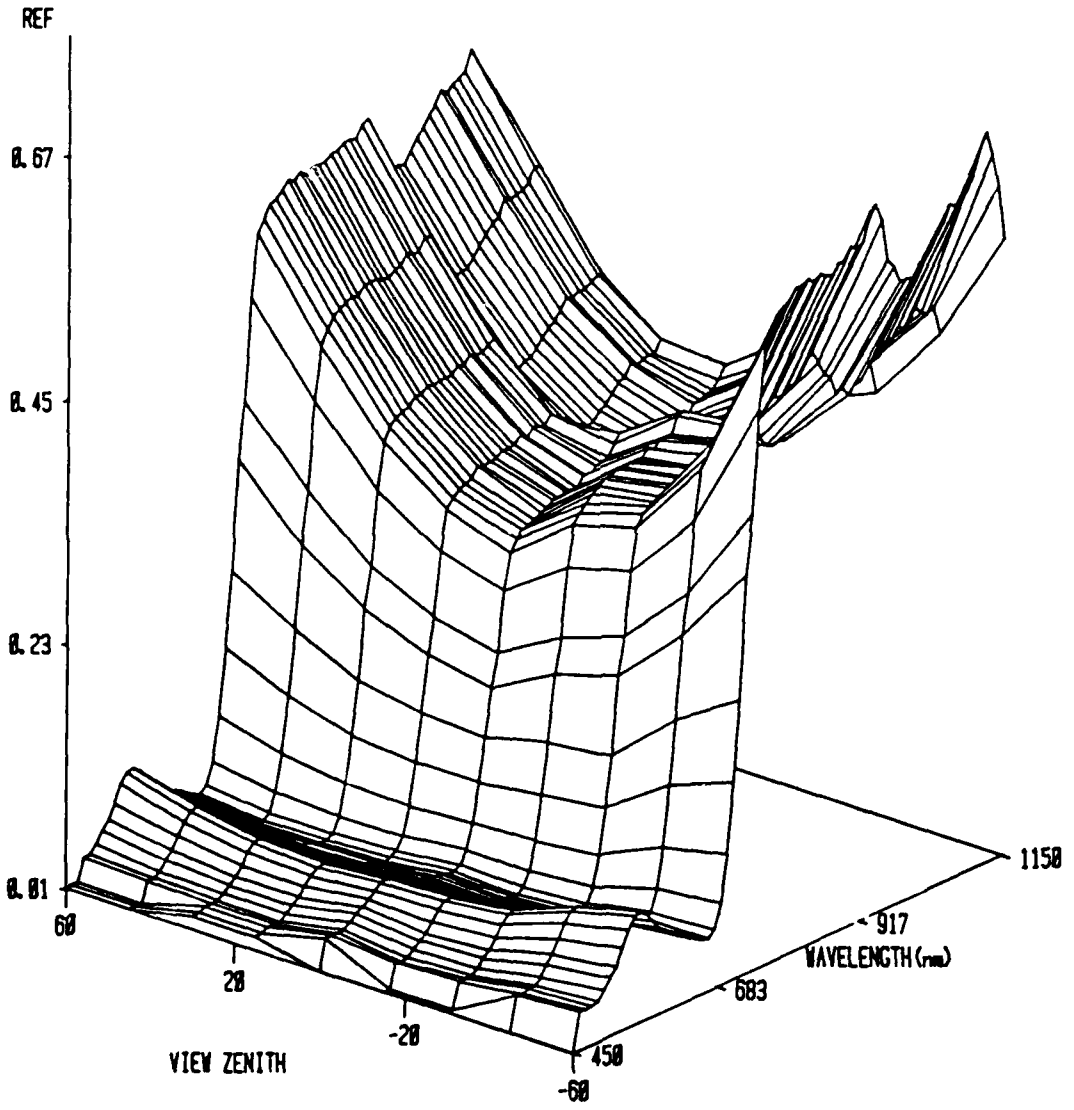

GRAPH NUMBER
VIEW ZENITH DOWNSUN=−60, UPSUN=+60

FIG. 6

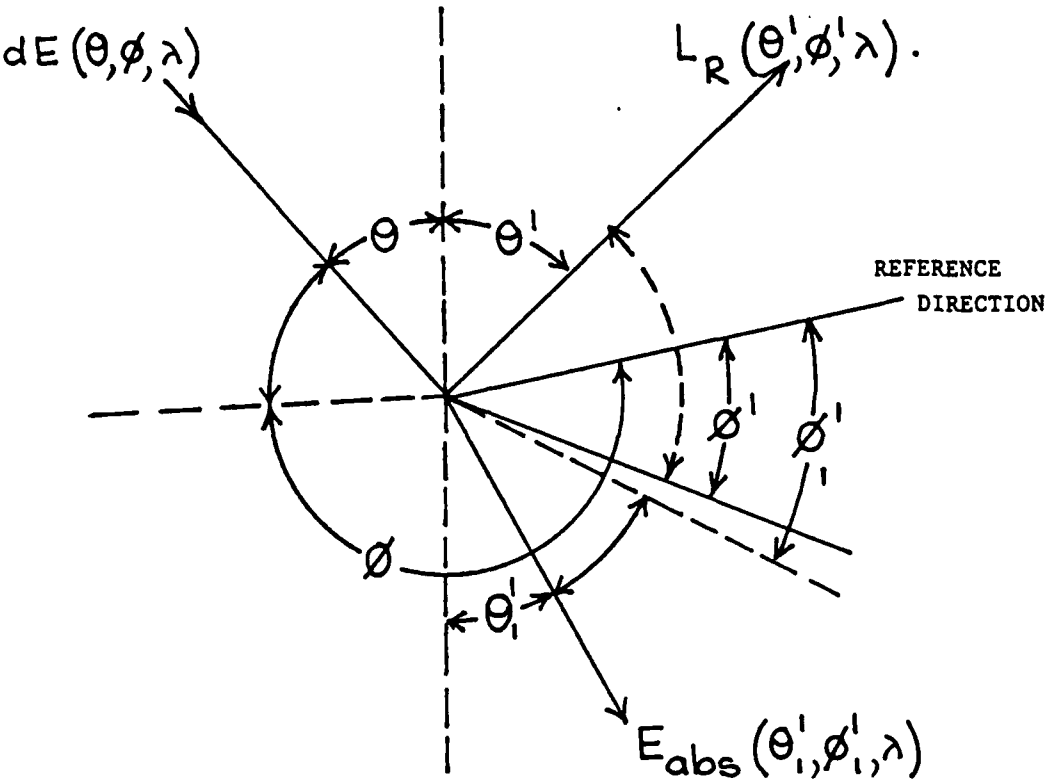

INCIDENT IRRADIANCE = REFLECTED RADIANCE + ABSORBED IRRADIANCE

$$E(\theta,\phi,\lambda) = \int_0^{\pi}\int_0^{\pi} L_R(\theta',\phi',\lambda)\ \mathrm{Cos}\ \theta'.d\theta'.d\phi' + \int_0^{\pi}\int_0^{\pi} E_{abs}(\theta'_i,\phi'_i,\lambda)\mathrm{Cos}\ \theta'_i.d\theta'_i.d\phi'_i$$

Fig. 7.

TRANSMITTED TARGET RADIANCE

$$\begin{bmatrix}\text{SPECTRAL}\\ \text{RADIANCE}\\ \text{INCIDENT}\\ \text{ON}\\ \text{DETECTOR}\end{bmatrix} = \begin{bmatrix}\text{TRANSMITTED}\\ \text{SPECTRAL}\\ \text{TARGET}\\ \text{RADIANCE}\end{bmatrix} + \begin{bmatrix}\text{PATH RADIANCE}\\ \text{(OPTICAL REFLECTIVE)}\\ \text{OR}\\ \text{SELF RADIANCE}\\ \text{(THERMAL IR)}\end{bmatrix}$$

TARGET RADIANCE — EXTINCTION COEFFICIENT

$$L_D(\theta,\phi;\theta',\phi',\lambda) = L_R(\theta,\phi;\theta',\phi',\lambda)\ .\exp\left[-\int_0^z\int_0^{\pi}\int_0^{\pi} \beta'_{ext}(\theta'',\phi'',\lambda,z)\,.\,d\theta''.d\phi''.dz\right]$$

$$+\int_0^{\pi}\int_0^{\pi} L_{path}\ (\theta,\phi;\theta',\phi',\lambda)\ d\theta\,.\,d\phi$$

ADDITIVE RADIANCE TERM DUE TO ATMOSPHERIC RADIANCE

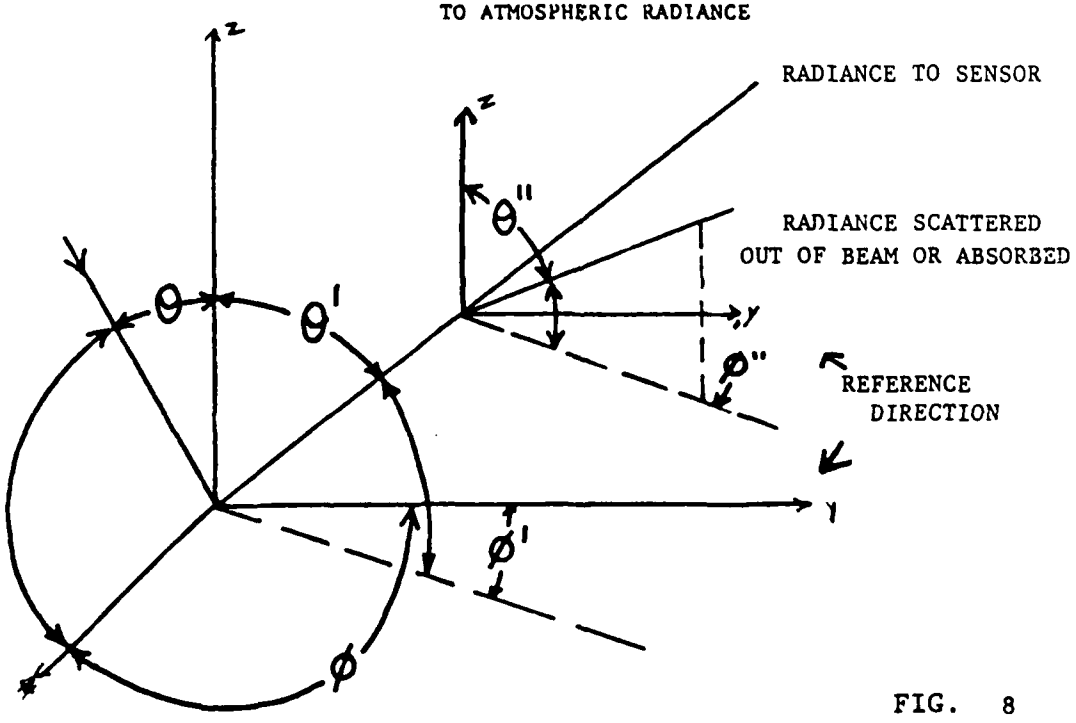

FIG. 8

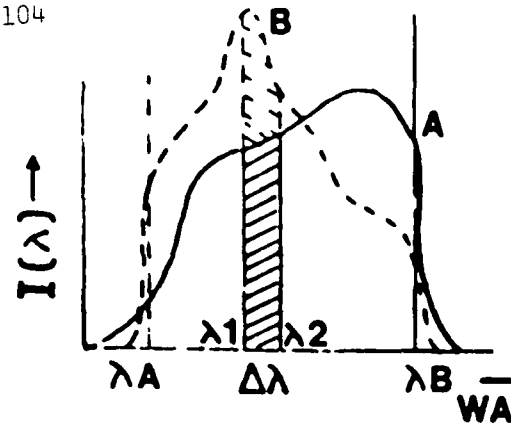

Spectral sensitivity of detector I(λ)

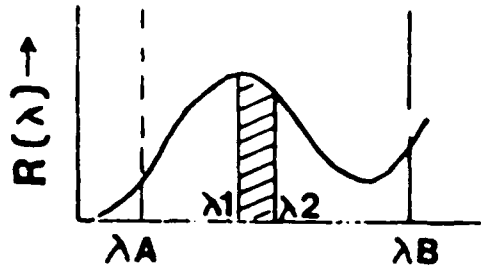

Spectral reflectance factor of target R(λ)

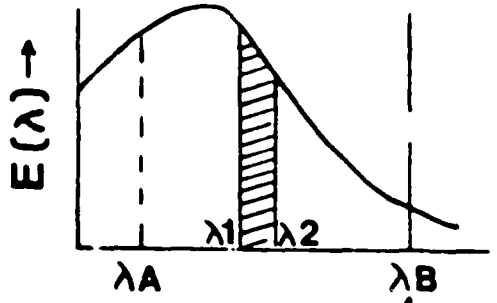

Spectral solar irradiance on target E(λ)

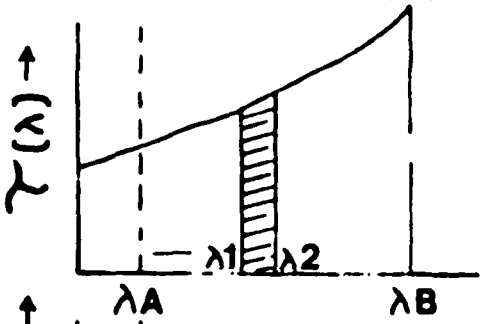

Spectral atmospheric transmission τ(λ)

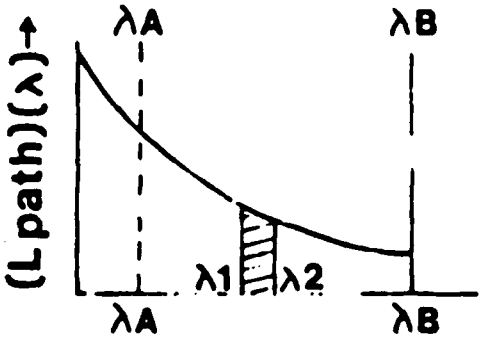

Spectral atmospheric path radiance (Lpath)(λ)

FIG. 9

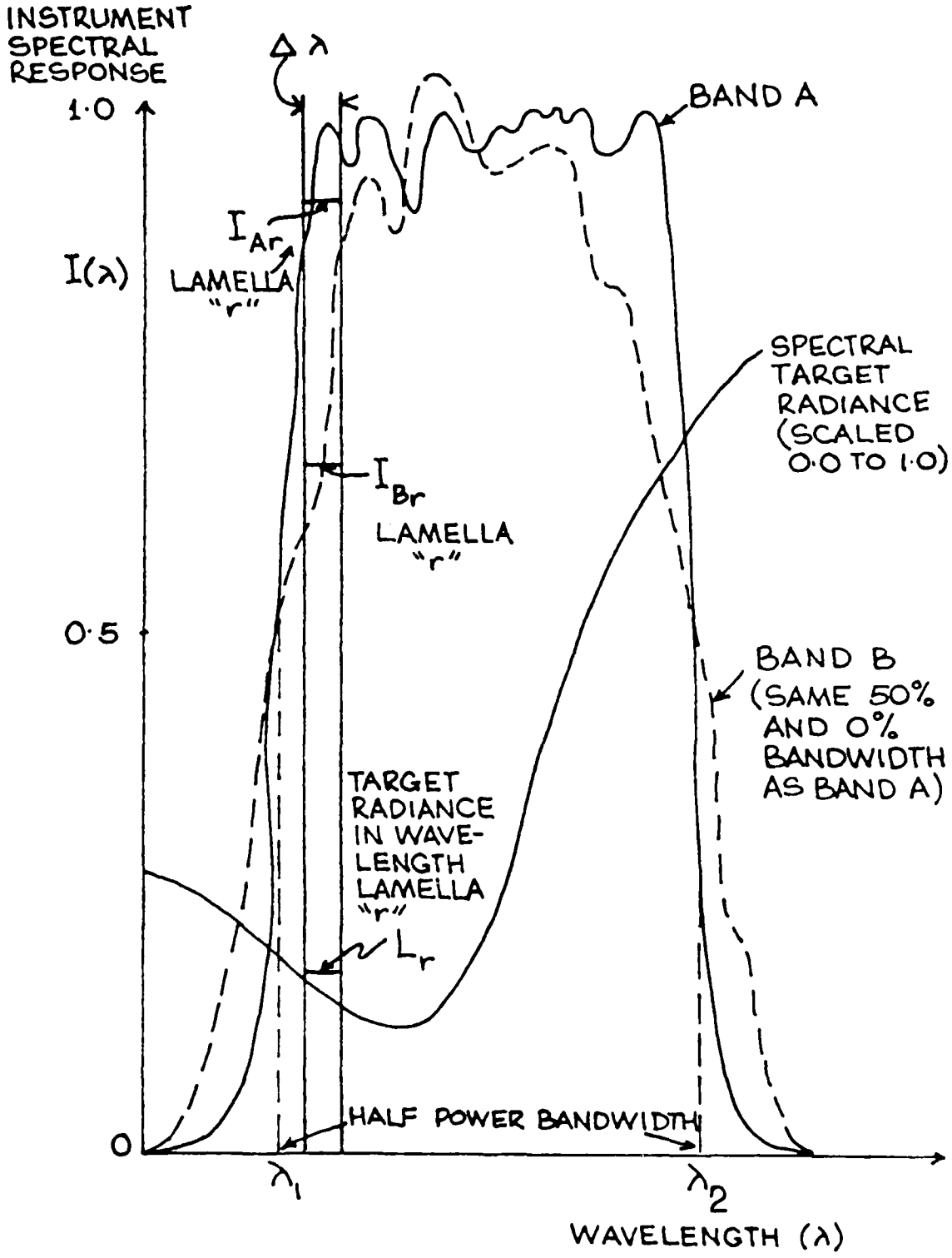

NOTE: $I_{Ar} \times L_r > I_{Br} \times L_r$

FIG. 10

DISCRIMINATION FUNCTION
SINGLE BAND DATA (11-12 MICRONS)
Atmospheric Transmissivity = 1.0 Emissivity of Background = 0.9

B2

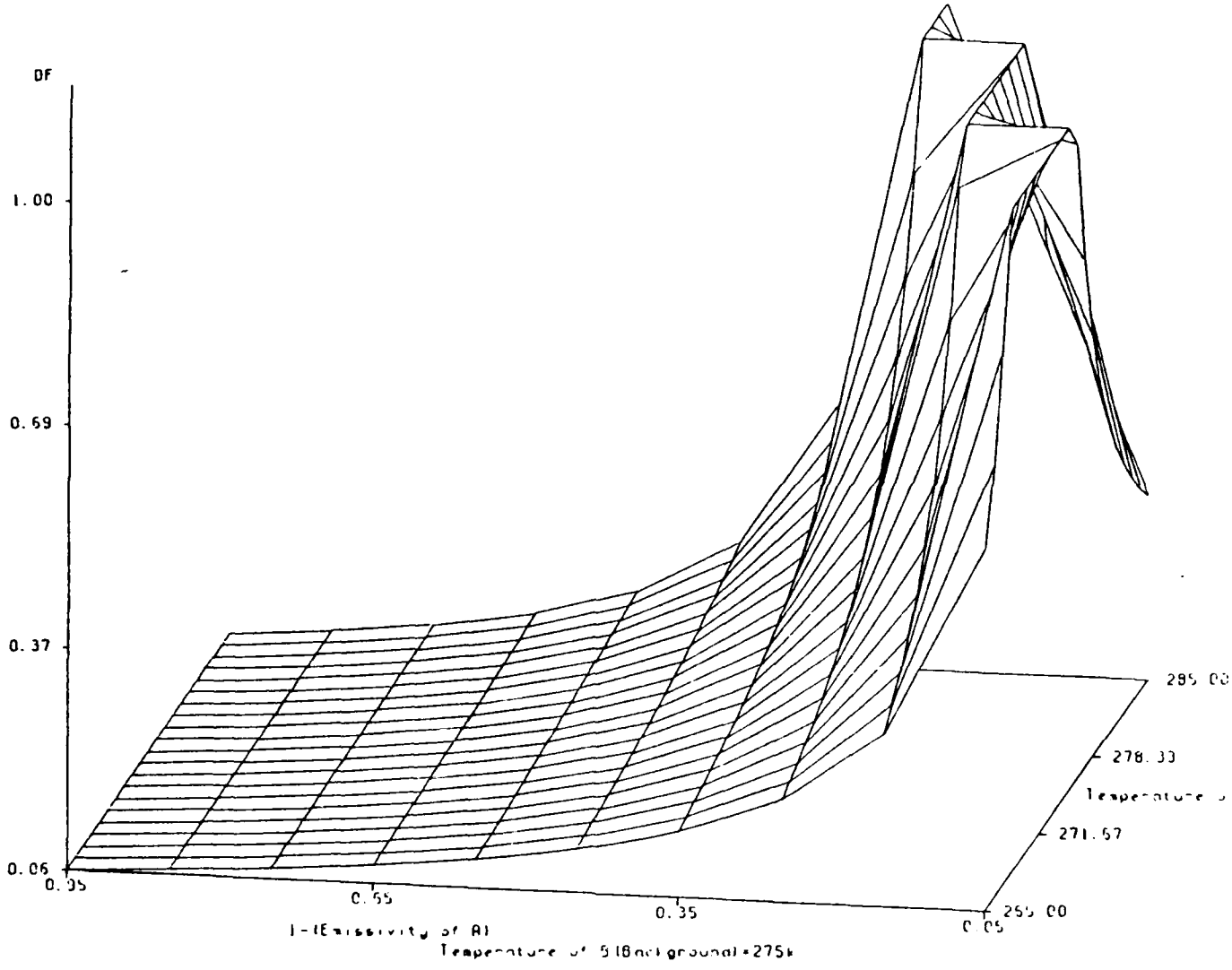

DISCRIMINATION FUNCTION
SINGLE BAND DATA (11-12 MICRONS)
Atmospheric Transmissivity= Emissivity of Background=0.0

B1

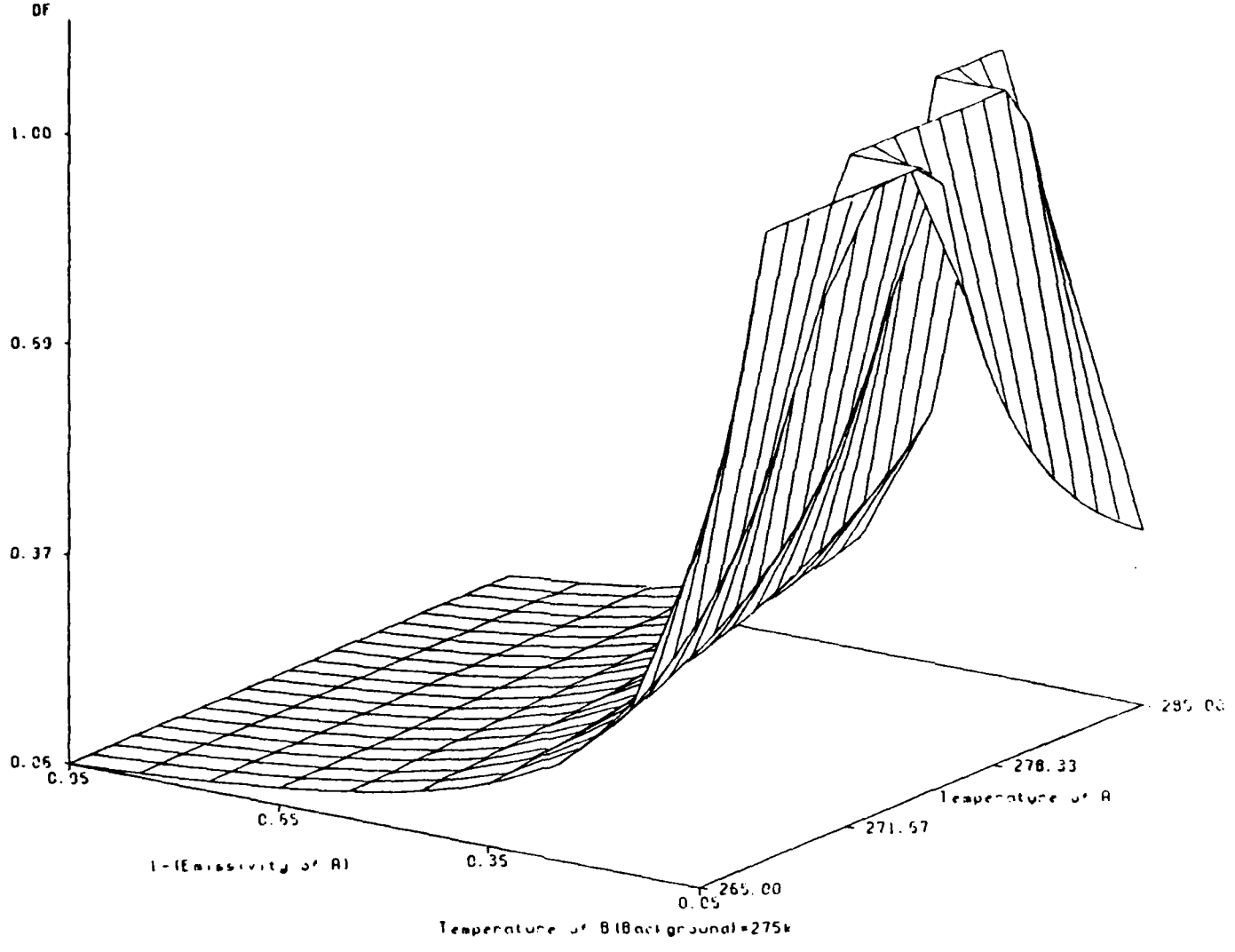

DISCRIMINATION FUNCTION
SINGLE BAND DATA (3.5-4.1MICRONS)
Atmospheric Transmission=0.7 Emissivity of B(Background)=0.35

A6

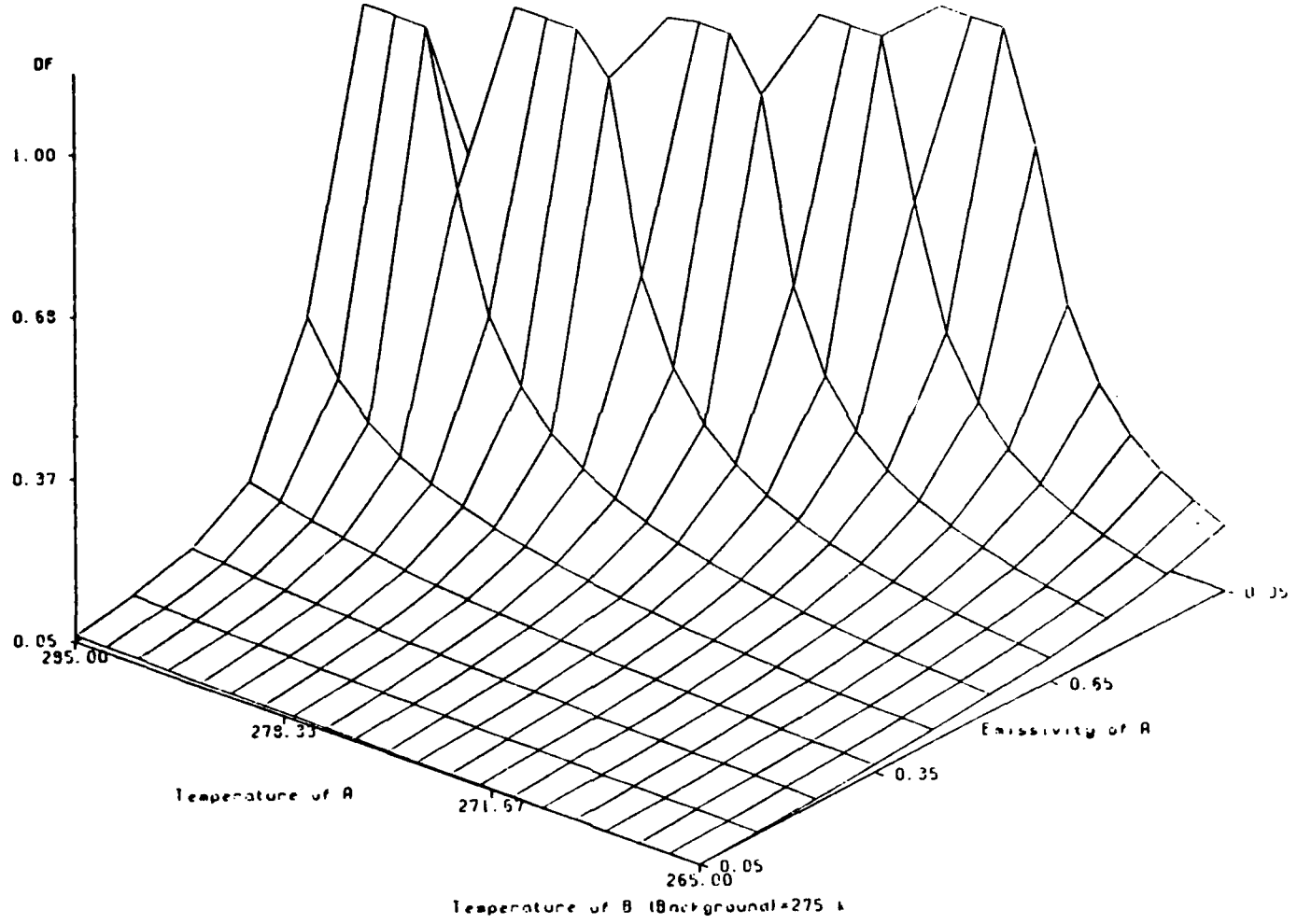

A5

DISCRIMINATION FUNCTION
SINGLE BAND DATA (3.5–4.1 MICRONS)
Atmospheric Transmission=0.7 Emissivity of Background=0.85

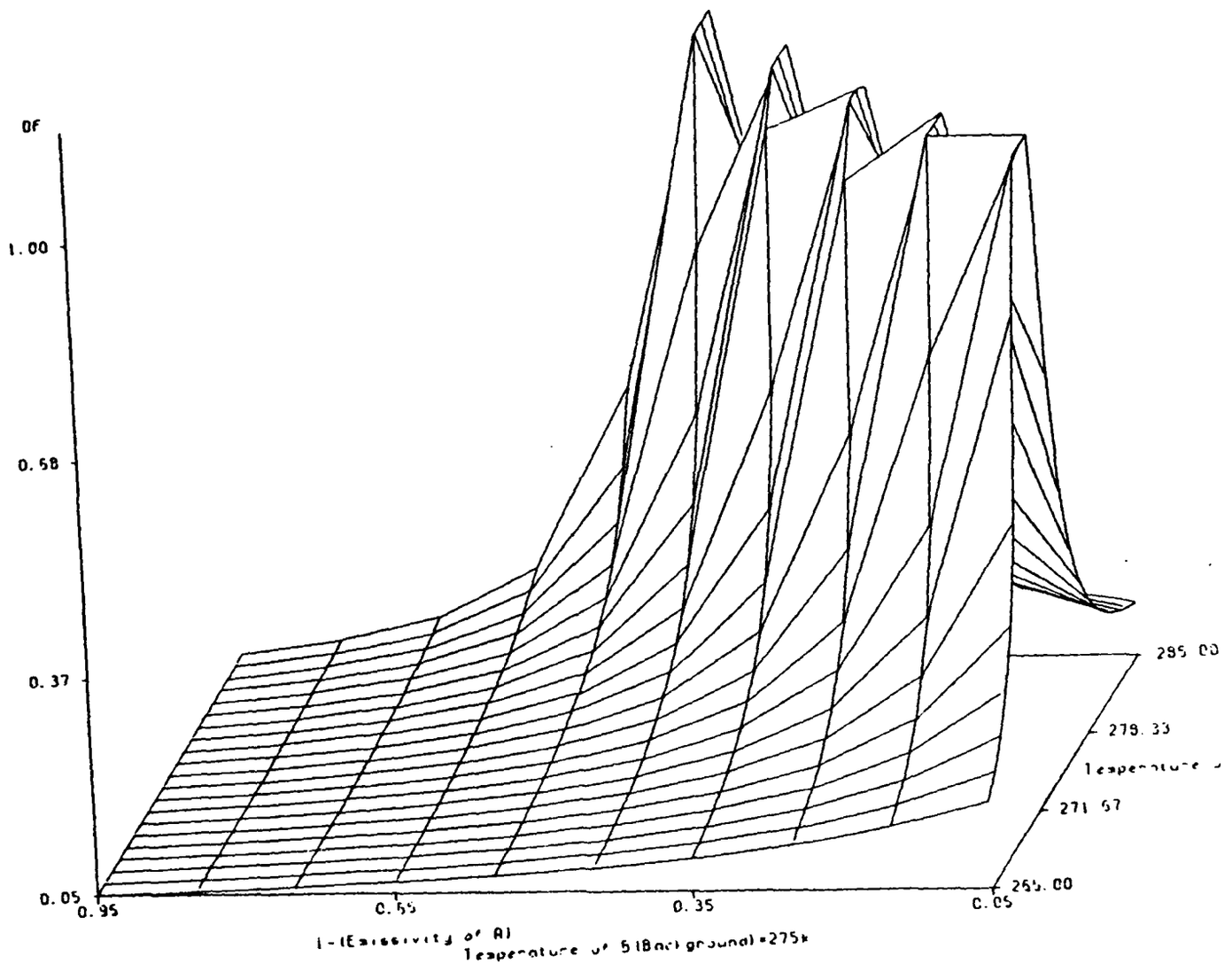

DISCRIMINATION FUNCTION
SINGLE BAND DATA (3.5-4.1 MICRONS)
Atmospheric Transmission=0.7 Emissivity of B(Background)=0.85

A4

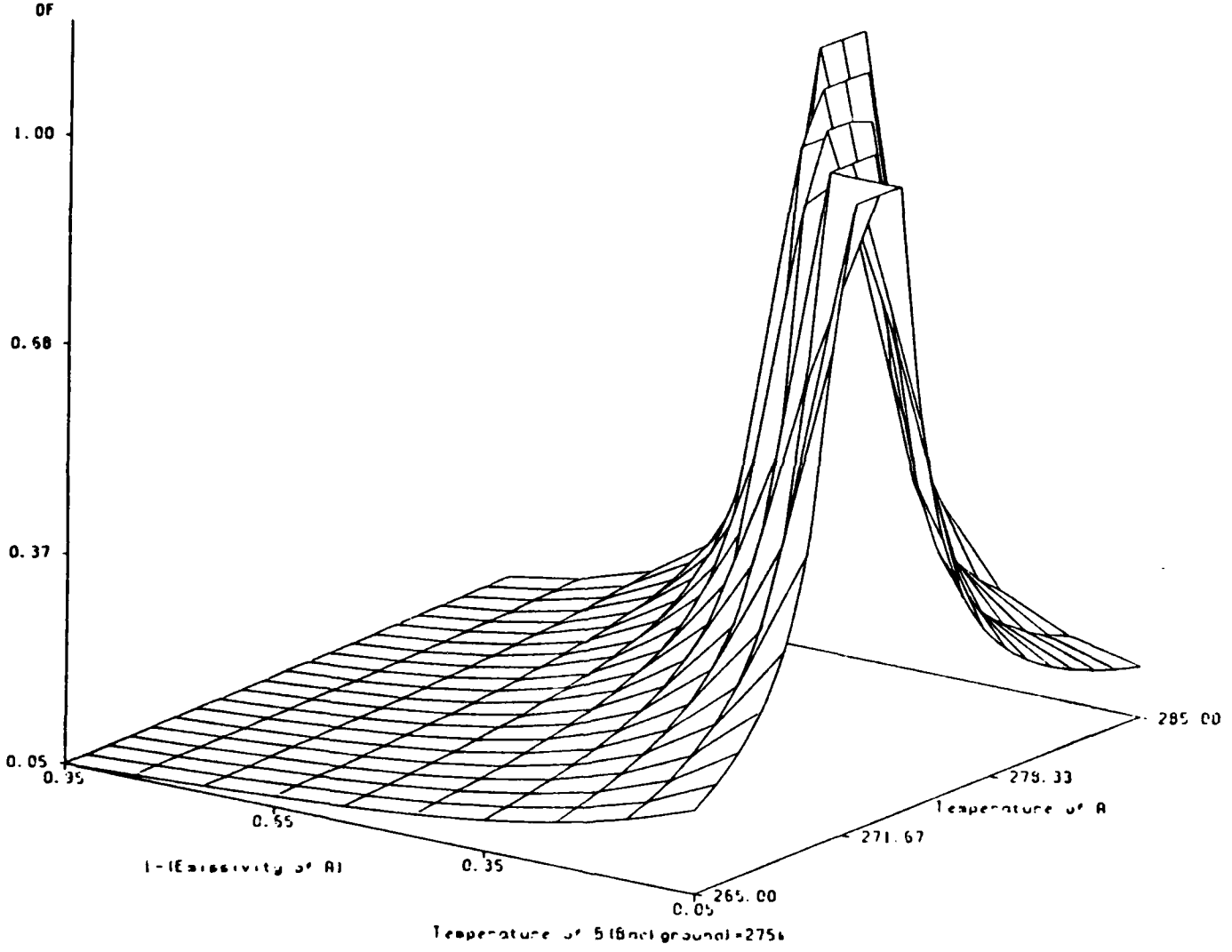

DISCRIMINATION FUNCTION
SINGLE BAND DATA (3.5-4.1MICRONS)
Atmospheric Transmissions=1 Emissivity of B(Background)=0.9

A3

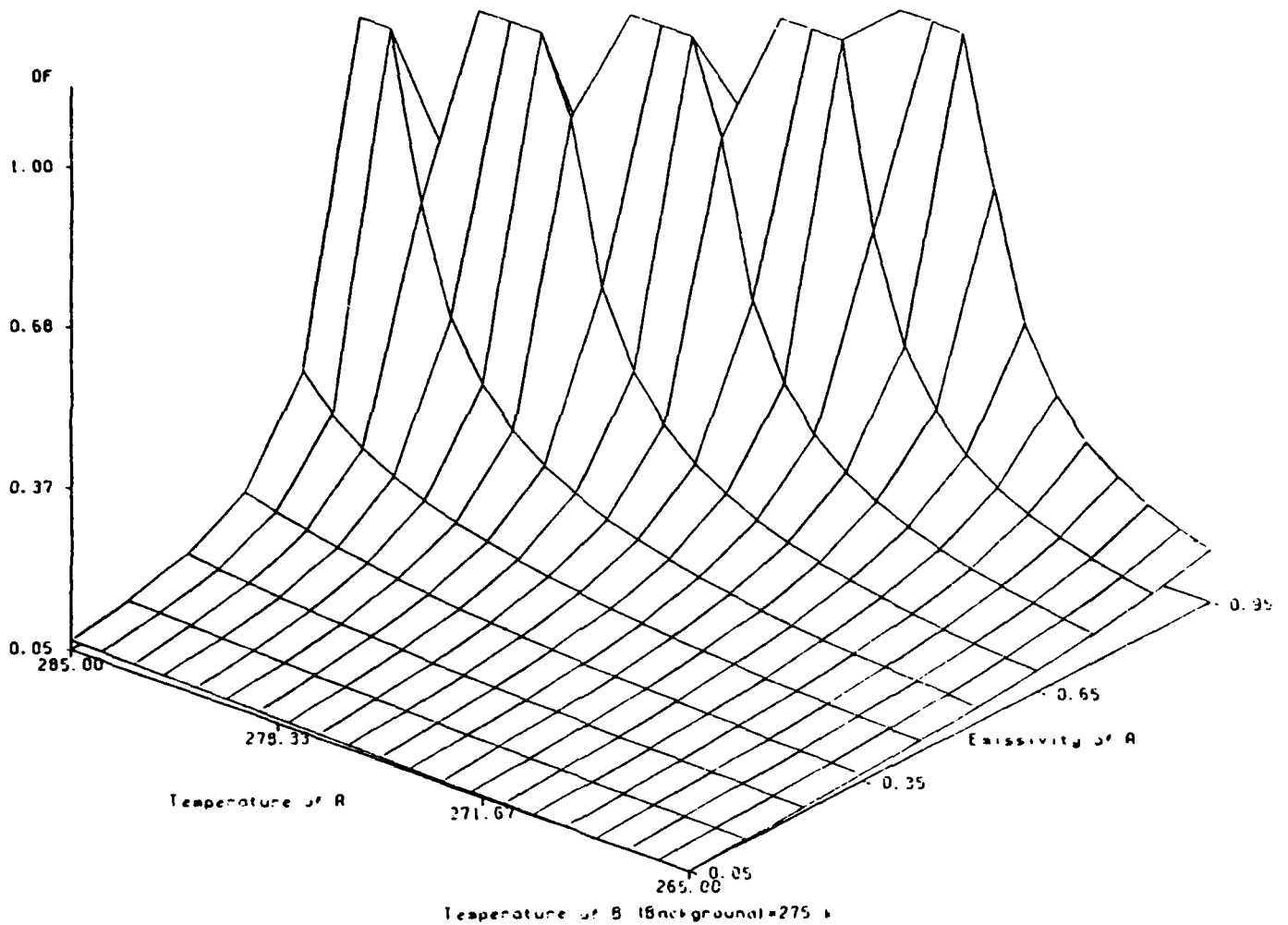

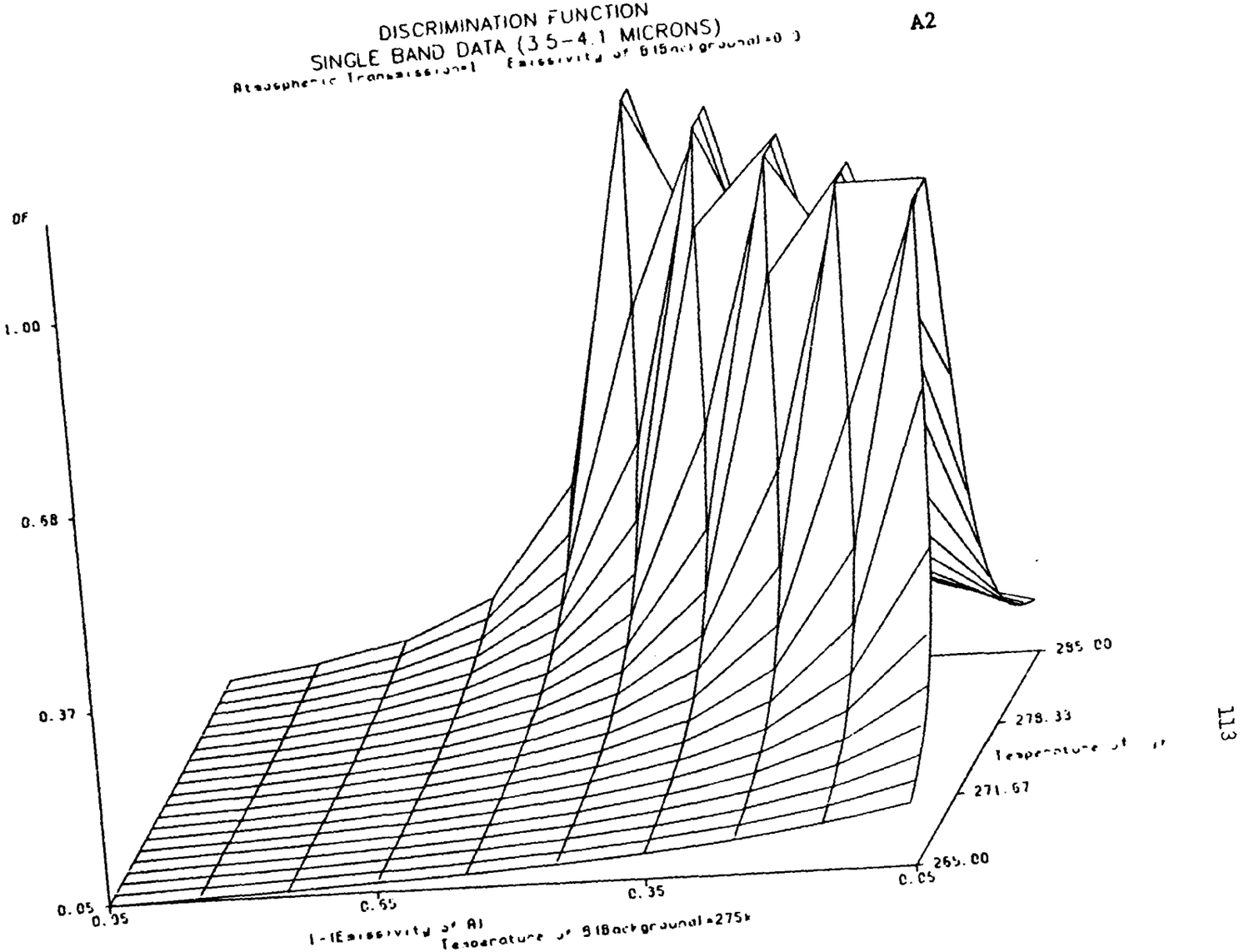
DISCRIMINATION FUNCTION
SINGLE BAND DATA (3.5-4.1 MICRONS)
A2
DF
1.00
0.68
0.37
0.05
0.05
0.35
0.65
0.95
1-(Emissivity of A)
Temperature of Background=275K
265.00
271.67
278.33
285.00

DISCRIMINATION FUNCTION
SINGLE BAND DATA (3.5–4.1 MICRONS)
Atmospheric Transmissivity = .51 Emissivity of Background = 0.5

Al

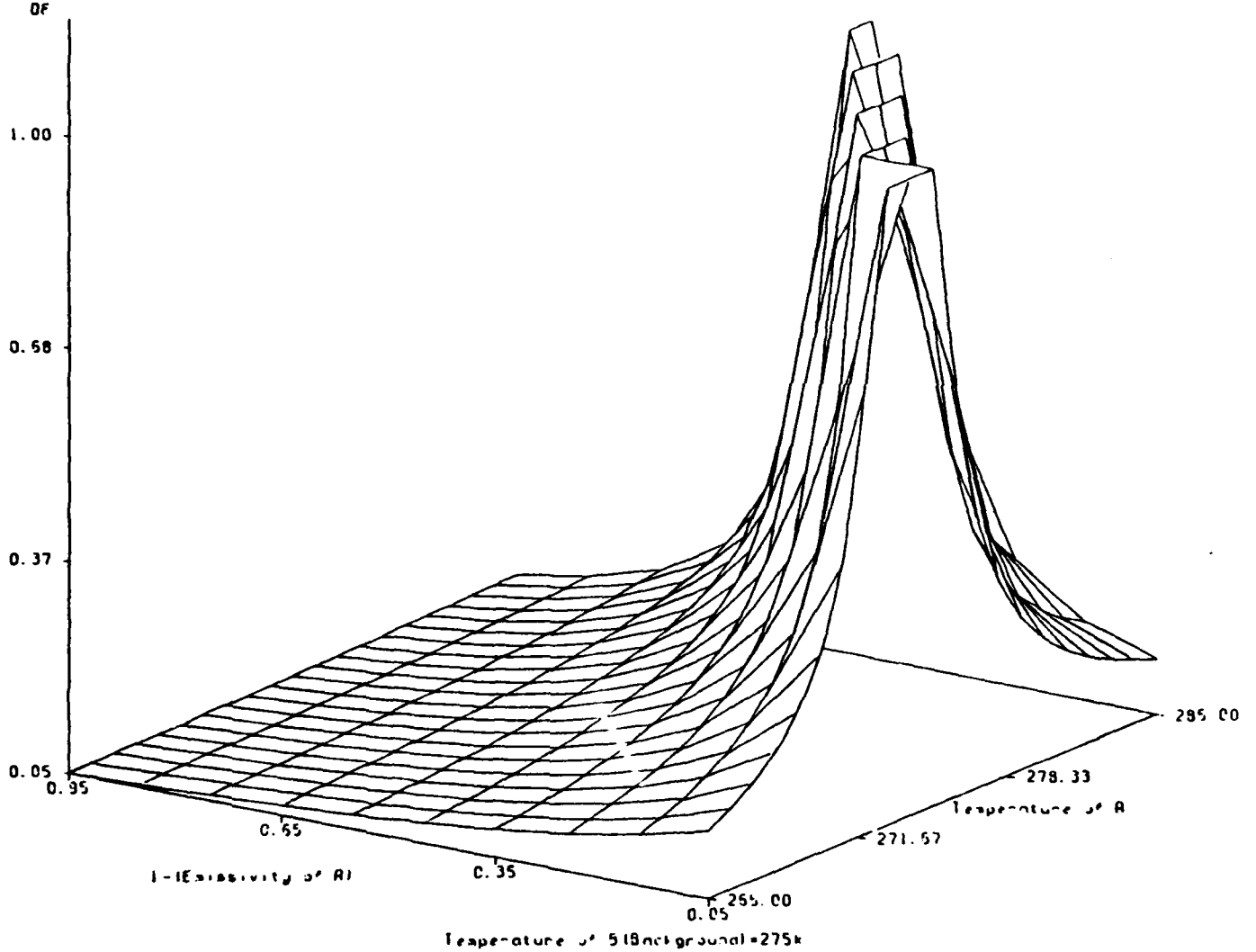

THERMAL IR CASE

$$\begin{bmatrix}\text{SPECTRAL}\\ \text{RADIANCE}\\ \text{AT}\\ \text{SENSOR}\end{bmatrix} = \begin{bmatrix}\text{SPECTRAL}\\ \text{TARGET}\\ \text{ELEMENT}\\ \text{EMISSIVITY}\\ \text{FOR GEOMETRY}\\ \text{CONSIDERED}\end{bmatrix} \times \begin{bmatrix}\text{BLACKBODY}\\ \text{RADIANT}\\ \text{EMITTANCE}\\ \text{AT TEMPERATURE}\\ \text{OF TARGET}\end{bmatrix} \times \begin{bmatrix}\text{ATMOSPHERIC}\\ \text{SPECTRAL}\\ \text{EXTINCTION}\\ \text{COEFFICIENT}\end{bmatrix}$$

$$+ \begin{bmatrix}\text{SPECTRAL}\\ \text{SKY RADIANCE}\end{bmatrix}$$

$$L_D(\theta',\phi',\lambda) = \varepsilon(\theta',\phi',\lambda) \times W(T,\lambda) \times \exp\left\{ \int_0^z \int_{-\pi}^{\pi} \int_0^{\pi} \beta'_{ext}(\theta'',\phi'',\lambda).d\theta''.d\phi''.dz \right\}$$

$$+ L_{sky}(\theta',\phi',\lambda)$$

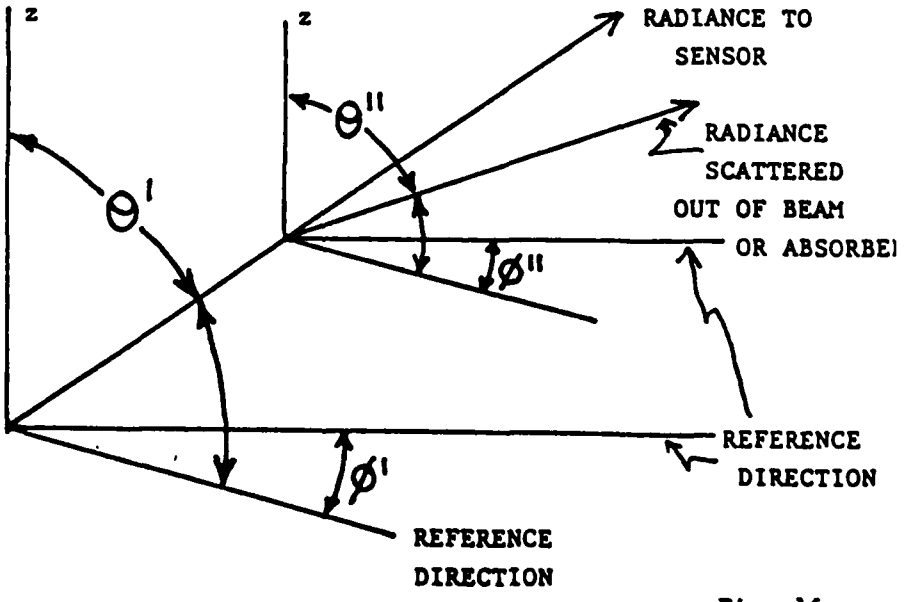

Fig. 16.

CONTRAST RATIO AS A FUNCTION OF SUB-I.F.O.V. CLOUD AND SCAN ANGLE

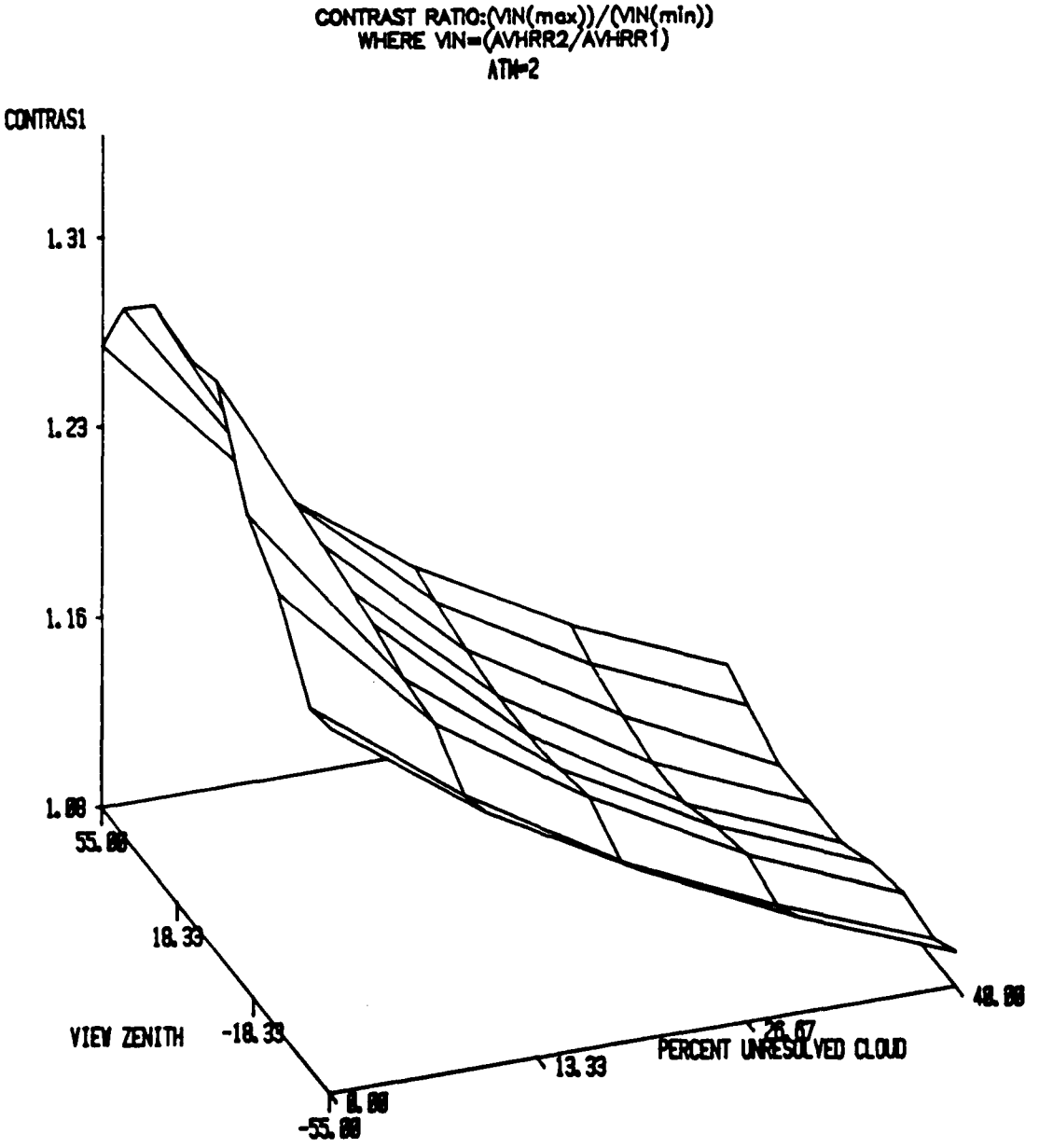

FIG. 15

3.5 BOOT ONLY (MAX/MIN) SOIL: DRY

CONTRAST RATIO AS A FUNCTION OF SUB-I.F.O.V. CLOUD AND SCAN ANGLE

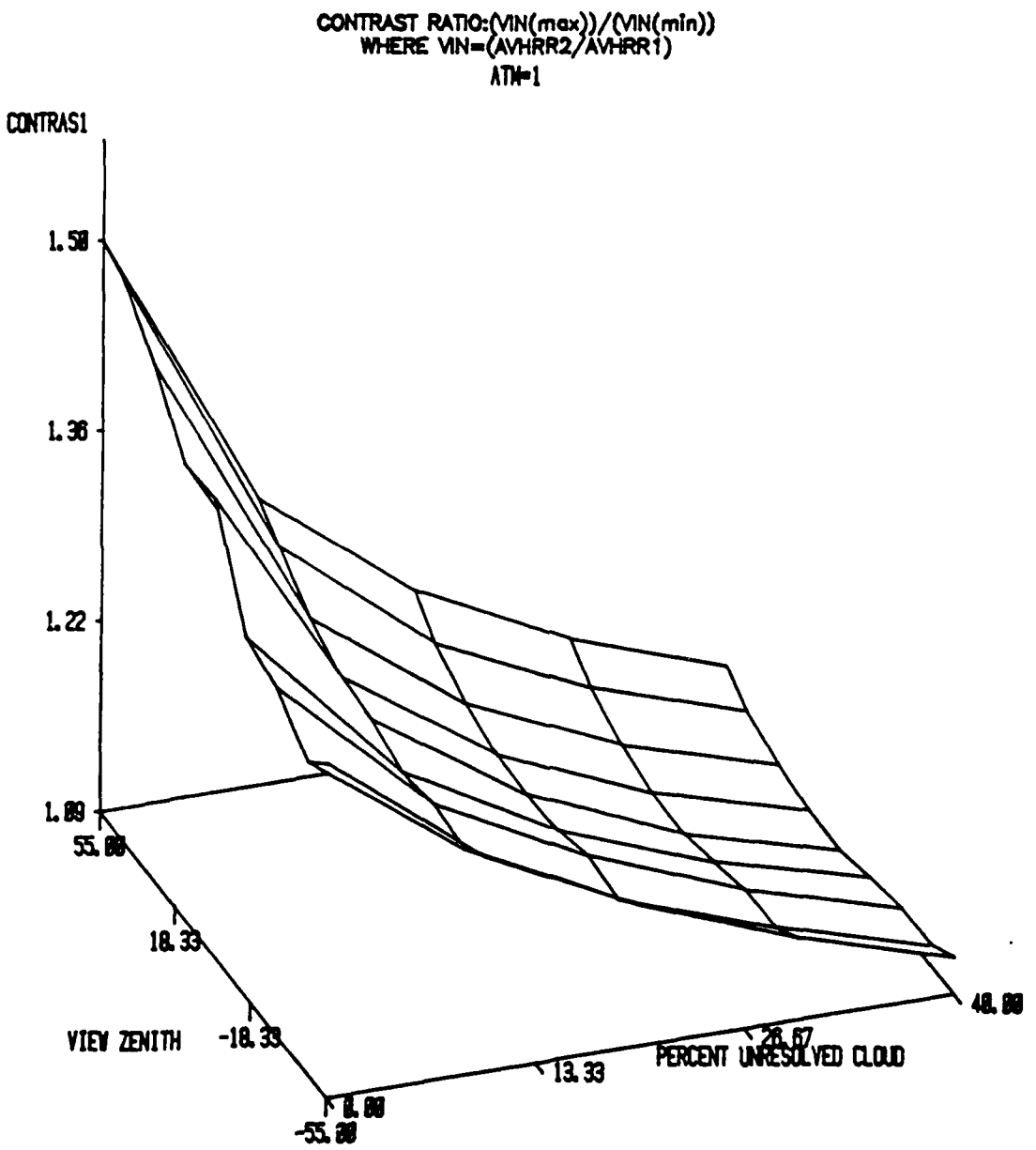

(ATM=1)=CLEAR ATMOSPHERE,(ATM=2)=TURBID
VIN(MAX)=100 WHEAT VIN(MIN)=70 WHEAT 30 SOIL
WHEAT AT 3.5 BOOT STAGE,WET SOIL

FIG. 14

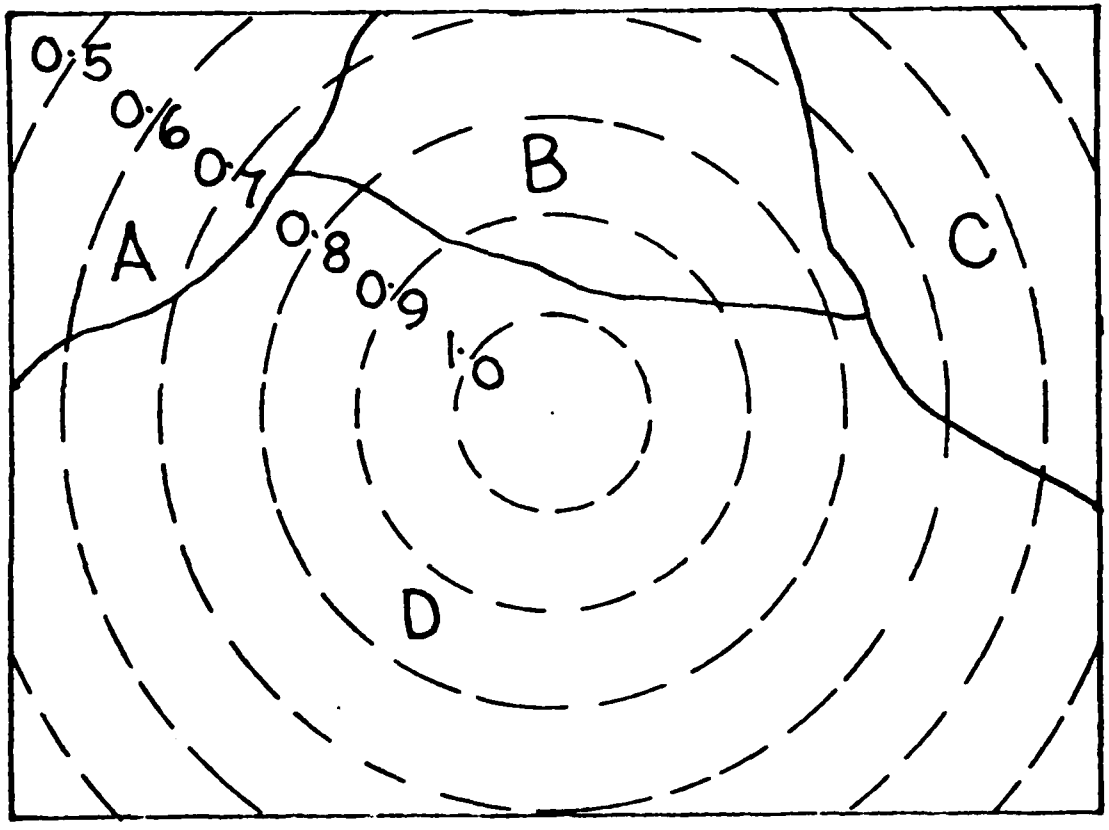

A TYPICAL MIXED PIXEL. ONE OF THE ELEMENTS MAY BE UNRESOLVED CLOUD. THE CONTOURS REPRESENT THE POINT-SPREAD FUNCTION OF THE SENSOR. THE RESPONSE OF THE SENSOR TO SPECTRAL RADIANCE FROM EACH ELEMENT DEPENDS UPON ITS POSITION IN THE IFOV.

FIG. 13

FIG. 12

2. THERMAL INFRARED REGION

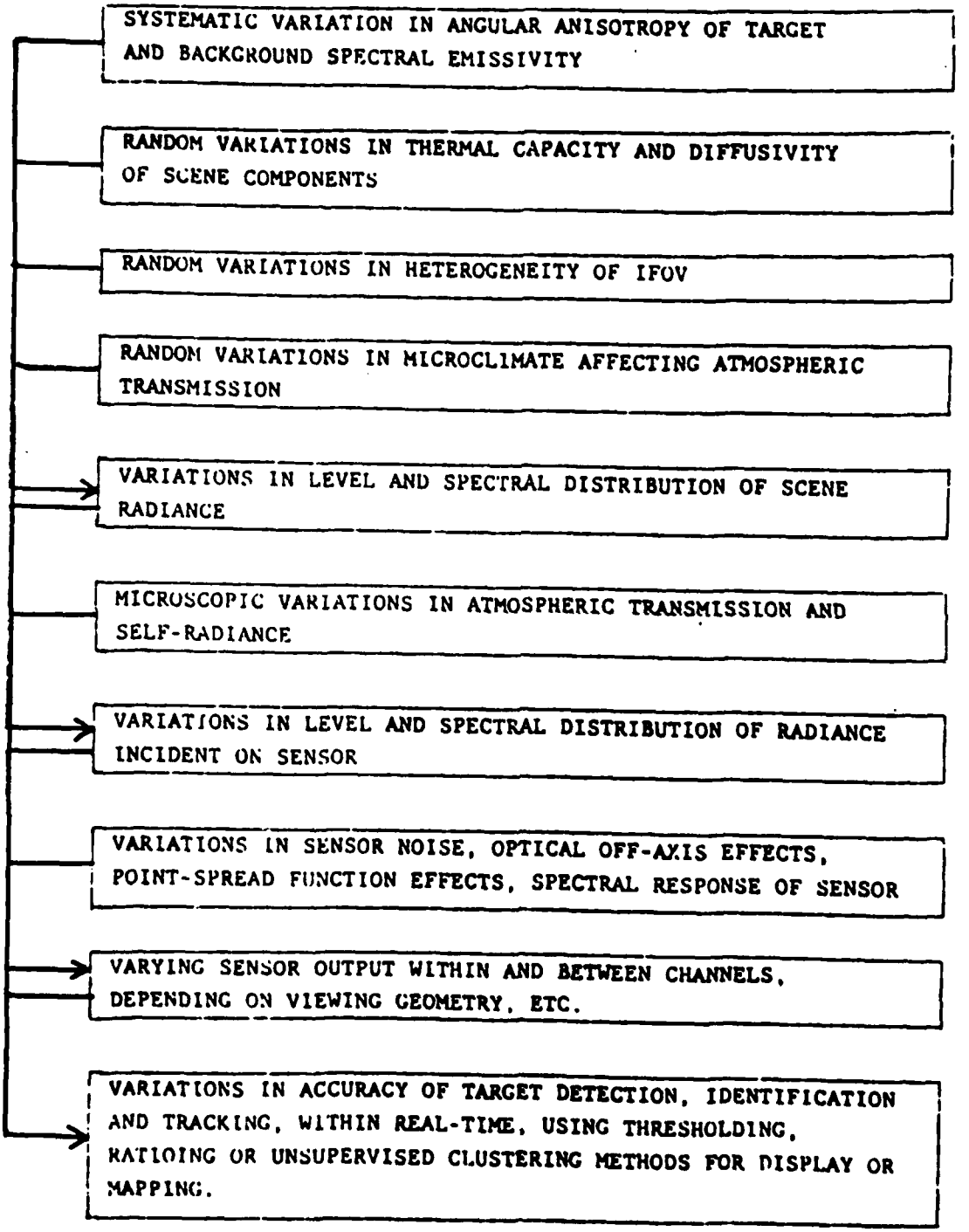

FIG. 11

1. OPTICAL-REFLECTIVE REGION

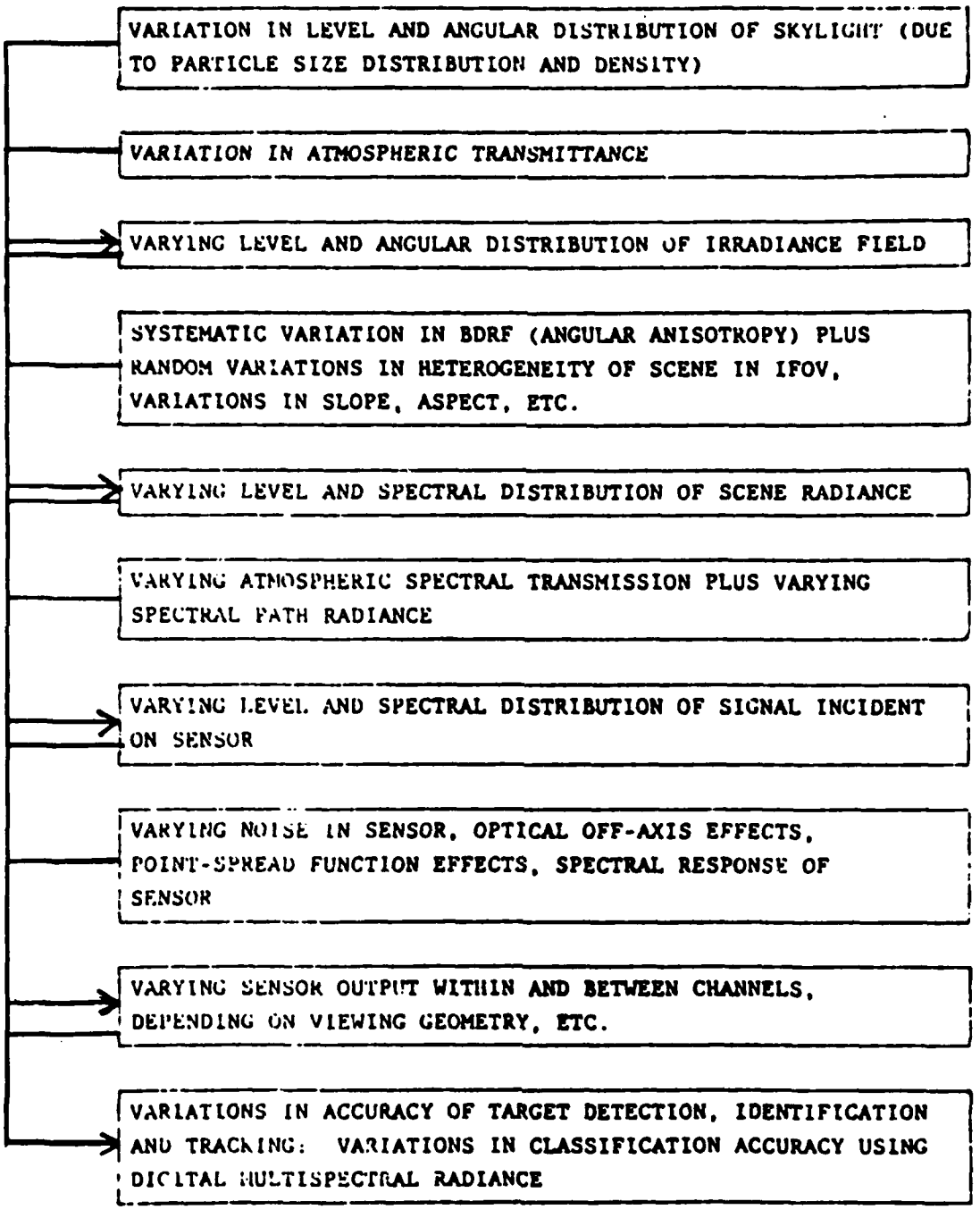

DISCRIMINATION FUNCTION
SINGLE BAND DATA (11-12MICRONS)
Atmospheric Transmissions1 Emissivity of B(Background)=0.9

B3

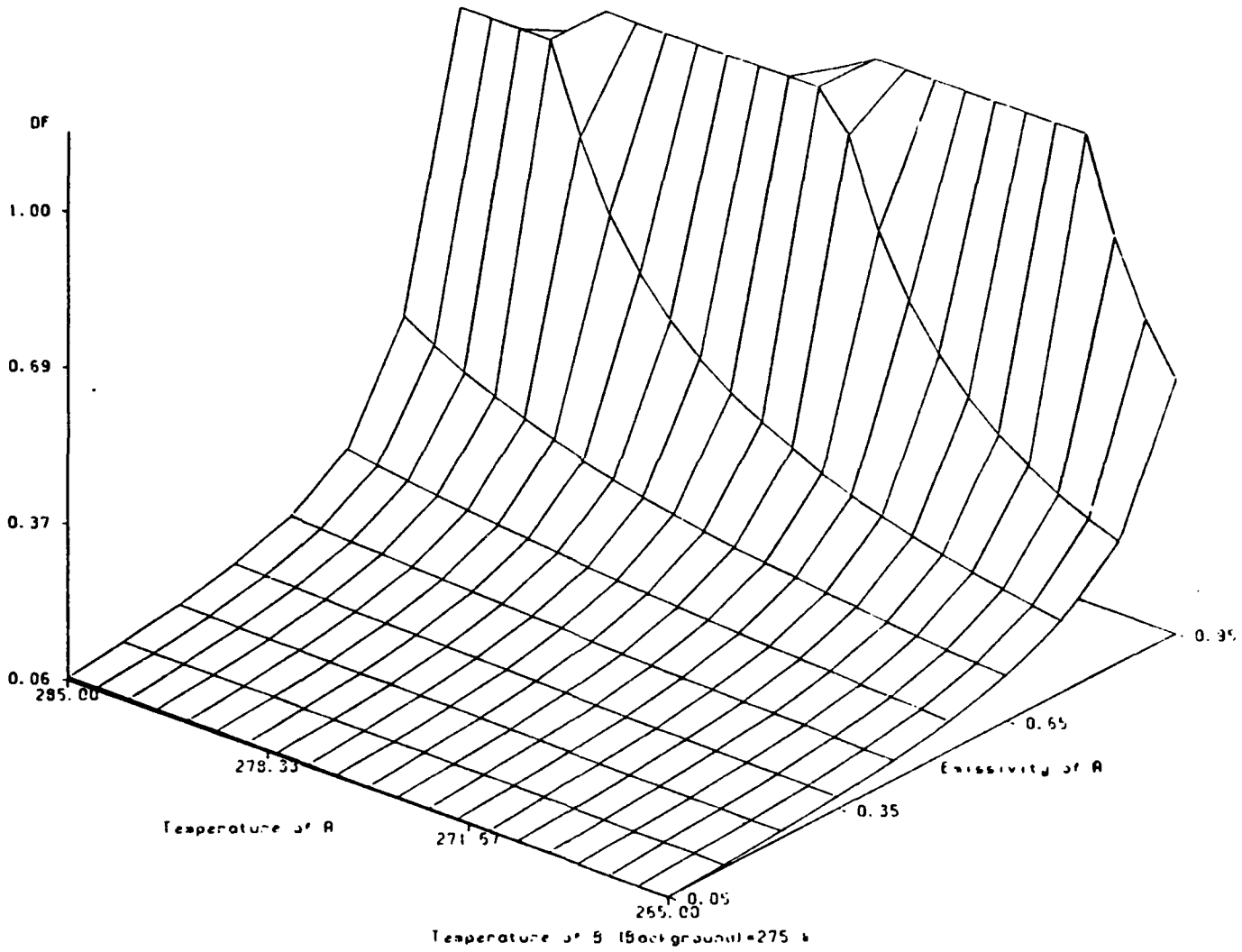

DISCRIMINATION FUNCTION
SINGLE BAND DATA (11-12 MICRONS)
Atmospheric Transmission=0.6 Emissivity of B(Background)=0.95

B4

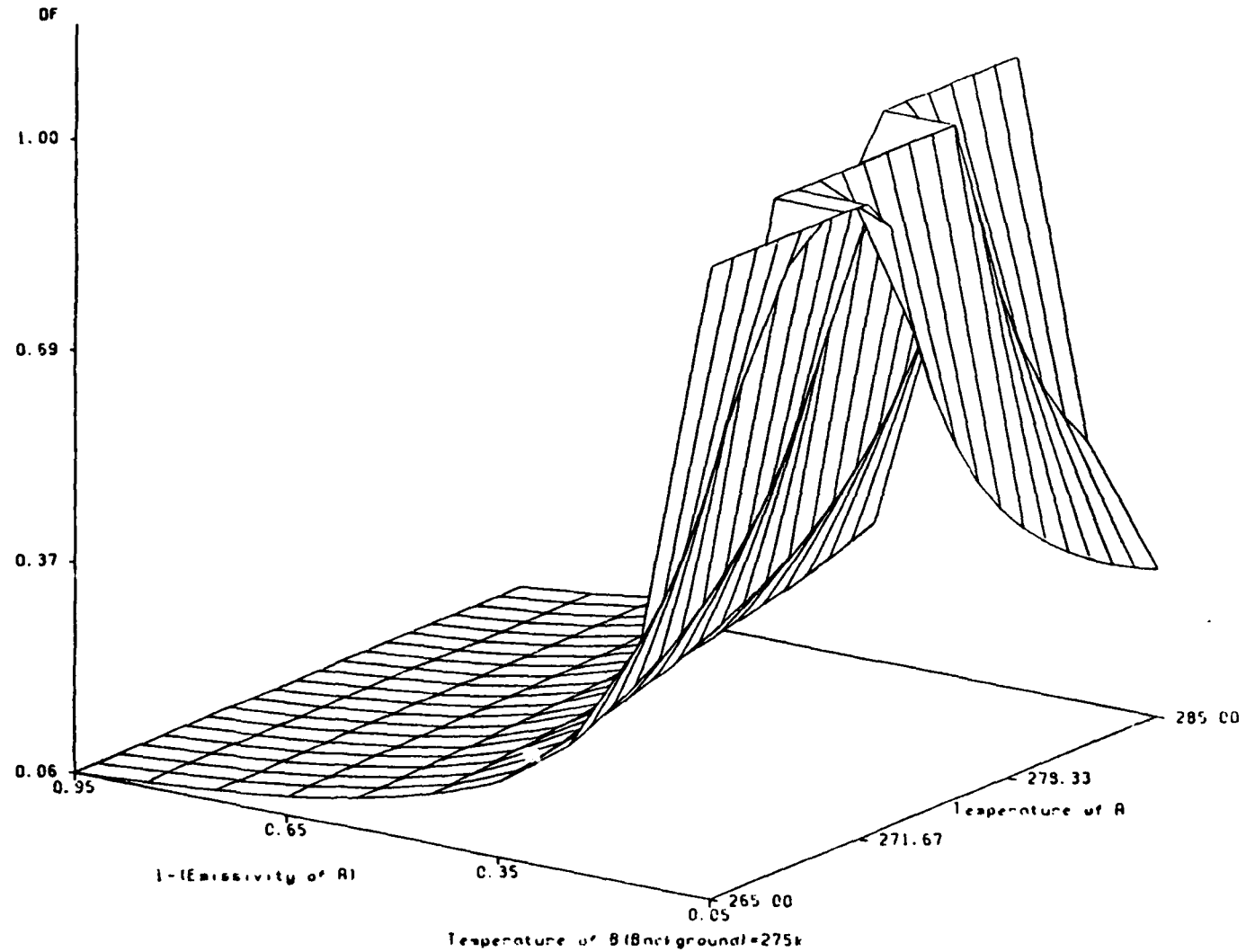

B5

DISCRIMINATION FUNCTION
SINGLE BAND DATA (11–12 MICRONS)
Atmospheric Transmission=0.6 Emissivity of Background=0.85

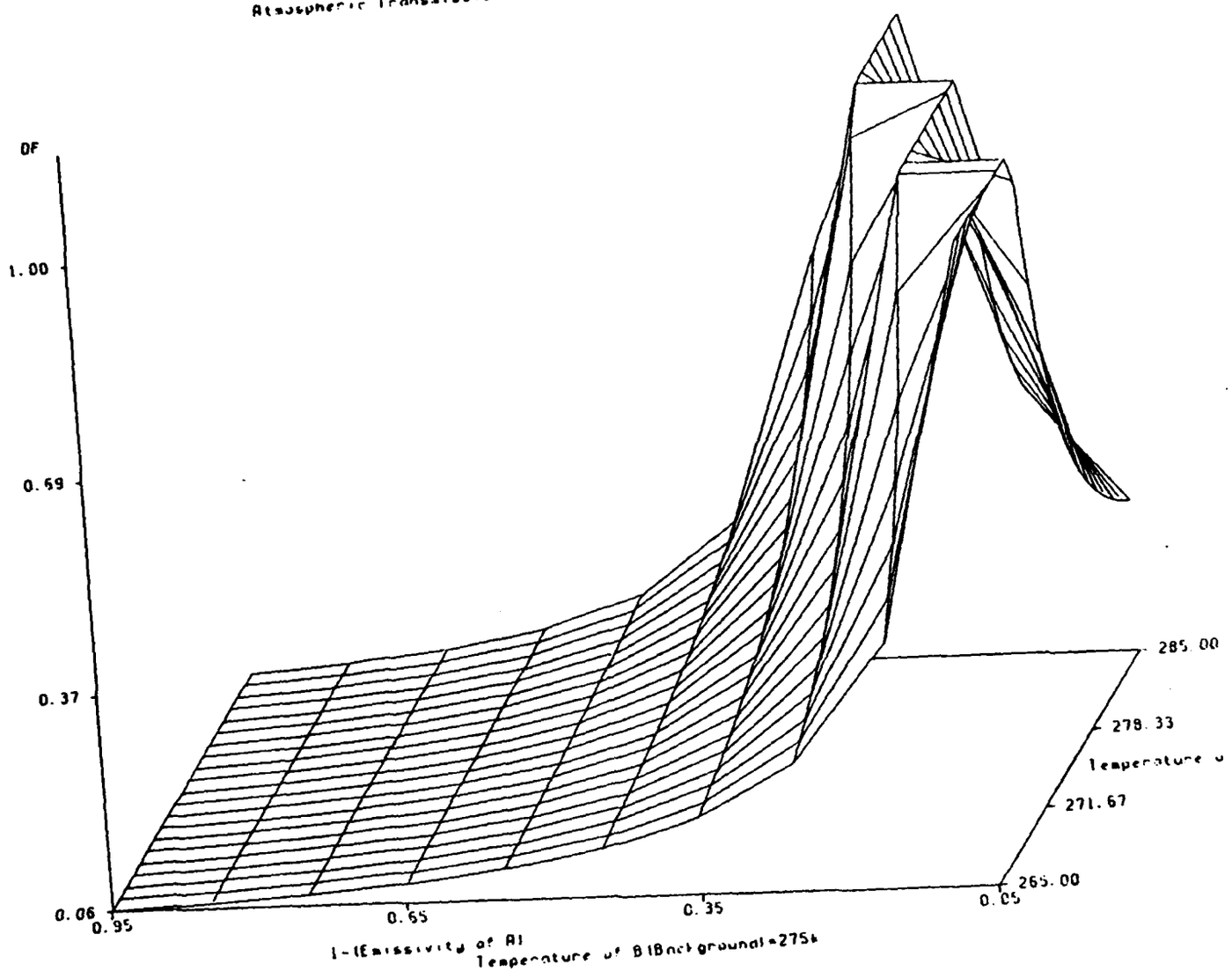

DISCRIMINATION FUNCTION
SINGLE BAND DATA (11-12MICRONS)
Atmospheric Transmission=0.6 Emissivity of Background=0.85

B6

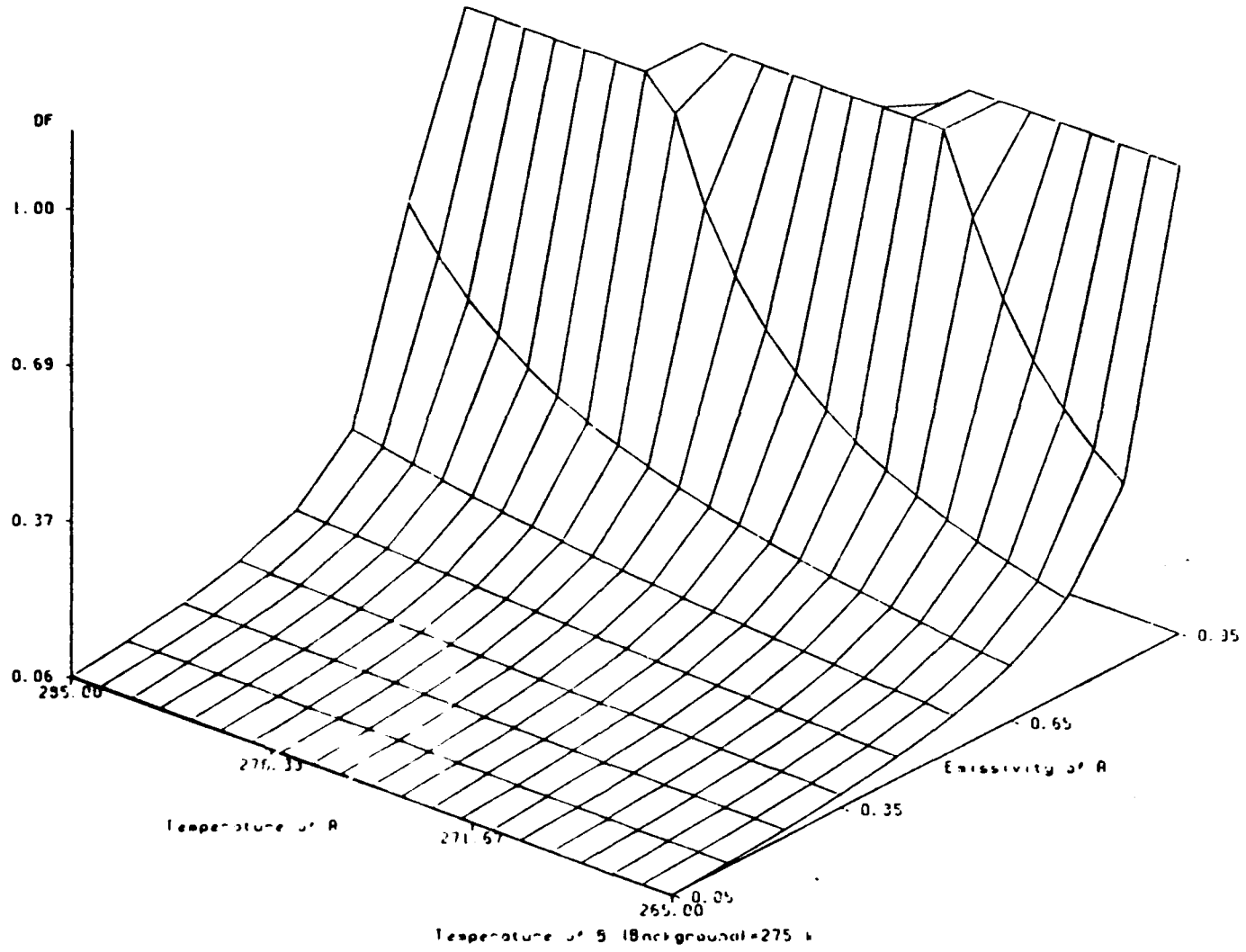

DEPENDENCE OF D.F. ON RELATIVE ATMOSPHERIC TRANSMISSION IN BANDS USED TO COMPUTE RADIANCE RATIO AND ON TEMPERATURE DIFFERENCE BETWEEN TARGET AND BACKGROUND

C1

Channel1 = 3.5 – 4.1 microns

Channel2 = 11 – 12 microns

Correlation Coefficient = 1

RUN=1

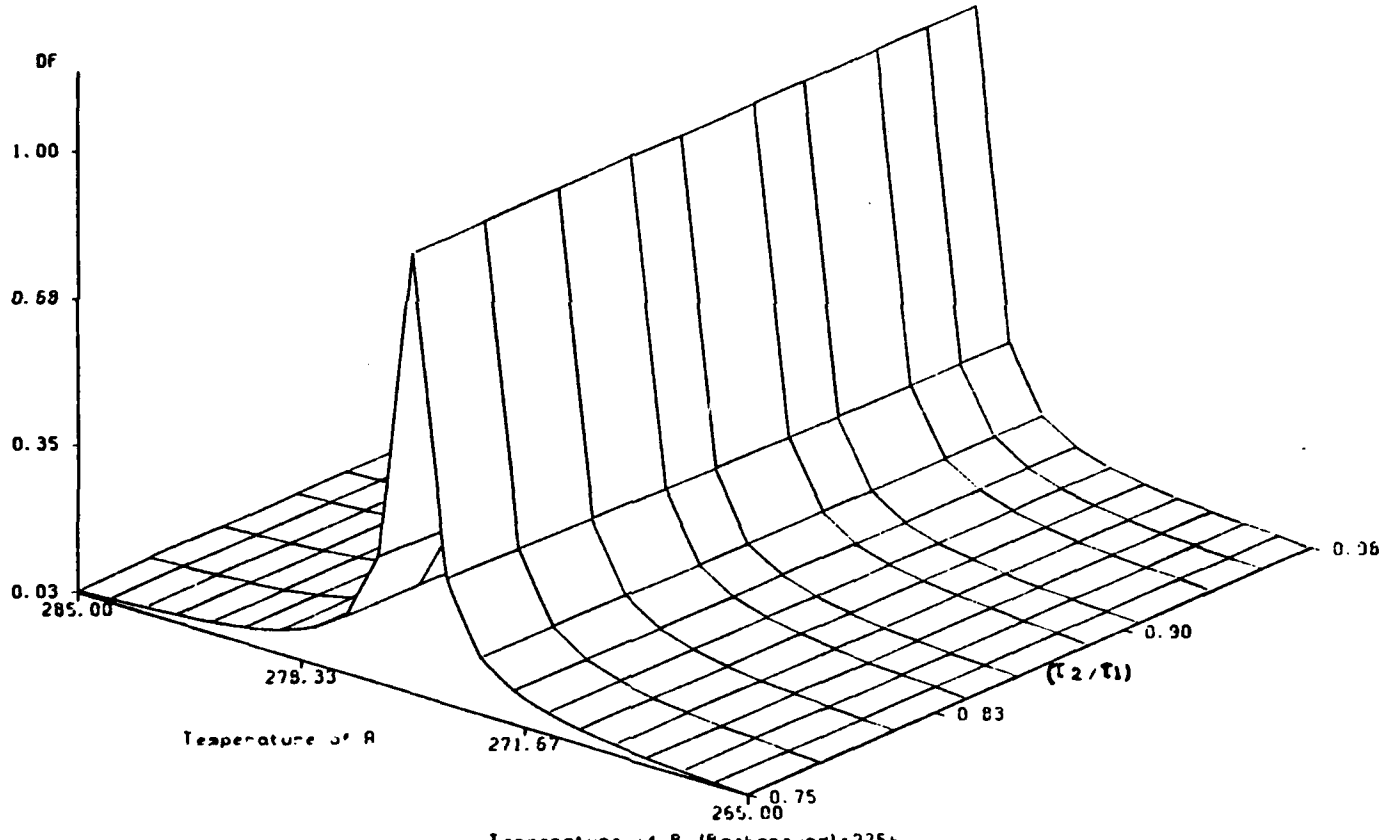

Temperature of B (Background) = 275k

(V. ... run1 - 5=.01 - .05 respectively

DEPENDENCE OF D.F. ON RELATIVE ATMOSPHERIC TRANSMISSION IN BANDS USED TO COMPUTE RADIANCE RATIO AND ON TEMPERATURE DIFFERENCE BETWEEN TARGET AND BACKGROUND

C2

Channel1 = 3.5 – 4.1 microns

Channel2 = 11 – 12 microns

Correlation Coefficient = .1

RUN=5

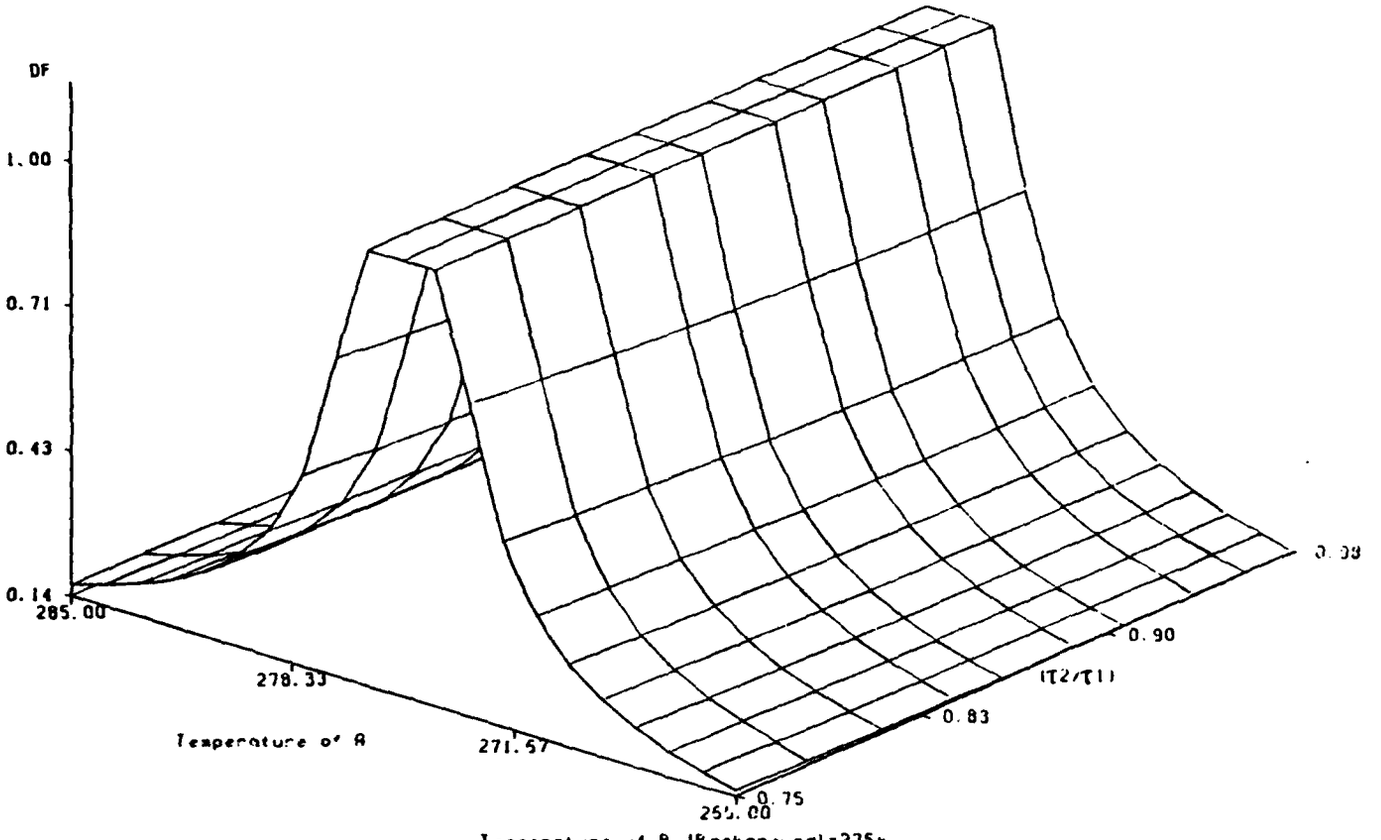

Temperature of B (Background=275K

C.V. --- run1-5=.01-.05 respectively

DEPENDENCE OF D.F. ON RELATIVE ATMOSPHERIC TRANSMISSION IN BANDS USED TO COMPUTE RADIANCE RATIO AND ON TEMPERATURE DIFFERENCE BETWEEN TARGET AND BACKGROUND

Channel1=3.5-4.1 microns

Channel2=11-12 microns

Correlation Coefficient= 9

RUN-5

C3

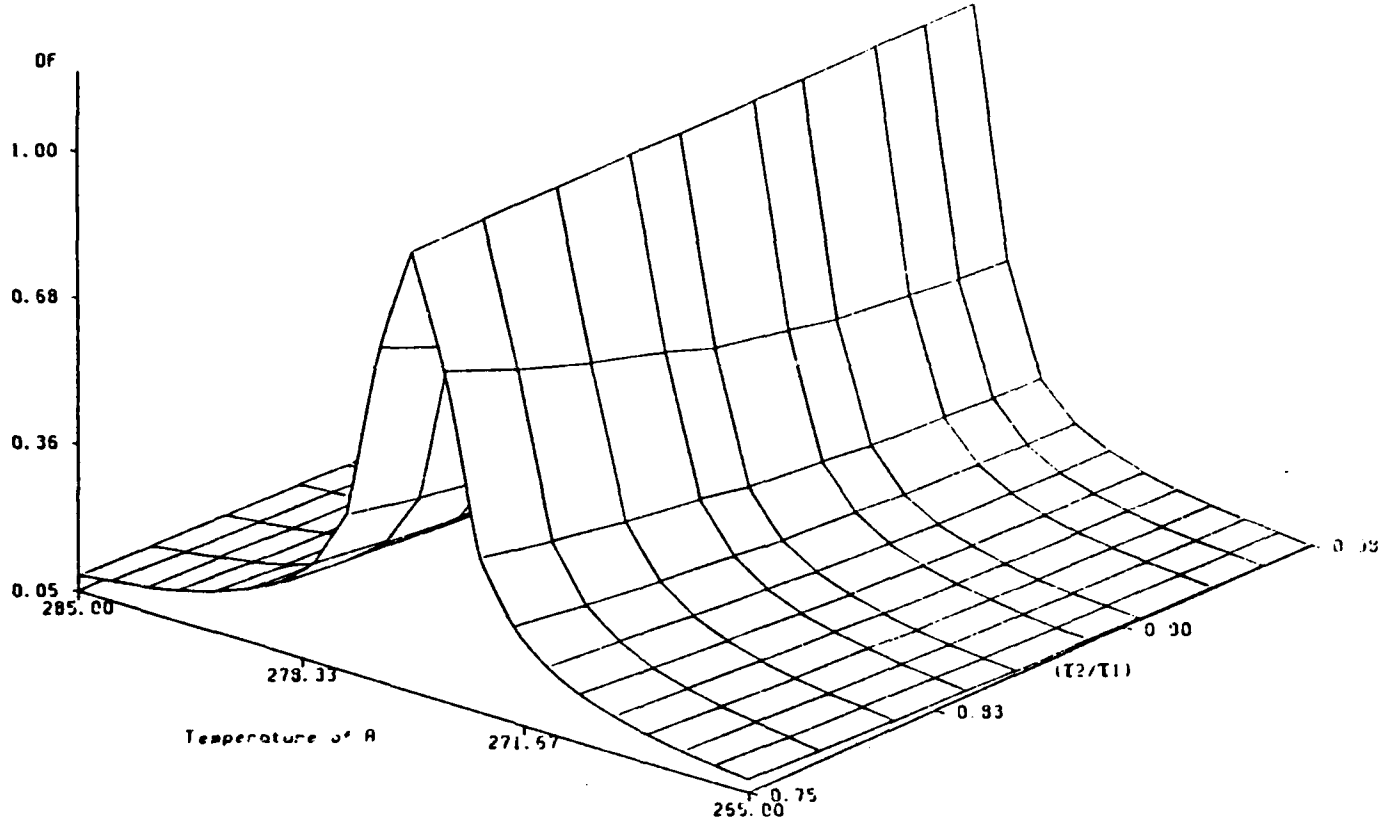

Temperature of B (Background=275k
C.V. --- run1-5=.01-.05 respectively

MISSION
of
Rome Air Development Center

RADC plans and executes research, development, test and selected acquisition programs in support of Command, Control Communications and Intelligence (C^3I) activities. Technical and engineering support within areas of technical competence is provided to ESD Program Offices (POs) and other ESD elements. The principal technical mission areas are communications, electromagnetic guidance and control, surveillance of ground and aerospace objects, intelligence data collection and handling, information system technology, ionospheric propagation, solid state sciences, microwave physics and electronic reliability, maintainability and compatibility.

END

FILMED

7-85

DTIC